THE UNIVERSITY
of EDINBURGH

Optical Profiling of Macrophages

Tom Speight

PhD
College of Medicine and Vetinary Medicine
University of Edinburgh
2019

Declaration

I can confirm that this thesis has been entirely composed by myself. The work represents experiments and studies undertaken by me, whilst working within a multidisciplinary research group and any contributions from others has been clearly indicated. None of this work has been submitted for any other degree or professional qualification.

Tom Speight

Abstract

Macrophages are required to show plasticity in how they react to their microenvironment and orchestrate an inflammatory response. With such an integral role in human immunity, aberrant macrophage function can directly contribute to a variety of pathologies: from driving chronic inflammation to a compromised clearance of invading pathogens. Although there are pharmaceutical opportunities to restore alveolar macrophage function in disease, there still remains a challenge to truly profile their activity *in situ*. The use of optical endomicroscopy - a non-invasive, fibre-optic imaging platform capable of accessing the alveolar space, may be used in combination with optical probes to profile alveolar macrophage activity in their native environment.

Work outlined in this thesis covers the characterisation of a human monocyte-derived macrophage model phenotype, performed using gold-standard *in vitro* systems including flow cytometric analysis of receptor expression and phagocytic activity. The work then moves on to explore alternative ways of optically profiling macrophages that may have clinical applications.

An optical probe was synthesised to target the mannose receptor, a cell-surface receptor expressed on macrophages, using a camelid nanobody fragment as a targeting ligand. Initial characterisation showed cell-type specificity of the probe towards macrophages. While labelling appeared to be via active internalisation by cells, more evidence is required to determine if this probe interacts specifically with the mannose receptor target.

A novel form of optical endomicroscopy was used to explore imaging macrophages, label-free, via their auto-fluorescent emission spectra. This was to distinguish macrophages following internalisation of a fluorescent target, without further labelling required to image negative cells. Initial imaging showed that *in vitro* monocyte-derived macrophages did not fluoresce brightly enough to be imaged label-free, though it is expected that primary lung macrophages – particularly from

COPD patients who smoke – would be sufficiently bright enough to profile with this technique.

Ultimately this work will be the foundation to profiling primary alveolar macrophages in health and disease. Using optical endomicroscopic imaging systems with optical probes for markers of cell phenotype, as well as other label-free methods in development, there is potential to profile the activity of alveolar macrophages directly in the alveolar space of the human lung and monitor pharmaceutical effects on their activity.

Lay Abstract

The macrophage immune cell is a key actor in how the human body responds to invading bacteria and control inflammation. Macrophages can recognise the bacteria that pose a threat and recruit other parts of the immune system to clear it. This is particularly important in the airways of the lung, as macrophages in this region are the first cells to come into contact with bacteria (and other debris) we breathe in.

The work in this thesis first describes the use of human monocyte immune cells being taken outside of the body and cultured into macrophages. This model is used to re-affirm standard techniques of interrogating the activity of macrophages, and how they respond to drugs. The work then moves onto more novel methods of interrogating macrophage activity, with a focus on being able to carry this out inside the human lung.

One method involves the use of a fluorescent antibody fragment as a probe to specifically target human macrophages by binding to a marker on the surface of the cells. While this novel probe appears to specifically label macrophages over other types of cells in the human lung, more work is required to show it binds to its intended target on the surface of macrophages.

Another method involves using a microscope connected to imaging fibres small enough to reach down into the lung to capture macrophages in their native environment. Macrophages in the lung can emit their own colour of fluorescent light which can be detected by the microscope. In order to show how this microscope could be used to interrogate macrophage activity in the lung, human macrophages were fed labelled targets (either bacteria or dying immune cells) that emitted light in a slightly different colour. Therefore, the microscope would be able to distinguish between macrophages that were capable of eating and those that weren't based on the colour of light they emit.

Dedication

This thesis is dedicated to my family. To my mum and dad, who have always trusted and supported me with whichever direction I chose to go. You encouraged my curiosity and have always pushed me to make my own contribution to making things better.

To Clara, you've been a rock when I needed you to be. You've been optimistic when I struggled to be. You've made me a stronger person, and a happy person with a loving family- Javi and Maeby included!

Acknowledgements

Firstly, I would like to thank each of my supervisors for their support throughout this thesis. Prof. Dhaliwal was an enduring source of optimisim and creativity throughout this project. I am grateful to him for giving me this opportunity to push my own scientific curiosity and to "give things a try!". Prof. Dransfield was always on hand to provide assistance and advice whenever I needed it. I appreciated all the meetings he made time for, to help make sense of the data. Prof. Bradley made sure this project was kept under the umbrella of the Proteus project- expanding the multidisciplinarity of this work. I would like to thank the EPSRC for their support in funding the work in this thesis.

I would like to thank the Proteus Group for providing an environment for me to contribute towards an overarching goal, working with other scientists from all disciplines. In particular I would like to thank Gavin Birch, Helen Parker, and Dominic Norberg. Without Gavin's chemistry expertise, there would not have been a macrophage probe to characterise. Also thanks to Christophe Portal of Edinburgh Molecular Imaging for his help synthesising the MR Nanobody. Thanks to Helen and Dominic, I was able to expand the interdisciplinarity of my project and combine optical physics and biology to work on something totally unique. Special thanks to Emma Scholefield, Beth Mills, Tom Craven and Ahsan Akram for getting me started in the lab and helping to build my confidence to work independently on this project. Thank you to members of the CIR community at the QMRI for any advice and assistance I sought- particularly the donation or sharing of blood for this work. Thank you to Brian McHugh for his help in setting up the transfection assay described in chapter four. Thank you to Eilise Ryan, Li Feng, and Cecilia Boz for providing alveolar macorphages to work with.

Thank you to the excellent facility staff of the QMRI for all of their help. The Flow facility (Shonna Johnston, Will Ramsey, Mairi Pattison) were invaluable in training on flow and help setting up assays. Thank you to Trudi Gillespie and Charlotte Buckley for their support and enthusiasm in setting up imaging assays.

Beyond academic work, thank you to the OPTIMA CDT for supporting me as an aligned student and providing career development courses outwith my project that helped broaden my aspirations following this project.

Last but not least, thank you to the close colleagues and friends I've made throughout my time at the University of Edinburgh. Philip and Shauni, Andrea and Mela, Dominic and Rachel, Duncan, Jamie, Jo and Katie: being part of such a close knit group of pals really kept me going during the difficult periods, as well as for celebrating the happier ones! Each of you have been integral to making my life outside of work so enjoyable.

Abbreviations

AM – Alveolar Macrophage

ARE – Antioxidant Response Elements

BAL – Broncho-alveolar lavage

BMDM – Bone Marrow Derived Macrophage

CHO – Chinese Hamster Ovary

CLSM – Confocal Laser Scanning Microscopy

CMFDA - Chloromethylfluorescein diacetate

COPD – Chronic Obstructive Pulmonary Disease

COX-2 – Cyclooxygenase 2

CT – Computerised Tomography

Dex - Dexamethasone

E. coli – Escherichia coli

FAM - Fluorescein

FCFM – Fibered Confocal Fluorescence Microscopy

FDA – Food and Drugs Authority

FDG - Fluorodeoxyglucose

FLIM – Fluorescence Lifetime Imaging Microscopy

FOV – Field of View

GM-CSF - Granulocyte-Macrophage Colony-Stimulating Factor

HSI – Hyper Spectral Imaging

ITAM - Immunoreceptor Tyrosine-based Activation Motif

LED – Light Emitting Diode

LoD – Limit of Detection

LPS – Lipopolysaccharide

mAb – Monoclonal Antibody

M-CSF - Macrophage Colony-Stimulating Factor

MDM – Monocyte Derived Macrophage

MFU – Mean Fluorescence Units

MR – Mannose Receptor

NBD – Nitrobenzoxadiazole

NHS- N-hydroxysuccinimide

NIR – Near Infrared

Nrf2 - Nuclear factor erythroid 2–related factor 2

NO – Nitric Oxide

OCT – Optical Coherence Tomography

OEM – Optical Endomicroscopy

OI – Optical Imaging

PAMP – Pathogen Associated Molecular Pattern

PBMC – Peripheral Blood Mononuclear Cell

PET – Positron Emission Tomography

PI3K - Phosphoinositide 3-kinase

PMN – Polymorphonuclear

PRR – Pattern Recognition Receptor

PS – Phosphatidylserine

ROS – Reactive Oxygen Species

SCy5 – Sulphonated Cyanine 5

SDCM – Spinning Disc Confocal Microscopy

SR – Spectral Ratio

TAM – Tumour Associated Macrophage

TGF ß – Transforming Growth Factor

TIM - T-cell immunoglobulin and mucin

TNF – Tumour Necrosis Factor

IFN – Interferon

Table of Contents

List of Figures

Chapter One: Introduction

1.1 A Brief Overview of Inflammation

Inflammation is an incredibly well conserved mechanism that ensures the human body can react effectively to any harmful stimuli [1]. Beneath the outward-facing signs of calor, dolor, rubor, and tumor, there are a host of interactions taking place at the cellular and molecular level to recognise the cause of harm, eliminate it, and begin repair [1].

At the outset of inflammation, neutrophils are recruited in large numbers to the site of injury [2]. Neutrophils represent the most common leukocyte population in the body and are key to an inflammatory response. As first responders to environmental challenges, they can identify and ingest foreign material [2]. Neutrophils can also release an arsenal of cytotoxic products such as reactive oxygen species (ROS) to neutralise pathogens in the environment [3]. In addition to neutrophils, monocytes are recruited to the inflammatory site from the circulation [4]. These monocytes differentiate into macrophages to drive forward the inflammatory response with the production of pro-inflammatory mediators, ranging from tumour necrosis factor α (TNF), interleukin-1 (IL-1) and nitric oxide (NO), each facilitating anti-microbial activity [5]. Production of interleukin-12 and 13 signal the start of T cell activation (Th1 and Th13) and differentiation, and a shift to adaptive immunity [6].

At some point during inflammation, a switch must be flipped: all the processes initiated at the onset of the inflammatory response must also be dampened in order for the tissue to return to a form of homeostasis. This clean-up operation entails the removal of pro-inflammatory cytokines (so that there is not a continuation of immune cell activation), cessation in signals for further immune cell recruitment (through stopping chemokine production), as well as clearance of already-extravasated cells that are no longer required [7]. Often the clearance of extravasated cells, mostly neutrophils, involves the onset of apoptosis, followed by efferocytosis by macrophages [8]. There is also the production of WNT ligands, transforming

growth factor beta (TGF-ß), and soluble mediators such as prostaglandins to commence tissue repair in the environment from any collateral damage that occurred during the inflammatory phase [9,10,11].

1.2 The Role of Macrophages in Inflammation

Macrophages are a member of the mononuclear phagocyte system which also encompasses monocytes and dendritic cells. The longstanding hypothesis of macrophage origin had been they arose from peripheral blood monocyte differentiation [4]. Circulating monocytes in the blood entered tissues when recruited during inflammation and differentiated into macrophages in the presence of growth factors (M-CSF, GM-CSF) and cytokines (interferon-gamma, IL-4) [12]. More recent studies have shown evidence for there being populations of tissue-resident macrophages present even before birth, developing in the yolk sac during embryonic development [13]. These populations of macrophages are also believed to have the capacity for self-renewal [14].

While the nomenclature has moved on in recent years, historically the activated states of macrophages were defined under two opposing forms: classical "M1" activation and alternative "M2" activation [15]. The M1 state is considered the pro-inflammatory form macrophages can take. This has typically been characterised as macrophages producing proinflammatory cytokines (TNF-α, IL-1) and reactive oxygen and nitrogen species, as well as being closely associated with promoting a Th1 immune response through antigen presentation [6]. This portrayed M1 macrophages as also having strong microbicidal and tumoricidal capabilities. Activation of macrophages into the M1 phenotype can be through stimulation of inflammatory cytokines such as interferon-γ (IFN and TNF-α), or from exposure to microbial products like lipopolysaccharide (LPS) [16].

By contrast, M2 macrophages represent the pro-restorative features also attributed to macrophages. This includes functions associated with tissue remodelling and stimulating the Th2 response [15]. The typical stimulant associated with M2 activation is interleukin-4 (IL-4) [17]. The metabolic functions of M2 macrophages also distinguish them from M1 macrophages: rather than metabolising arginine to nitric oxide (an M1 trait), M2 cells metabolise the amino acid into ornithine and polyamines for tissue repair purposes [18,19].

The M1/M2 dichotomy appealed to the notion that inflammation vacillates between two overarching states: activation and resolution. Therefore macrophages were given defined states that reflected this. However, over the years it became clearer that macrophages do not fall into one of these two rigid states. Instead, M1/M2 became classed as two polarised states, between which is an entire spectrum of activation that macrophages could adopt. In addition to this, further evidence showed that tissue resident macrophages would adopt their own unique phenotype, comprising a combination of markers from the M1/M2 dichotomy [20,21]. This makes intuitive sense, as there would likely be an assortment of stimulants in a given microenvironment that seek to polarise macrophages one way or another. Therefore, as the tissue microenvironment govern the ultimate phenotype of resident macrophages, they were characterised as unique tissue-resident populations depending on where in the body they reside: Langerhans cells in the skin, Kupffer cells in the liver, microglia within the brain, , peritoneal macrophages in the peritoneum, osteoclasts in the bone, and alveolar macrophages in the lung [22].

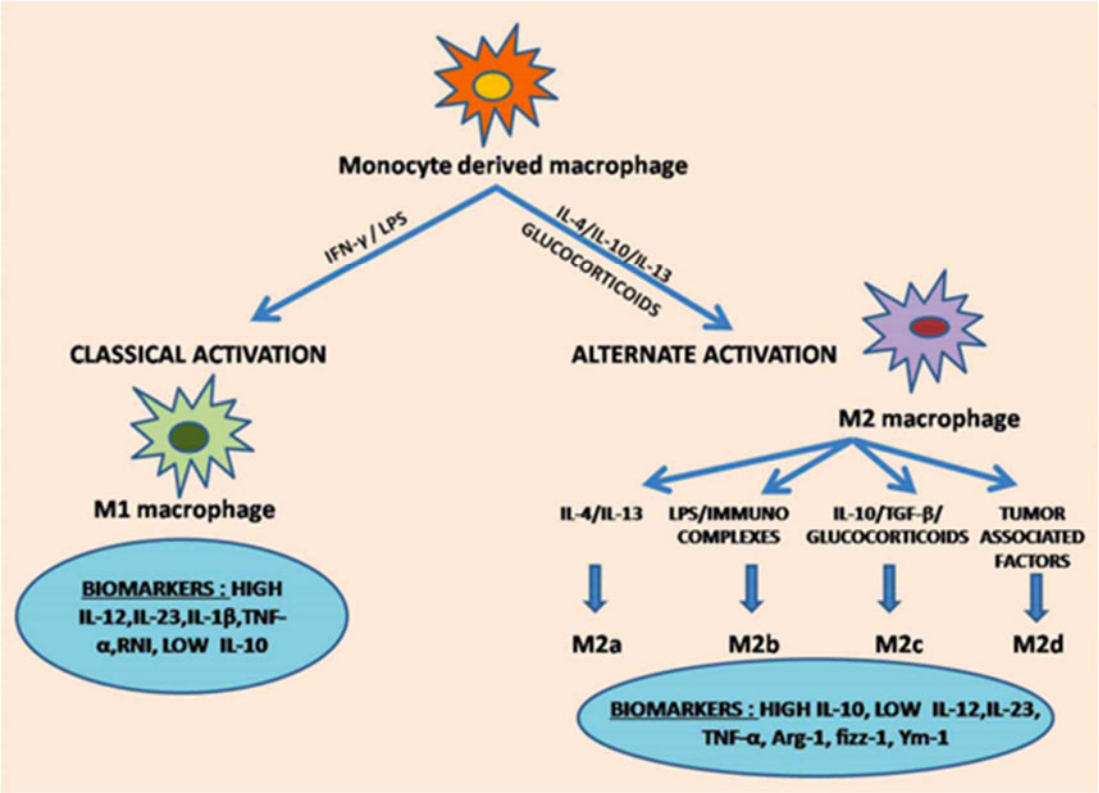

Figure 1.1 The alternate pathways of macrophage polarisations and the biomarkers associated with the two ends of the polarised spectrum. From Arora et al. (2018) [23]

1.2.1 Macrophage Phagocytosis: "the big eater"

The professional phagocyte system comprises of: macrophages, dendritic cells, monocytes, neutrophils, and eosinophils [24]. Metchnikov gave macrophages their name to describe one of their classic functions in immunity [25]. The key role for "the big eater" is to orchestrate the response to foreign material by first engulfing it. Phagocytosis is the integral process that facilitates the programmed responses to what material a macrophage has come into contact with, therefore what type of process is required [26].

Phagocytosis is a receptor-mediated event [27]. Plasma membrane receptors on the surface of the macrophage dictate the specific nature of phagocytosis, as each will have specific binding affinity for mediating phagocytosis of different target ligands (Figure 1.2A). Microbial ligands for phagocytic recognition are proteins and lipids

that distinguish the microbe as foreign, such as lipopolysaccharide (LPS) and lipoteichoic acids [27]. These are commonly known as pathogen-associated molecular patterns (PAMP) [28]. Toll-like receptors on the surface of macrophages aid in the recognition of PAMPs on the surface of microbes, while other pattern recognition receptors (PRR) help recognise damage associated molecular patterns (DAMP) on self-tissue [29,30]. For example, sugars such as glucan that are present on pathogens are recognised by the PRR Dectin-1, while LPS present on the surface of gram-negative bacteria is recognised by the Scavenger Receptor A [31,32]. The scavenger receptor A, as well as other PRRs such as MARCO, are also responsible for the clearance of other waste in the local environment such as oxidised lipids that, if left, would trigger unwarranted inflammation [33]. Microbes and other foreign bodies can be targeted by soluble molecules in the blood, such as immunoglobulins and complement, that are recognisied by opsonic receptors that stimulate phagocytosis [34]. Fcγ receptors (FcγRI, FcγRIIA, FcγRIIB, FcγRIIC, FcγRIIIA, and FcγRIIIB) on macrophages bind to the Fc portion of IgG antibodies [35]. Upon binding, activated FcγRs stimulate immunoreceptor tyrosine-based activation or inhibitory motifs (ITAM) which in turn activate phosphatidylinositol 3-kinases (PI3K) that activate GTPases to initiate phagocytosis [34].

On apoptotic cells, certain phospholipids such as phosphatidylserine (PS) serve as "eat me" signals to macrophages, marking the apoptotic cell for clearance [36]. A number of receptors can recognise exposed PS to elicit efferocytosis- the internalisation of apoptotic cells. The T cell immunoglobulin mucin family (TIM), BAI1, and Stabilin-2 can directly interact with PS on apoptotic cells, while the TAM phagocytic receptor family (Tyro3, Axl, Mer) bind to bridging molecules protein S and Gas6 to facilitate efferocytosis [37,38,39,40].

Once a target has been internalised, an early phagosome vacuole is formed within the cytoplasm of the macrophage, to compartmentalise the ingested material (Figure 1.2B) [41]. This phagosome subsequently fuses with lysosomes and other

products of the endoplasmic reticulum and Golgi network to form a secondary phagolysosome [42]. Acidification of the phagolysosome reduces the pH to ~4.5 to hasten the degradation of the ingested material [43].

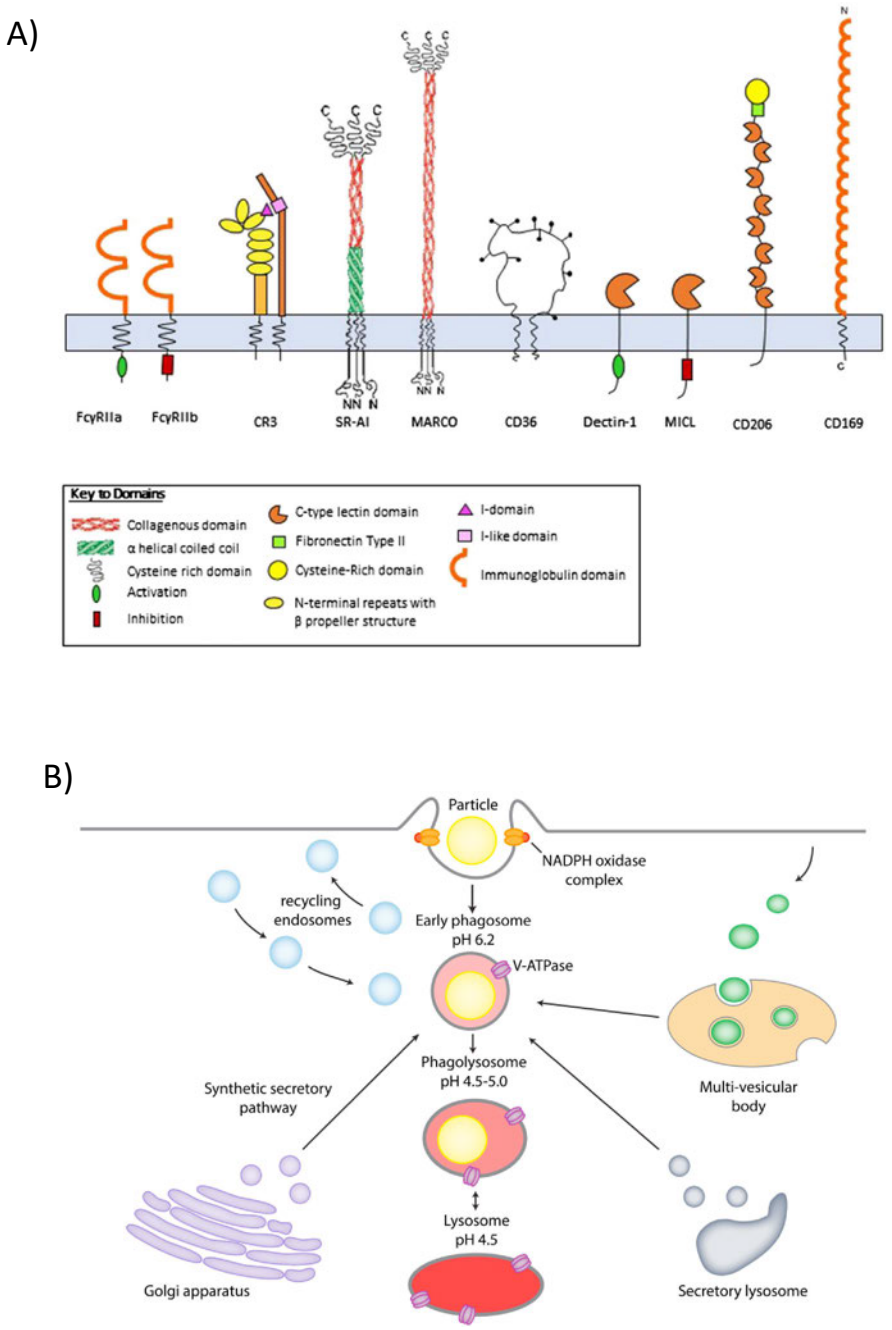

Figure 1.2 A) A selection of cell surface receptors expressed on macrophages that mediate phagocytosis of microbes and other foreign material, and apoptotic bodies. B) Overview of the phagocytic pathway. Adapted from Gordon (2016) [27]

1.3 Alveolar Macrophages

Every day the human lung faces a number of environmental challenges: from inhalation of infectious agents to any other potentially harmful particulate matter. The alveolar-capillary barrier, the site of gas exchange in the lung, is the key site where potential pathogens or particles can gain access to the bloodstream. Maintaining control of this barrier is essential to not only preventing infections, but to maintain inflammatory homeostasis in the lung, including the prevention of excess inflammation that could also hinder gas exchange [44]. The orchestrator of inflammatory responses in this space is the cell that first comes into contact with inhaled material: the alveolar macrophage (AM).

AMs are a unique and important population of resident macrophages within the body's immune network [45]. Over 90% of the pulmonary leucocyte population are AMs [46]. While circulating monocytes can differentiate into AM-like cells to fulfill this specialised role, there is evidence to suggest a bespoke AM population is present soon after birth [47]. AMs can reside for a long time in the alveolar space, lasting weeks to months [48]. In some cases, there has been evidence of cigarette products being present within AMs years after cessation of smoking, further highlighting their long life-span [49]. Resident AMs have also shown a stable capacity for self-renewal [14].

There appears to be an important role for GM-CSF in maintaining the AM population in the lung [50]. Higher levels of GM-CSF enable migrating monocytes to the lung to differentiate into the unique AM phenotype, including adhesion to the alveolar walls [51]. The alveolar epithelial cell wall provides a continuous source of GM-CSF [52]. In addition to GM-CSF, the nuclear receptor PPAR-γ has also been shown as a key regulator of alveolar macrophage differentiation and maintenance, something which is more unique AMs compared to other tissue resident populations [53,54]. This reveals that alveolar macrophages, like other tissue macrophages, possess a unique transcriptional program in order to regulate their unique phenotype [55].

Some have suggested that the quiescent state of AMs revolves around a predominantly anti-inflammatory phenotype, as depletion of these cells in animal models has resulted in excessive production of pro-inflammatory mediators [56]. AMs are thought to show a reduced response to foreign material at first. This is exemplified by low basal expression of CD86 (a pro-inflammatory, co-stimulatory molecule for T cell activation) on the AM surface [57]. It has also been established that AMs are comparatively poor at antigen presentation to T cells as well as having a limited capacity for respiratory burst [58,59]. These factors contribute to minimal responses of unstimulated AM to particulate material they encounter.

AMs possess a number of mechanisms to non-specifically target foreign material in the lung. This involves the expression of PRRs and scavenger receptors [60]. This form of response to microorganisms is capable of countering up to 10^9 intra-tracheal bacteria before further engagement of the immune system is required [61]. Two receptors that are closely associated with the AM phenotype are the mannose receptor (MR) and MARCO [62]. These receptors aid in the recognition of unopsonised bacteria, by binding to sugars (mannose, fucose, N-Acetylglucosamine) present on these pathogens [62]. The oxidative stress that AMs encounter in the presence of pathogens leads to the expression of TLR4 on their surface, which in turn stimulates expression of other TLRs [63,64]. This then endows the AMs with a greater phagocytic capacity and supports pro-inflammatory cytokine production [65,66].

As sentinels of the alveolar-capillary barrier, AMs are charged with walking an inflammatory tightrope in their resident environment. They must show a higher tolerance to foreign material than is expected of other tissue macrophages, while also being proficient in inciting and dampening inflammatory responses efficiently enough to avoid damage to lung tissue. With so many roles to play, aberration in one or more of their functions quickly implicates AMs in lung pathology.

1.3.1 Alveolar macrophages in disease: COPD as a case example

Often associated as a smoker's disease, chronic obstructive pulmonary disease (COPD) is an increasingly threatening inflammatory disease throughout the world. In the coming years, COPD is expected to become the third leading cause of death globally [67]. Back in 2010, the economic costs of treating COPD topped $2.1 trillion, half of which from developing nations [68]. The pathology of COPD is characterised as progressive lung function decline- caused by aberrant and persistent inflammation in response to cigarette smoke exposure and other environmental pollutants [69].

AMs are closely linked to the pathology of COPD, due to defects in the cell phenotype that contribute to the common hallmarks of COPD (persistent inflammation and recurring infections) [70]. There is an increase in AM cell number during COPD [71]. The increased numbers likely stem from aberrant chemokine production in the airways, such as MCP-1, causing continual recruitment of monocytes to the alveolar space [72]. This is supported by evidence of increased amounts of MCP-1 being present in the sputum of COPD patients [73]. Other factors possibly contributing to increased AM numbers in COPD are expansion of local proliferation in the alveolar space with prolonged survival [74].

While COPD appears to increase the number of AMs present in the lung, macrophages show little capacity at relieving inflammatory symptoms or preventing recurring infection. It is now well established that there are clear phagocytic defects in AMs during COPD [75]. Studies have shown that alveolar macrophages retrieved from broncho-alveolar lavage (BAL) fluid of COPD patients, as well as macrophages cultured *in vitro* from monocytes retrieved from the blood of COPD patients, show a diminished ability to phagocytose pathogens often associated with infections during COPD, including: *Haemophilus influenzae*, *Pseudomonas aeruginosa* and *Streptococcus pneumoniae* [75,76]. Further studies on AM function in COPD show that phagocytic dysfunction is not limited to microbial clearance, as AM

efferocytosis is also impaired during COPD, resulting in a lack of apoptotic cell clearance in the alveolar space [77]. Interestingly, the AM phagocytic defect in COPD does not extend to inert particle clearance, which relies more on scavenger receptor activity [76,78].

While it has been hypothesised that possible reasons for defective AM phagocytosis in COPD may be due to diminished PAMP recognition or expression of phagocytic receptors, there is limited evidence to support this [79]. One study found that cigarette exposure (which is often the case in COPD) decreased TLR3 expression, though no changes were found for other TLRs [80]. Another study showed that COPD had little impact on the expression of phagocytic receptors, such as CD44, CD36, CD51, CD61, CD14, and CR3 [81]. The same study did find some effect on other receptor expression in COPD, as there was a reduction in HLA-DR and CD80 [81]. In considering receptor expression as a marker for COPD, one study did find that the scavenger receptor CD163 is predominantly expressed on isolated AMs from the BAL of COPD patients [82]. Another reason for poor phagocytic activity could be continual AM exposure to oxidative stress, due to chronic exposure to cigarette smoke [78]. Sustained oxidative stress can lead to AM deficiency of both bacterial clearance and apoptotic cell removal [78,83]. Although, one study has shown that AM phagocytic defects are not limited to active smokers [83].

Studies have focussed on elucidating the phenotype of AMs during COPD. There is a rise in production of chemokines that recruit more immune cell types, for example interleukin-8 (IL-8) has found to be elevated in COPD airways [84]. There is also a characteristic cytokine profile in COPD that can be attributed to AMs, such as elevated levels of the pro-inflammatory mediator TNF-α found in the sputum of COPD patients [84]. In addition, there is increased production of matrix metalloproteases and cathepsins, which likely contribute to persistent remodelling of lung tissue [85]. This profile likely stems from altered regulation of transcription factors that influence AM cytokine production. For example, the activation of NF-kB

- which plays a well-established role in the production of pro-inflammatory mediators including TNF and iNOS – correlates to exacerbations of COPD [86].

Reviewing the cytokine and receptor profiles of AMs during COPD reveals how macrophages in disease can present as antithetical to the linear spectrum of activated states. While AMs show increased expression of pro-inflammatory cytokine products, they also express receptors and other markers associated with an M2, pro-resolution state. AMs appear to be trapped in facilitating the vicious cycle that occurs during COPD: incapable of resolving inflammation in the airways, the AMs maintain a pro-resolving phenotype in their continued attempts to recapture some form of lung homeostasis. This in turn leaves the AMs ill-prepared for recurring infections that exacerbate the oxidative stress in the microenvironment, triggering pro-inflammatory mediators that recruit even more immune cells which won't be effectively cleared- perpetuating the inflammatory cycle (Figure 1.3).

The current treatment for COPD largely focuses on alleviating the restriction airflow in the disease [87]. There is still a gap in COPD therapy that effectively slows down the decline of lung function or restore activities integral to recapturing the inflammatory homeostasis of the lung.

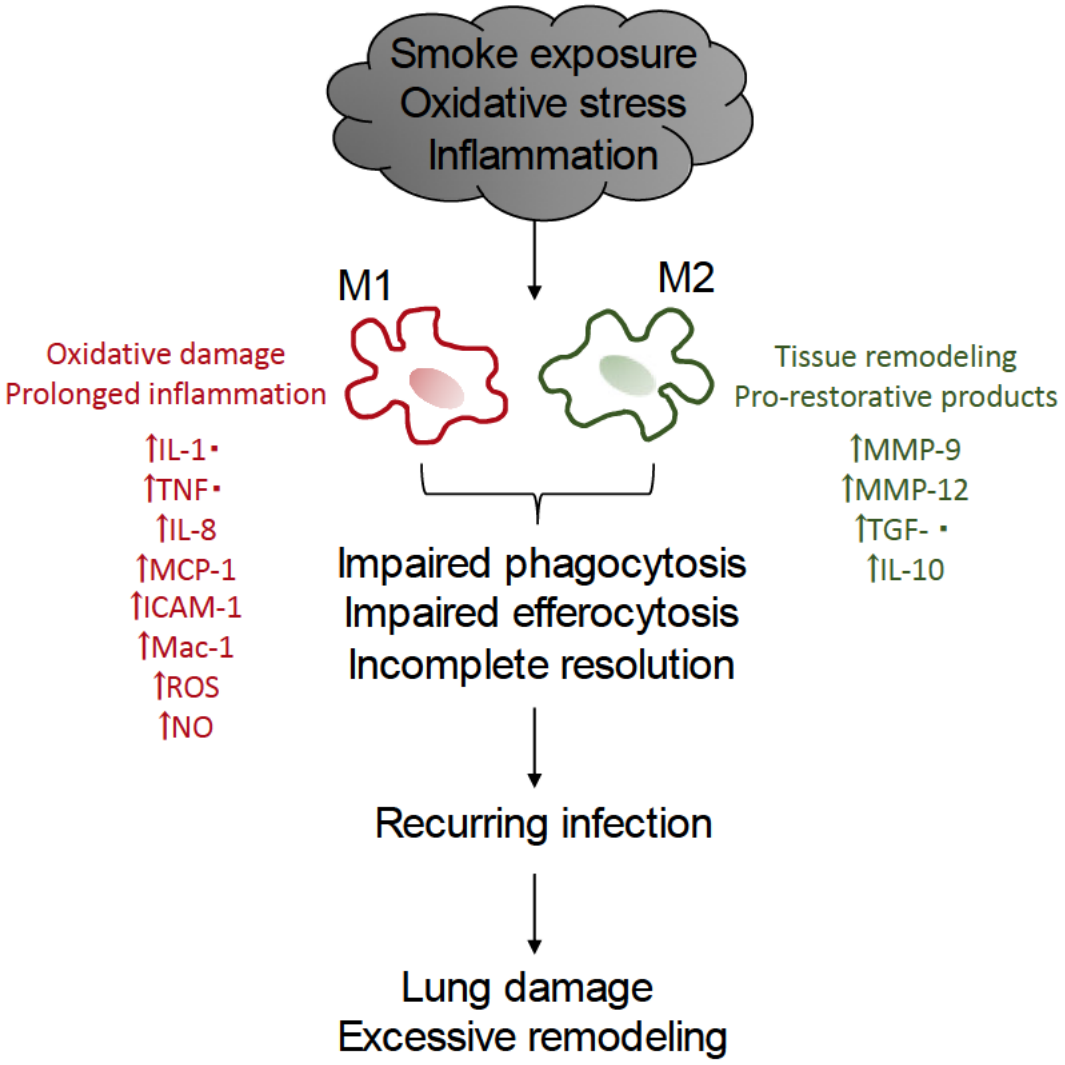

Figure 1.3 The COPD alveolar macrophage. Adapted from Vlahos and Blozinovski (2014) and Barnes (2004) [88,72]

1.3.2 Therapies to restore alveolar macrophage function

The plasticity of macrophage responses to environmental stimuli mean they can drastically adapt their phenotype. From expression of receptors, production of cell products, to phagocytic activity, each can be modified to varying degrees depending on the stimuli and even the disease environment a macrophage resides in. The reality of this means there are a plethora of macrophage states in disease, making it difficult to create applicable and directed therapies. But, by aligning potential therapies with a detailed knowledge of the activated state of macrophages in

different pathologies, there would be new avenues opened up for personalised medicine in diseases where macrophages are implicated.

Nanoparticle-based approaches have been explored to therapeutically manipulate macrophage function [89,90,91]. Use of nanoparticles has largely focussed on improving the specificity of molecular imaging techniques for detecting macrophages. For example, one study used a radiolabelled nanoparticle to be specifically taken up by inflammatory monocytes and macrophages in atherosclerotic plaques, while also showing promise as a marker for cell responses to anti-inflammatory treatment [92]. Another study developed liposomes that present phosphatidylserine to mimic apoptotic cells in order to encourage macrophages to adopt an anti-inflammatory phenotype [93]. *In vitro* and some *in vivo* studies in mice showed these nanoparticles were taken up by macrophages in atherosclerosis models [93]. These macrophages subsequently showed upregulation of CD206 (the mannose receptor) and downregulation of CD86, aligning with a change in phenotype [93]. Other strategies using nanoparticles to modulate macrophage activity have been deployed to limit the production of pro-inflammatory mediators, such as TNF-a, cyclooxygenase-2 (COX-2) and reactive oxygen species (ROS) [94,95,96]. These strategies highlight the potential for more directed macrophage therapy, focussing on specific products of their phenotype rather than general targeting of cells that could have unintended consequences [89].

In the context of COPD, macrophage therapy has previously struggled to make headway. An abundance of pro-inflammatory mediators stemming from AMs in COPD contribute to the pathology, but the use of corticosteroids – a mainstay anti-inflammatory therapy – have shown little effect in suppressing these mediators [97,98]. One study found that insensitivity to corticosteroids – specifically dexamethasone - was specific to COPD AMs when compared to AMs from regular smokers [99].

As oxidative stress is postulated to be influential on AM function during COPD, a range of antioxidant therapies have been explored to restore lost activities. Some studies have directed efforts to the activation of transcription factor nuclear erythroid–related factor 2 (Nrf2), as it is responsible for the transcription of anti-oxidant proteins [100,101]. Nrf2 is stimulated during oxidative stress to dissociate from its inhibitor (Keap1) and is then translocated to the nucleus where it binds to antioxidant response elements (ARE) [102]. This process has been shown to be disrupted in mice models following exposure to cigarette smoke, as well as a decline in its transcriptional activity has been confirmed in AMs from COPD patients [103,104]. Treatment with sulforaphane, a natural agonist for Nrf2, initially improved phagocytosis by AMs in a COPD mouse model and in isolated AMs from COPD patients [100]. This restoration in activity coincided with increased expression of the MARCO scavenger receptor and anti-oxidant elements [100]. Further studies have shown that defective phagocytosis of opsonised bacteria is also a unique element of COPD, which is also treatable with Nrf2-agonists [105].

A randomised clinical trial has shown that use of macrolide antibiotics, such as azithromycin, can reduce the number of exacerbations in COPD. Improvement in AM function in COPD has been shown from the use of macrolide antibiotics [106]. Studying the effects of azithromycin on COPD AMs using *in vitro* methodology found a significant improvement to AM phagocytic activity following azithromycin treatment [107]. The improvement in AM activity coincided with changes in receptor expression. Expression of CD206 (the mannose receptor) has previously been shown to be reduced during COPD, though expression was increased by up to 50% following azithromycin treatment [107]. Multiple studies present conflicting data on the actual effect azithromycin treatment has on COPD patient cohorts, suggesting more detailed analysis is required to pinpoint what mechanisms by which macrolide antibiotics effect AMs so as to restore phagocytic function [108,106].

1.4 Optical Molecular Imaging

Molecular imaging provides a window to the inside of living systems. Depending on the spatial resolution of the system involved, it is possible to detect, characterise, even measure biological processes taking place, right down to the cellular level with micromolar resolutions [109]. Improvement in the resolution is directly proportional to the level of detailed information that can be observed: this can range from simple anatomical structures to cellular interactions [110]. Development of new generations of molecular imaging technology widens the possibility of identifying new targets for pathology as well as improving our understanding of mechanisms that take place in health and disease [111]. A priority of modern imaging systems is to ensure they are non-invasive, whilst maintaining a resolution that is high enough to deliver the information required. Effective implementation of such devices would bring a direct improvement to clinical medicine as well as basic scientific research.

1.4.1 Molecular imaging of the human lung

One area of clinical need for improved molecular imaging is the human lung, as the distal regions of these organs have been challenging to study despite being such a critical site of infection and inflammation [112]. The standard forms of imaging the human lung have been chest x-rays, computed tomography (CT) scanning, and positron emission tomography (PET) [113,114,115]. Each of these imaging modalities have provided insight into different areas of the lung. Chest x-rays provide a two-dimensional image as ionizing radiation would pass through the body to a detector on the other side [114]. The resultant image resolves areas of opacity where there should be (such as bone) as where there shouldn't be, as is the cased in the diseased lung. CT scanning built upon this by compiling multiple two dimensional images of the lung around a single axis of rotation, providing a reconstructed three dimensional image of the tissue structures [113,116]. While x-rays and CT scans provide structural information of the lung, the development of PET scanning offered the

opportunity to image biological functions of the lung [115]. PET imaging involves the use of radionucleotides as contrast agents. The radionucleotides emit a positively charged positron as they decay, which travels through the tissue until it collides with an electron. The resulting gamma rays following collision are intercepted by multiple detectors as they travel outside of the body; these detectors can determine the relative position of the positron-electron collision in the body. The functional imaging capabilities of PET are due to the radionucleotides acting as radioisotope substitutes for essential biological molecules, such as carbon and nitrogen [117]. A prominent example is the use of 18-fluorodeoxyglucose (FDG) to act as a glucose substitute for PET-based imaging of glucose metabolism [118]. PET advanced molecular imaging to go beyond just structural information, as well as highlighting the benefit of coupling an imaging system with an imaging agent to retrieve more detailed information about the body. But historically a gap remained in molecular imaging: the ability to resolve disease processes down to the cellular level *in vivo*. The potential to carry out microscopic imaging inside of the body, in particular the human lung, would be a powerful tool in efforts to improve our understanding of what actually happens inside of these tissues, both in disease and in health. The rapidly developing field of optical imaging has been making strides to achieve this and advance molecular imaging in the medical field even further [112].

Optical imaging (OI) seeks to harness light from the visible spectrum right the way through to near infra-red as a means to develop systems that provide high resolution with *in vivo* imaging capabilities and clinical applications [112]. Use of OI-based technologies should be minimally invasive and relatively low-cost. OI involves the absorption of light at a particular wavelength, which excites a fluorophore to emit fluorescent light at a slightly higher wavelength; this emitted light can subsequently be detected [119]. The excited fluorophore can be intrinsic to biological tissue or part of an externally administered optical imaging probe, used in conjunction with an imaging system to "light up" specific cells or molecular processes, both *in vitro* and *in vivo* [120,112]. The source of the excitation can be from a laser or a light emitting diode

(LED), each capable of producing specific wavelengths of light [121]. Multiplexing of fluorophores is a key feature of OI as different fluorophores can require different wavelengths of light to be excited. The stokes shift that fluorophores undergo – the difference in wavelength from excitation to emission of light – can be in distinct parts of the light spectrum. Therefore, so long as their excitation and emission spectra are not too close together, multiple fluorophores can be used at the same time with multiple excitation light sources. OI has been a mainstay in biological research, with the development of fluorescent proteins and fluorescently-tagged antibodies to be used with bench-top optical imaging systems such as flow cytometry and confocal laser scanning microscopy [122,123,124,125].

The use of OI has been an attractive modality for *in vivo* imaging in humans [112]. In comparison to radiological molecular imaging modalities described earlier in the chapter, optical imaging does not require the use of ionising radiation [109]. The excitation and subsequent emission and detection of light is a fast process, while micrometre resolution of some optical imaging systems means imaging can be performed in the body to visualise cells in detail [112,109]. However, OI is not without its own drawbacks. One significant challenge of using OI *in vivo* is the lack of transparency in the human body; photons can be absorbed, light scattered and reflected back as it travels through tissue [121]. This varies between tissue sites depending on structural differences such as their level of vascularisation and the density of organelles such as mitochondria [110]. The use of near-infrared light (NIR) can partially mitigate this, as light in this spectral range of 650-900 nm has greater penetration through human tissue when compared to visible light further down the spectrum [126]. This is because light in the NIR spectral range undergoes very little absorption by water and haemoglobin as it travels through the body [110]. Another method to overcome light absorption is to develop detection systems that are able to access distal regions of the body and image *in situ.* This has high clinical potential in imaging the distal regions of the human lung, if the OI system is small enough to access these airways.

1.4.2 Optical Endomicroscopy: a cellular exploration of the alveolar space

Optical microendoscopy (OEM) sought to minimise the dimensions of specific parts of an OI system in order to have the ability to image areas of the body that could not previously have been accessed. This technology has the potential to image the distal lung not only *in situ*, but also in real time [127]. The *in situ* capabilities of OEM stem from utilising a flexible fibre bundle that allows excitation light to pass down. The excitation light is from an LED source at the proximal end of the fibre; any emitted light at the distal end can travel back up the fibre bundle where it meets a photodetector [128,129,130].

One of the first commercialised optical detection systems to use fibre-based OEM technology was Cell-viZio™ (Mauna Kea Technologies, France). This system uses a laser scanning unit coupled to a fibre bundle so that fibred confocal scanning fluorescence microscopy (FCFM) can be carried out in the human lung, *in situ,* and is approved by the US Food and Drug Administration (FDA) [131]. FCFM systems like Cell-viZio™ are able to take advantage of the benefits confocal laser scanning microscopy offers to OI. That is, the ability to perform high resolution imaging across a single focal plane, eliminating out of focus light that could disturb the field of view (FOV) [132]. Some groups have used FCFM to image structures such as bronchial tissue, which can be fluorescently excited 488nm (using blue excitation light) due to the autofluorescence of the elastin in this tissue (Figure 1.4)[128]. Further work has shown the high degree of inter-observer reliability with this form of optical imaging [127]. In addition to FCFM, widefield fibre-based OEM system have since been developed and clinically translated as low-cost systems for pulmonary imaging [130].

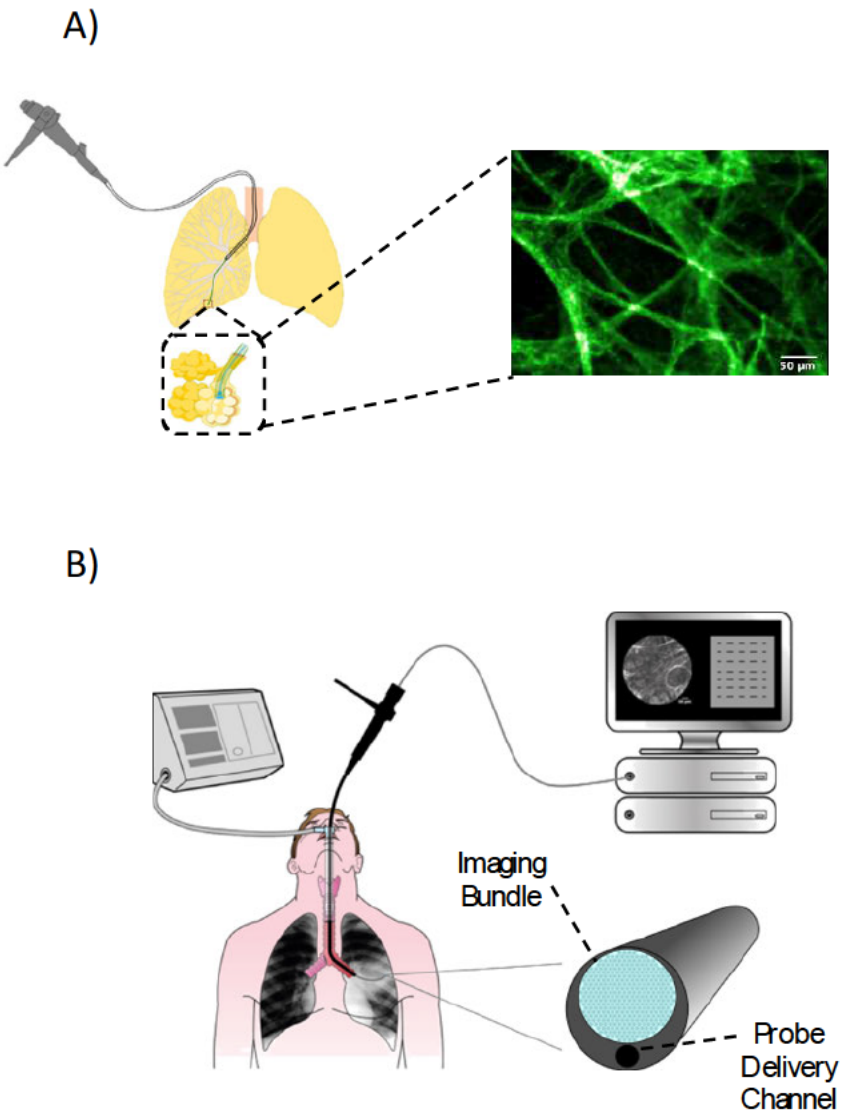

Figure 1.4 Development of optical endimicroscopy (OEM) imaging platforms to image the alveolar space. A) OEM platforms are capable of accessing regions beyond what is capable of standard bronchoscopy. It is possible to use imaging fibres small enough to reach the alveolar space and perform fluorescence-based imaging, visualising autofluorescent structures such as elastin and collagen componants of lung tissue. B) OEM platforms can be coupled to bespoke imaging fibres that can provide a probe delivery channel as well as imaging bundles. This provides scope to directly administer fluorescent imaging probes to multiplex OEM imaging in the alveolar space.

1.4.3 Optical Probes for imaging macrophages

As with other forms of molecular imaging, OEM can be aligned with compatible probes to enhance the specificity and sensitivity of imaging, as well as tracking of dynamic biological events. These probes typically consist of a ligand with a specific affinity for a molecular target, conjugated to a fluorescent reporter [133]. The application of clinically translatable optical probes together with OEM has been demonstrated previously by using antimicrobial peptides conjugated to fluorescent reporters to label bacteria and activated neutrophils in lung tissue [134,135,136].

The probes must be able to function suitably in the dynamic environment of human tissue and amplify their signal to be detected by optical imaging systems [111]. Background noise can be an issue for detecting fluorescent molecular probes, which can be exacerbated by unbound probes contributing to the poor signal to noise ratio [111].

The ligand of optical probes can be specific to a target cell; this is often achieved via targeting surface receptors that are uniquely expressed by specific cell populations. The use of optical probes to label macrophages has been considered as expression of receptors on the surface of macrophages can indicate their activation state and activity. Targeting these receptors for optical labelling may provide phenotypic information about a macrophage in addition to labelling the cell. One example of this involves targeting the folate receptor [137]. This receptor is used for the uptake of folic acid, an essential nutrient for amino acid synthesis.[138] Cells increasing their metabolic rate upregulate the folate receptor, likely to increase folate uptake to support the glycolytic pathway [139]. Increased activity of the folate receptor beta isoform has been reported on the surface of macrophages following stimulation with LPS, a common pathogen associated molecular pattern (PAMP) [137]. In one study, an optical probe for folate receptor – via fluorescently conjugated folic acid - was developed for targeting macrophage populations that may be associated with pro-

inflammatory activity and contributing to acute lung inflammation [137]. Another study sought to use a fluorescent folic acid conjugate to target inflammatory macrophages, while simultaneously using a fluorescent mannose conjugate (targeting the mannose receptor) to target anti-inflammatory macrophages [140]. They used an *in vitro* infection model to demonstrate multiplexing of these optical probes to stratify the phenotypic changes in macrophages post-stimulation [140].

Development of other macrophage-targeting probes have involved tracking the activity of the cell. For example, a library of probes was synthesised with specific cleavage sites for Hydrogen peroxide (H_2O_2), a common ROS produced by macrophages [141]. The chemical cleavage by H_2O_2 on the probe changes the electron transfer properties, resulting in fluorophore emission. This is an example of a "smartprobe": probes that dynamically change their fluorescent properties upon interaction with their target. The benefit of using smartprobes is their signal is only amplified when interacting with a target [142]. Background noise can be an issue for detecting fluorescent molecular probes, which can be exacerbated by unbound probes contributing to the noise [111]. The use of smartprobes can mitigate this issue [142]. Novel smartprobes have also been synthesised to track the phagocytic activity of macrophages. For example, one study developed a pH-sensitive fluorophore scaffold that could be selectively internalised by macrophages [143]. Emission of fluorescence by the probe coincides with a drop in pH, an indication of phagolysosome maturation [144].

The development of fluorescent probes to target macrophages carry a lot of potential to couple these imaging agents with OEM systems that can take forward their macrophage targeting to *in situ* settings. One study has already used a smart fluorophore to detect myeloperoxidase activity in macrophages of rat models of acute lung injury [145]. There is however limited use of combining fluorescent probes for macrophages with OEM systems. With increased efforts to marry the two, the potential for profiling macrophages *in situ* rises inexorably. To have a library of

probes that can track the activity or phenotypic state of macrophages – in the alveolar space or in other tissues – would be a powerful tool in experimental medicine.

1.5 Hypotheses and Aims

The introduction to this thesis provides an overview of key elements of inflammation, with a particular focus on the activity of alveolar macrophages and how aberrant function is implicated in lung diseases. While there is an active field of research studying how to effectively profile alveolar macrophages and therapeutically modulate their activity, there still remains a limited understanding of how AMs function *in situ,* and whether therapeutic drugs work as effectively *in situ* as they do using *in vitro* methodologies.

In light of this, the aims of my research have been to establish novel ways of profiling macrophages that could be performed in the alveolar space. The overarching hypothesis has been that surface receptor probes and optical endomicroscopy imaging systems can be used to profile alveolar macrophages *in situ.*

The work in chapter three of this thesis will cover the establishment of a cell culture model to differentiate monocytes into macrophages, as well as assays to profile the cell surface receptor phenotype and phagocytic activity.

Chapter four introduces a novel fluorescent nanobody designed to selectively label macrophages via the mannose receptor. Studies in this chapter include biological characterisation of the nanobody: cell and target specificity and labelling characteristics.

The use of fibre based optical endomicroscopy imaging platforms to profile the phagocytic activity of monocyte-derived macrophages and autofluorescent alveolar macrophages is described in chapter five.

Chapter Two: Materials and Methods

2.1 Materials

Gibco Life Technologies (UK)			
Phosphate Buffered Saline (PBS), 14190-94	PBS (10x), 70011-044	Iscoves Modified Dulbecco's Media (IMDM), 12440-053	IMDM, no phenol red, 21056023
0.9% Sodium Chloride (NaCl), UKF7124	Hanks Balanced Salt Solution (HBSS), 14025092	Percoll, 17-0891	Dextran T500, 5510 0500 8007
Dulbecco's Modified Eagle Medium (DMEM), 12491-015			

Sigma Aldrich (now Merck) (MA, USA)			
Cytochalasin D, C8273	Fetal Bovine Serum (FBS, F0804	L-glutamine, G7513	Trypsin-EDTA, 59418C
Dimethyl Sulfoxide (DMSO), 472301	Bovine Serum Albumin (BSA), 05470	Penicillin Streptomycin, P4458	Human AB Serum, H4522
Lipopolysaccharides from *Escherichia coli, L2630*	Sulforaphane,, S4441	Dexamethasone, D4902	

Thermofisher (MA, USA)			
pHrodo Green STP Ester, P35369	pHrodo Green *Escherichia coli* Bioparticles, P35366	T-75 Cell Culture Flask, 130190	Cell Tracker Green CMFDA, C2925
SYTO™ 82 Orange Fluorescent Nucleic Acid Stain, S11363	SYTO™ 64 Red Fluorescent Nucleic Acid Stain, S11346	Lipofectamine 3000 Reagent, L3000001	Opti-MEM™ Reduced Serum Medium, 31985062

Biolegend (CA, USA)			
PE anti human CD11b antibody, 301305	PE anti human HLA-DR antibody, 307605	PE anti human CD80 antibody, 104707	PE anti human CD163 antibody, 333605
PE anti human CD206 antibody, 321105	PE anti human IgG1 isotope control antibody, 403503		

R and D Sytems (MN, USA)			
Recombinant Human IL-4 Protein, 204-IL-010	Recombinant Human interferon gamma Protein, 285-IF-100		

Other			
8-Well Lab-Tek II Confocal Chambers (VWR, PA, USA), Z734853	NucleoCassette Cell Viability Counter (Chemometec, Allerod, Denmark), 9410002	Human Pan Monocyte Isolation Kit (Miltenyi Biotec)	Reastain Quick-Diff Red and Blue (Centaur (Kampenhout, Belgium)
Fuse-It-Color Red (Ibidi, UK), 60200	Fluoresbrite® YG Microspheres 1.00µm (Polysciences, Germany), 17154	Mannose Receptor (MRC1) (NM_002438) Human Untagged Clone (Origene, Germany), SC303200	

2.2 Ethics

The phlebotomy of healthy volunteers was approved by the Lothian Local Research Ethics committee AMREC Reference number 15-HV-013 Volunteers gave full informed consent to participate. Bronchoalveolar lavage samples were collected following guidelines of the Edinburgh BioResource (PI Kev Dhaliwal)

2.3 Leukocyte Isolation and Culture

2.3.1 Isolation of human leukocytes

Peripheral blood leukocytes were isolated from healthy donor whole blood following the methods previously described [146]. Venous blood was collected from healthy donors, following consent, and mixed with Sodium Citrate (3.8%) in a 50 ml falcon tube. Following gentle inversion, the falcon tubes were centrifuged at 350g for 20 min (0 brake) to separate out the platelet-rich plasma. The plasma layer was removed following centrifugation and mixed with Calcium Chloride to extract platelets. The remaining layer of blood was mixed with Dextran (6%) and diluted with 0.9% sodium chloride (NaCl) solution to the top of a 50 ml falcon tube. Dextran stock was previously prepared using sterile dextran powder (Sigma-Aldrich, UK)

solubilised in 0.9% Baxter's saline. The Falcon tube was gently inverted before allowing sedimentation to occur (25 min). Following sedimentation, the top layer of blood was aspirated into a fresh 50 ml falcon tube and again topped up to 50ml with NaCl, before being centrifuged at 350g for 6 min (brake 9, acceleration 9). Pelleted cells from centrifugation is then resuspended in 3 ml of 55% Percoll solution (diluted in HBSS). A discontinuous Percoll gradiant was set up of 55%, 68%, and 81% Percoll with DPBS. 3 ml of 81% Percoll was added to a 15 ml Falcon tube, followed by 3 ml of 68% Percoll gently layered on top dropwise to avoid mixing. The Leukocytes suspended in 55% Percoll were subsequently layered on top in the same fashion, before being centrifuged at 350g for 20 min (0 brake). Centrifugation allowed remaining erythrocytes to pellet at the bottom of the tube, while a suspended band of polymorphonuclear cells collected at the 81/68% Percoll interface and a suspended band of mononuclear cells collected at the 68/55% interface. Isolated cell populations were removed using a Pasteur pipette. The cell populations were counted using an NC-100 Nucleocounter Automatic Cell Counter (Chemometec, Denmark). The abundance of individual leukocyte populations in each isolated fraction was assessed using a BD FACSCalibur flow cytometer (Becton Dickinson NJ, USA) based on cellular side scatter for granularity and forward scatter for size. Cytospin slides were prepared of the cell populations to examine cell morphology and cell-type distribution. 2 x 10^5 cells were centrifuged onto glass slides using a Cytospin 2 centrifuge at 300 g for 3 min. The cell smear was left to air dry then stained with DIFF Quick Red and Blue to stain cytoplasm and nuclei, respectively.

2.3.2 Monocyte purification

Peripheral blood monocytes were isolated from the mononuclear cell fraction described above by using a MACS pan-monocyte separation kit (Miltenyi Biotec, Germany). The mononuclear layer was suspended in PBS and placed on ice for 20 min, before being centrifuged at 350 g for 5 min (acceleration 9, brake 9) and all the media removed. The pelleted cells were resuspended in DPBS at a rate of 30 µl for every 10^6 cells. 10µl of Fc-blocking reagent was added for every 10^6 cells, as well as 10 µl antibody cocktail at the same rate. This mixture was placed on ice for 5 min. Another 30 µl of DPBS was added per 10^6 cells, plus 20 µl of magnetic microbead solution at the same rate. The mixture was placed on ice for 10 min. The cell mixture was passed through a MACS LS column, attached to a MACS separator that created a magnetic field around the column. During cell mixture flow through of the column, non-monocytes labelled by the antibody cocktail (and subsequently labelled with anti-biotin microbeads) bound to the sides of the column, allowing unbound monocytes to be collected in a tube below the column. The collected population was counted again using a Nucleocounter and the scatter properties assessed using flow cytometry.

2.3.3 Monocyte-derived macrophage culture

A purified monocyte population was suspended in IMDM (pre-heated to 37 ºC) at a concentration of 6 x10^5 cells per ml. 500 µl of the cell mixture was added to individual wells of a 48 well polystyrene tissue culture plate, or LabTek 8-well confocal chamber, and incubated at 37 ºC for 1hr to allow adherence to the bottom of the wells. The wells were aspirated and the IMDM replaced with culture media containing: 500 µl IMDM (+5% autologous serum, +1% Penicillin/Streptomycin) per well. The adherent cells were incubated at 37 ºC, 5% CO_2 for 6 days to allow for differentiation to monocyte-derived macrophages.

2.3.4 Macrophage stimulation and pharmacological treatment

The use of macrophage stimulation during culture and the stimulants used is highlighted in figures of future chapters. Interferon-gamma (IFN) was used at a final concentration of 10 ng/ml and added for the final 24 hr of cell culture. Lipopolysaccharide (LPS) was used at a final concentration of 20ng/ml for the final 24 hr of culture. Interleukin-4 (IL-4) was used at a final concentration of 10ng/ml for the final 24 hr of culture. Dexamethasone was used at a final concentration of 250 nM and added at day 0 of the MDM culture. Sulforaphane was used at a final concentration of 10 μM and added for the final 18 hr of culture.

2.3.5 Macrophage receptor phenotyping

Isolated mononuclear cell, monocyte or differentiated MDM populations were seeded on 96-well round bottomed tissue culture plates and pelleted by centrifugation at 2000 rpm for 2 mins at 4 °C. Cells were kept on ice for the duration of the assay. The media was removed and 10 μl of rabbit serum was added for 5 mins. Antibodies included: PE-CD11b, PE-HLA-DR, PE-CD80, PE-CD163, PE-CD206, PE-isotype control (BD Pharminigen; all mouse IgG1 κ anti-human). Antibodies were diluted 1:20 from stock concentration in flow buffer (PBS + 0.5% bovine serum albumin (BSA). 50 μl of diluted antibodies was added for 20 min on ice, away from light. 100 μl of flow buffer was added and the plate was again pelleted to remove buffer. Pelleted cells were then suspended in 200 μl flow buffer and analysed using a BD FACSCalibur. Cell populations were gated on FSC/SSC and analysed for FL2+ (488nm laser excitation filtered through a 585nm dichroic bandpass filter) . PE isotype control was used to define FL2 negative events. Samples were collected in duplicate. For analysis performed using an Attune NxT flow cytometer, cell populations were also gated using FSC/SSC and analysed for staining using the YL1 channel (561nm laser excitation filtered through a 585nm dichroic bandpass filter). Cell positivity for labelling was defined above isotype control labelling signal.

2.4 Phagocytic Assays

2.4.1 Phagocytosis of polystyrene beads

1 µm polystyrene microspheres (polysciences, Switzerland) were diluted in cell culture media described above or fresh IMDM and sonicated for 5 min. The final concentration used is outlined in specific figures in chapter three. The MDM culture media was aspirated and replaced with the microsphere suspension ± 5 µg/ml Cytochalasin D. The culture plate was incubated at 37 °C, 5% CO_2 for 45 min to allow for phagocytic interaction. Following co-culture, cells were detached by incubating with Trypsin+EDTA for 5 min at 37 °C followed by pipette mixing. Cell populations were analysed using a BD FACSCalibur. Macrophages were gated on using FSC/SSC scatter properties before being analysed for FL1+ (488 nm laser excitation filtered through a 530nm dichroic bandpass filter) for microsphere signal. Up to 5000 gated events were collected with samples recorded in duplicate.

2.4.2 Phagocytosis of bacteria

pHrodo Green E. Coli Bioparticles were suspended in DPBS and diluted in cell culture media or fresh IMDM. The final concentrations used in experiments are indicated in figure legends of the results. The phagocytic assay setup is as described in section 2.4.1. Following detachment post co-culture, the cell populations were analysed using Attune NxT flow cytometer. Macrophages were gated on using FSC/SSC scatter properties and doublets excluded from analysis. The gated population was analysed for BL2+ (488 nm laser excitation filtered through a 590nm dichroic bandpass filter) for pHrodo signal. Up to 5000 gated events were collected with samples recorded in duplicate.

2.4.3 Efferocytosis of apoptotic neutrophils

Peripheral blood polymorphonuclear cells (PMN) were isolated as described in section 2.3.1, then cultured in a T-25 tissue culture flask at a density of $5x10^7$/ml in IMDM (+2% autologous serum, 1% Penicillin-Streptomycin) for 20 hr to induce apoptosis. This method of inducing apoptosis has been established previously to yield an apoptotic population of ~70% [7]. The apoptotic Neutrophils were labelled with 1 µg/ml CellTracker Green 5-chloromethylfluorescein diacetate (CMFDA) for 30 mins at 37 ºC, then washed and suspended in cell culture media or fresh IMDM. The final concentration of neutrophils for each was meant six neutrophils to one macrophage per condition. The phagocytic assay setup is as described in section 2.4.1. The analysis of the cell population was either carried out using a BD FACSCalibur, as described in section 2.4.1, or using an Attune NxT, as described in section 2.4.2.

2.4.4 Phagocytosis assay gating strategy

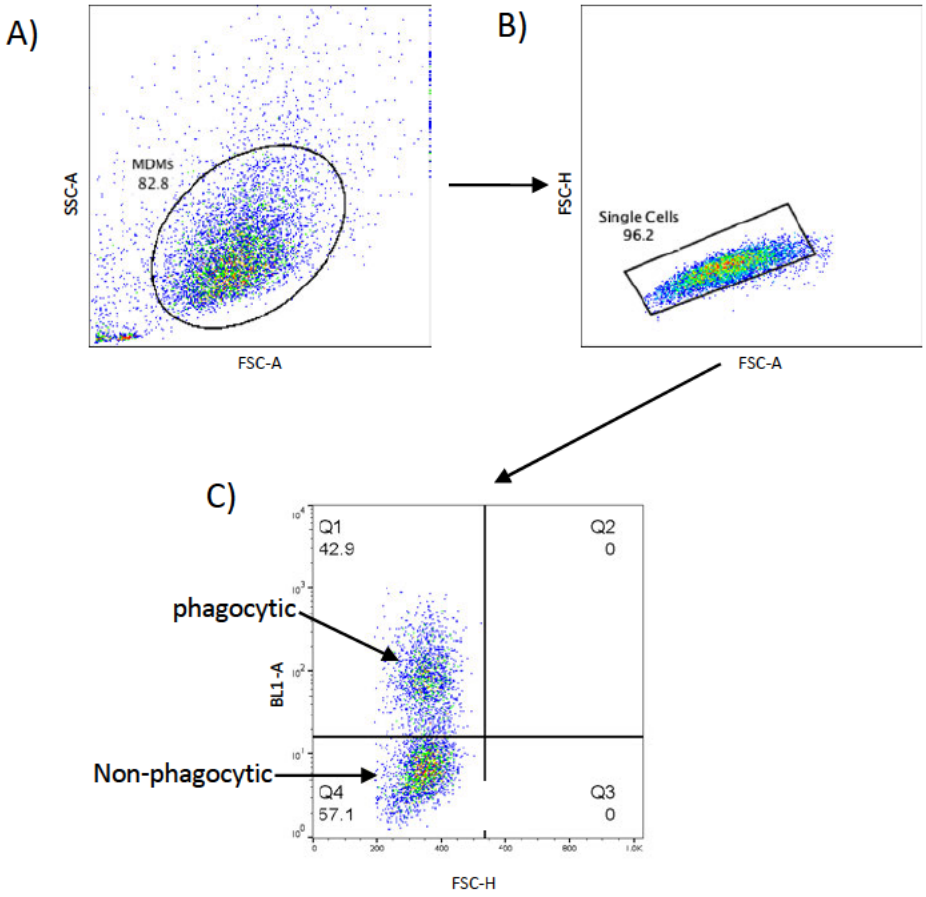

Figure 2.1 Phagocytosis assay gating strategy. Monocyte derived macrophages were gated from unbound targets and debris using forward and side scatter characteristics (A). Single cells were gated on using forward scatter signal area and height characteristics to eliminate doublets and clumps of cells (B). The percentage uptake of phagocytic targets was determined through plotting target fluorescence signal channel against forward scatter of the gated macrophage population (C). Plot C) shows identification of phagocytic and non-phagocytic macrophages as a percentage of the total population

2.4.5 Real-time confocal microscopy of efferocytosis

An MDM/apoptotic neutrophil co-culture was performed as described in section 2.4.3, but in a LabTek II confocal chamber as described previously and imaged using a laser-scanning confocal microscope (LSM 510, Carl Zeiss). Apoptotic neutrophils were labelled with Cell Tracker Green (as described above). Images were taken using a 63x oil objective. Fluorescence of green labelled neutrophils was captured by

exciting with a 488 nm laser. A time-series was performed with 180 frames at 15 sec intervals (45 min total).

2.4.6 Real-time spinning-disc confocal microscopy of efferocytosis

Macrophages were labelled with Fuse-it-Color Red membrane dye (Ibidi, UK) according to manufacturer's instructions and excited using a 561 nm laser. Apoptotic neutrophils were labelled with 1µg/ml pHrodo Green STP Ester for 30 mins at RT. The pHrodo fluorescence was excited with a 488 nm laser. Fuse-it Color fluorescence was excited with a 561 nm laser. The camera EM gain and exposure time were kept the same throughout the imaging. The imaging was performed in a heated chamber that was maintained at 37 ºC +5% CO_2. A time-series was performed in 3 fields of view (FOV) with 15 frames taken at 3 min intervals (45 mins total). For each timeframe a Z stack of 95 optical planes over 32 µm was taken.

2.5 Cell Line Culture

A549 (pulmonary adenocarcinoma cell line, ATCC, CCL185) cells and Chinese Hamster Ovary (epithelial-like cell line) cells were provided by Brian Mchugh (University of Edinburgh) were cultured in DMEM, +10% fetal bovine serum (FBS), +2mM L-glutamine, +1% Penicillin/Streptomycin, in T75 tissue culture flasks or 8 well Lab-Tek II Confocal Chambers. Cell proliferation was monitored using an inverted light microscope until the population was ~75% confluent. At confluency, cells were washed with pre-warmed DPBS and detached using 2ml of Trypsin- EDTA at 37 ºC for 5 min. The detached cells were either diluted into fresh culture media in a T75 tissue culture flask or used for experiments.

2.6 MR-Nanobody Characterisation

2.6.1 Probe synthesis

MMR-Nanobody synthesis was performed by Gavin Birch (Bradley Group, University of Edinburgh) as a collaborator on this project. The nanobody structure was originally obtained from Vrije Universiteit Brussel, in collaboration with Edinburgh Molecular Imaging. The protein sequence was published in the European patent EP2855526B1. The following fluorophore conjugation method has been provided and used with permission by Gavin Birch: Fluorophore labelling of this protein was carried out through mild conditions with the N-hydroxysuccinimidyl (NHS) ester reactive dye which, upon reaction with a lysine, would form an amide bond between the protein and fluorophore. The fluorophore used was a sulfonated Cy5 dye. To purify the labelled protein from residual dye both PD-10 gel filtration and spin centrifugation (Amicon spin concentrators) were used.

2.6.2 Stock concentrations and spectral reads

The stock concentration of the probe was validated using a fluorescent spectrophotometer exciting at 630 nm. Concentration was interpolated from fluorescent intensity from a standard curve of known sulphonated Cyanine 5 dye concentrations.

2.6.3 Confocal imaging for cell-type specificity

Peripheral blood monocytes were isolated as described in section 2.3.2 and adhered to wells of Lab-Tek II Confocal Chambers for 45 min in IMDM media. MDMs were cultured on the surface of the confocal chambers as described in section 2.3.3. Human polymorphonuclear cells were isolated as described in section 2.3.1 and adhered to the bottom of Lab-Tek II Confocal Chambers that had been previously coated with Fibronectin to aid adherence. A549 cells were cultured on the confocal

chambers as described in section 2.5. Between 100,000 and 200,000 cells were used per well. Monocytes and MDMs were counterstained with 1 µM of Cell Tracker Green CMFDA dye for 10 min at 37 ºC then washed with fresh IMDM. The MMR-nanobody was diluted to 50 nM final concentration in IMDM media (+5% autologous serum) and 500 µl was added per well. The MMR-nanobody was incubated with cells for 20 min before being analysed using a confocal laser-scanning microscope (CLSM). CLSM systems used for this assay were Leica Sp5 and Leica Sp8, using 40x oil or 63x oil immersion lens. A 488 nm Argon laser and emitted light detected with meta detector (500-530nm) was used to excite Cell Tracker Green if used in the assay. For MMR-Nanobody excitation, a 633 nm HeNe laser was used and emitted light detected with meta detector (660-750nm). with a pixel dwell time of 4 µs with a pinhole diameter corresponding to 1 Airy unit. Fields of view were chosen using Cell Tracker Green channel or brightfield.

2.6.4 Flow cytometric analysis of cell-type specificity

Monocytes and MDMs were adhered to the bottom of 48 well tissue culture plates. The cell media was aspirated and replaced with 500 µl of IMDM (+5% autologous serum) with 50 nM of MMR-nanobody and incubated at 37 ºC for 20 min. The nanobody-containing media was aspirated, and cells were detached using Trypsin-EDTA at 37 ºC for 5 min before being analysed using a BD FACS Calibur or Attune NxT flow cytometer. During flow cytometric analysis, voltages remained constant throughout the experiment and data was collected on a logarithmic scale, collecting 5,000 events. Samples were run in duplicate. Post-experiment analysis was performed using FlowJo version 10.6. FSC/SSC characteristics were used to gate on cells and eliminate debris. The MMR-nanobody signal was excited using the FL4 channel of a BD FACS Calibur or the RL1 channel of Attune NxT flow cytometer. For quantification, the geometric mean of the MMR-nanobody signal was used, with data presented as mean fluorescent units (MFU) from independent experiments.

2.6.5 Labelling bronchoalveolar lavage cells

Bronchoalveolar lavage cells were isolated by first passing through a 70 µm cell strainer to exclude large debris. The cell population was centrifuged at 300 g for 5 min to pellet cells, and subsequently resuspended in IMDM. The cells were counted using a Nucleocounter and a cytospin was used to determine cell morphology. Cells were adhered to 8 well LabTek Confocal chambers for 1 hr at 37 ºC, at 100,000 cells per well. Following adherence the media was aspirated and replaced with IMDM (+5% human AB serum) with 50 nM MMR-nanobody and left to incubate at 37 ºC for 20 min. Confocal imaging was carried out as described in section 2.6.3.

2.6.6 Mannan blocking

Dry Mannan from *Saccharomyces cerevisiae* was acquired from Sigma Aldrich and solubilised in PBS. Solubilised mannan was used at a final concentration of 2 mg/ml together with 50 nM of MMR-nanobody when labelling MDMs. The effect of mannan was assessed using flow cytometric analysis as described in section 2.6.4.

2.6.7 Transfection of MRC1 into CHO cells

Adherent CHO cells were grown on 6 well tissue culture flasks in DMEM without antibiotics until 90% confluent. An MRC1 expression plasmid coding for a human mannose receptor was obtained from Origene (Germany, SC303200), using a pCMV6 tag-free Entry vector. The dry plasmid was solubilised in 100 µl of sterile H20. 50 µl of plasmid DNA solution was diluted in 50 µl of Opti-MEM reduced Serum Medium (Thermofisher, 31985062) and gently mixed. 2 µl of Lipofectamine 3000 (Thermofisher) was diluted in 50 µl od Opti-MEM medium and mixed gently, before incubated at RT for 5 min. The DNA and Lipofectamine mixtures were combined and incubated at RT for 20 min. 100 µl of Lipofectamine-plasmid mixture was added to individual wells of confluent cells. A lipofectamine-only control was added to

separate wells. The plate was incubated for 48 hr at 37 ºC 5% CO_2 before being assessed for transgene expression using flow cytometry. Flow cytometric analysis followed the same protocol described in sections 2.3.5 and 2.6.4, using a PE anti-CD206 mAb and an isotype control to determine mannose receptor expression, and 50 nM of MR-Nanobody to determine labelling.

2.6.8 Spinning-disc confocal microscopy of probe localisation and labelling kinetics

MDMs were cultured on wells of an 8 well LabTek confocal chamber. For probe localisation assays, the cells were labelled with 1 µM of Cell Tracker Green CMFDA for 10 min at 37 ºC +5% CO_2. The media was aspirated and replaced with IMDM (+5% autologous serum) with a final concentration of 50 nM MMR-Nanobody. The cells were incubated for 20 min at 37 ºC +5% CO_2 before being analysed on an SDCM. Cell Tracker Green fluorescence was excited with a 488 nm laser, while MMR-nanobody fluorescence was excited with a 640 nm laser. The camera EM gain and exposure times were kept the same for each channel throughout imaging. For each image a Z stack of 135 optical planes over 31 µm was taken. For imaging kinetics assays, the same labelling steps applied, though prior to imaging, the MDM media was aspirated and replaced with 25 µl fresh IMDM to cover the surface of the well and taken to SDCM for imaging. A time-series was taken at 30 sec intervals for 15 min. Following the first timeframe, 500 µl of 50 nM MMR-nanobody was added to the well as subsequent timeframes captured the labelling kinetics.

2.6.9 Image analysis of spinning-disc confocal data

Using the green 488 nm channel on Imaris (Bitplane, Switzerland) image analysis programme, a region of interest (ROI) was drawn in a 3D space around an individual macrophage labelled with Cell Tracker Green. A 3D isosurface was created from the

green signal within the ROI (surface detail of 2µm, thresholding on absolute intensity to cover the entire cell). Touching objects (cells, debris) were split using the region growing tool (seed point diameter 12 µm) and seed points manually classified as the centre of the macrophage in the ROI. An isosurface was generated from this seed point based on a voxel number threshold that recognised the whole macrophage cell surface. This semi-automated algorithm was subsequently applied to the whole FOV to create isosurface of all cells. Cells touching the edge of the FOV were eliminated from analysis. The intensity mean of the 640 nm (MR-nanobody signal) channel was quantified in each isosurface (macrophage cell mask).

2.7 Optical Endomicroscopy of Macrophage Phagocytosis

2.7.1 Phagocytosis imaging assay using a widefield OEM system

MDMs were cultured on wells of polystyrene 48 well tissue culture plates. They were labelled with 1 µM Syto 82 far-red nucleic acid stain for 10 min at 37 ºC +5% CO_2. Apoptotic neutrophils were labelled with 1 µg/ml of pHrodo Green STP Ester for 30 min at RT before being pelleted and resuspended in IMDM +5% autologous serum. MDM media was aspirated and replaced with apoptotic neutrophils at a ratio of six neutrophils per macrophage in each well (each well contained 300,000 macrophages and 1,800,000 neutrophils). This co-culture was incubated for 45 min at 37 ºC +5% CO_2 before imaging with a widefield OEM system. The imaging system comprised of three LED excitation sources, as described previously [130]. A 470 nm LED was used to excite pHrodo Green fluorescence. A 625 nm LED was used to excite Syto 82 fluorescence. Images were captured with a 25 ms exposure time. An Alveoflex (Mauna Kea Technologies) commercial imaging fibre bundle was used to direct excited light onto the tissue culture plate. The imaging fibre had a zero working distance, meaning the fibre had to be physically touching the cell culture to perform imaging. Emitted light from the tissue culture plates returned back up the imaging

fibre and detecting using a monochromatic camera connected to a computer. Recordings of the tissue culture plate in real time was 10 frames per second.

2.7.2 Emission spectroscopy of primary human alveolar macrophages and lung tissue

A commercial spectrometer (VIS-NIR-ES, Ocean Optics) was coupled to an Alveoflex imaging fibre. Primary human alveolar macrophages were isolated from bronchoalveolar lavage samples as described in section 2.6.5. Human lung tissue was acquired from the Edinburgh BioResource. Isolated AMs and lung tissue were adhered to tissue culture plates and the spectra captured by touching the imaging fibre against the well (for adhered cells) or directly onto lung tissue.

2.7.3 Spectral Ratio Imaging system setup

The SR imaging system described in this thesis was built by Helen Parker, University of Edinburgh, who collaborated on this work by supplying the system and helping with imaging acquisition of samples. The following is a description of the SR system which has been adapted with permission from Helen Parker and has been previously published [147].

A 470 nm LED excitation source was directed through a standard epi-fluorescence arrangement of excitation filter and dichroic (FITC-Ex01-Clin-25, Semrock). The excitation light was then coupled to a bespoke fibre imaging bundle described previously [148]. The emitted fluorescence from the target propagated through the fibre and, after passing through the epi-fluorescence dichroic and emission filter, was split into two optical paths according to a cut-off wavelength defined by the dichroic mirror. An optical chopper was installed into the long wavelength path. The two paths were recombined using another dichroic mirror and focused onto a

monochromatic CMOS camera (GS3-U3-23S6M-C Grasshopper, Point Grey, Canada). A PC operated a triggering unit to synchronise the chopper rotation with camera acquisition. This ensured that the sequential full wavelength and short wavelength images were taken at 50 ms exposure time. From this, we derived a short wavelength channel (< 605 nm) and a long wavelength channel (> 605 nm) whilst acquiring images at 10 fps video rate.

2.7.4 Spectral Ratio phagocytosis imaging

MDMs were cultured on the wells of 48 well tissue culture plates. In assays where the MDMs were labelled, 1 µM of Syto 81 Orange nucleic acid stain was used to label the cells for 20 min at 37 ºC +5% CO_2. Targets used for the SR assays were either apoptotic neutrophils, labelled with pHrodo Green STP as described in section 2.4.6, or pHrodo Green E. Coli Bioparticles, prepared as described in section 2.4.2. Macrophages were co-cultured with a target population for 45 min at 37º C +5% CO_2. Following incubation the co-culture plate was imaged using the SR system coupled to a bespoke imaging fibre bundle described in section 2.7.3 and published previously [148].

2.8 Statistical analysis

All experiments were performed twice or three times and is outlined in figure legends. Paired data columns (from crlls of the same culture) were evaluated using a paired Student's t test with GraphPad Prism version 8.00 for Mac OS (GraphPad Software, San Diego, USA). A P value less than 0.05 was considered significant.

Chapter Three: Characterising an in vitro Model of Human Macrophage Phenotype and Activity

3.1 Introduction

The study of macrophage phenotype – such as the receptors they express, cytokines they produce and their morphology - is an important avenue to improving our understanding of how tissues maintain inflammatory homeostasis [149]. Macrophages play an integral role in maintaining this homeostasis: whether mounting an inflammatory response to invading pathogens or switching activity to resolve an immune response that is no longer required [150,151]. If this niche role for macrophages

to orchestrate inflammatory homeostasis becomes perturbed, the consequence is often the manifestation of a range of inflammatory diseases [152,75].

In order to improve our knowledge of how macrophages carry out their functions of orchestrating inflammatory responses, model systems are required to interrogate macrophages in detail [153,154]. This is due limited avenues available to profile these cells *in situ.* Systems capable of capturing dynamic cell functions such as phagocytosis inside the human body have not yet been established. Model systems can be used to observe the plasticity of macrophage phenotype in different inflammatory environments - including their receptor expression and downstream signalling - to how they specifically interact with phagocytic targets [154]. Model systems used for these purposes have been developed to carry out this interrogation in a controlled, *in vitro* setting. These have taken the form of immortal cell lines from the monocyte lineage, such as THP-1 cells, U937, and RAW cells [155,156,157]. These cell lines allow for rapid expansion of readily available monocyte-like populations that can be differentiated under defined experimental conditions into macrophages. An alternative *in vitro* model is of isolating peripheral blood monocytes from whole blood and culturing them *in vitro* in the presence of serum and other stimulants to differentiate and adopt a mature macrophage phenotype [158]. Each approach can have advantages and drawbacks over the other. While freshly isolated monocyte differentiation may offer a more biologically relevant macrophage model, there can be ethical and logistical barriers to consistently use this approach [154]. Working with healthy human cells requires the setup of a blood retrieval resources that allows for collection of samples that is ethically regulated. Freshly isolated human cells also have a limited lifespan that requires multiple donations for repeated experiments. Cells lines are more readily available, with a more homogenous genetic background [159]. However, this genetic homogeneity may yield results that are less biologically relevant or difficult to replicate in more complex biological systems. There is a growing evidence base behind how any given macrophage population can be highly heterogenous, therefore the effects of potential therapies that target macrophages

in disease could generate inconclusive results depending on how representative a model population is [160,55]. Indeed, previous work has shown functional differences between cell line models and MDM models, such as phagocytic activity [154]. If these functions are relevant to the area of macrophage biology in a particular study, then choice of model becomes an important factor.

Ascertaining which cell-surface receptors are present on macrophages under specific conditions carry therapeutic and diagnostic applications. Characterising these markers can aid in targeting macrophages, either for pharmaceutical delivery or simply to aid in potential approaches in experimental medicine to profile macrophages [161,22]. Often these markers are cell-surface receptors, for which targeting ligands can be generated. However, the receptor expression phenotype on model cell lines, such as THP-1, can differ significantly from blood-derived macrophages, which may skew the conclusions made about the relationship between certain receptors and a cell phenotype [162]. The expression profile of a given receptor could also vary significantly between *in vivo* macrophage populations something that is difficult to replicate in some models [163].

In addition to the establishment of *in vitro systems* to study macrophage biology, assays also need to be in place to interrogate their phenotype (receptor expression, cytokine production) and how they perform certain activities such as phagocytosis. The process of macrophage phagocytosis is typically examined using *in vitro* methodology [164,165]. It is also possible that primary macrophages can be acquired directly from tissue (or from a broncho-alveolar lavage in the case of acquiring alveolar macrophages for *ex vivo* experiments) [166]. Phagocytic targets can be cultured bacteria (live, fixed, or killed), human cells and immortal cell lines induced to undergo apoptosis, or inert non-physiological particles [167]. The targets are often labelled in some way to track their internalisation into a macrophage. Following incubation with labelled targets, macrophages that acquire the target's label can be identified using optical systems such as flow cytometry or imaged with microscopy

to confirm internalisation [168,169]. The use of flow cytometry in this context can provide accurate quantification of phagocytosis by macrophages on a single-cell basis.

Macrophages can serve as therapeutic targets to alter their function and rebalance immune systems homeostasis. Efforts to modulate macrophage receptor expression, cytokine production and phagocytic activity have been established through *in vitro* methodology, which opens up further avenues to modulate their phenotype *in vivo* in a disease setting [160,55]. A common example of pharmacological manipulation of macrophages to promote the resolution of inflammation is the use of synthetic glucocorticoids, which can be potent anti-inflammatory agents, down-regulating a number of inflammatory processes (such as a reduction in IL-1, IL-6 and TNF, and IFN production) in macrophages and instead promoting resolution mechanisms such as clearance of apoptotic material [170,171].

In vitro assay systems have also been used to confirm the phagocytic dysfunction of macrophages in disease states that are associated with poor pathogen clearance. For example, AMs acquired from patients with COPD have shown reduced capacity to phagocytose apoptotic human cells and different strains of bacteria associated with COPD [77,76]. As restoring phagocytic function to AMs may reduce exacerbations in COPD, these *in vitro* assays have been used to assess the restorative effects of compounds on AM phagocytosis. One example is sulforaphane: a naturally occurring compound extracted from broccoli [172]. Sulforaphane is an agonist for the transcription factor Nrf2, promoting anti-oxidant gene transcription and ultimately a microbicidal phenotype [173,100]. Pre-clinical use of sulforaphane has shown to improve the bacterial clearance by AMs of COPD patient macrophages [100].

The aims of the following chapter were to:

• Set up an *in vitro* cell culture model of differentiating human peripheral blood monocytes into macrophages

• Use the monocyte-derived macrophages to establish assays profiling the phagocytic activity of macrophages with different biologically relevant targets, as well as tracking their response to pharmacological stimulation

3.2 An *in vitro* Model of Human Monocyte-Derived Macrophages

As the overarching goal of this thesis was to explore novel approaches to profiling macrophages, a suitable *in vitro* cell model was required to carry out my investigations into macrophage phenotype and activity. I identified blood-derived monocytes differentiated into macrophages as the most suitable, as I anticipated they would closer reflect how macrophages would present *in vitro*. Peripheral blood mononuclear cells (PBMC) were isolated from the whole blood of healthy human volunteers. The flow scatter plot shown in Figure 3.1B shows that the scatter characteristics (which provide broad information on the size and granularity of cells) of the PBMC layer represent the majority being lymphocytes, with fewer than 20% being monocytes. In order to further enrich the monocyte population, I used an immunomagnetic cell separation procedure employing negative selection. A biotinylated antibody cocktail was used to label all non-monocytes present in the PBMC population, followed by binding of anti-biotin-labelled magnetic microbeads. The cells were passed through a magnetic separation column to negatively select for monocytes. Figure 3.1D shows that, following this magnetic separation, the purity of the monocyte population was greater than 80%, with a small minority of lymphocytes remaining. An accompanying cell cytospin shown in Figure 3.1C showed the morphology of the of cells following magnetic separation are representative of monocytes, based on a typical cell diameter of over 15 µm and a lobular "horseshoe" nuclear shape [174].

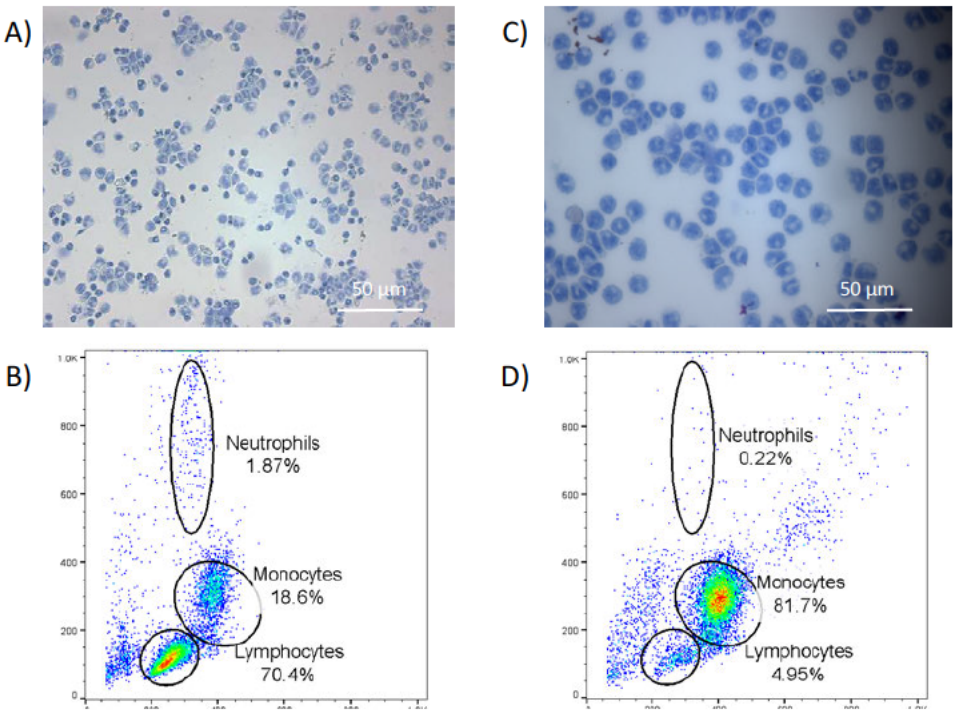

Figure 3.1 The purification of human monocytes from whole blood. Mononuclear cells were isolated from whole blood via dextran sedimentation followed by separation centrifugation across a Percoll gradient. A) Cytospin image of isolated mononuclear cell population. B) Mononuclear cell fraction laser scatter properties when assessed on flowcytometry. Monocytes were isolated further from the mononuclear cell fraction via magnetic bead negative selection. C) Cell cytospin image of isolated monocytes. D) Isolated monocyte population laser scatter properties. The relative proportion of cell types was analysed using the laser scatter properties when analysed with a BD FACS Calibur. Representative cytospins and flow plots of three independent experiments.

The process for differentiating the monocyte population into macrophages involved culturing in IMDM media, containing 5% autologous serum from the donor. This protocol followed a culture method previously published for the differentiation of human monocytes to macrophages [175]. Monocytes isolated by negative immunomagnetic selection were first adhered to the bottom of either tissue culture plate wells or glass coverslip confocal chambers before being cultured *in vitro* at 37 ºC (+5% CO_2) for 6 days. The cell phenotype (morphology and receptor expression) following this 6-day culture was assessed to confirm the cells had differentiated into monocyte-derived macrophages (MDM). Figure 3.2B shows that the cell morphology at day 6 of the culture was more characteristic of macrophages, with a larger cell size and cytoplasmic ratio [176]. In addition to these morphological changes, the cell-surface receptor expression changed following the culture. A panel of monoclonal antibodies (mAb) recognising different cell-surface receptors was

chosen in order to distinguish monocytes and macrophages. The rationale behind the choice for each mAb is outlined in Table 3.1. Flow cytometric analysis of the expression pattern of the different cell-surface receptors showed that that common markers for monocytes and macrophages, such as CD11b and HLA-DR, were expressed on freshly isolated monocytes and monocytes cultured for 6 days *in vitro* (Figure 3.2A). However, cells post-culture showed significantly higher expression of more macrophage-specific markers, such as CD80, CD163, and CD206 (Figure 3.2C). This data suggests that the monocyte-derived macrophages (MDM) represented a suitable *in vitro* model for further investigation of the function of human macrophages.

Phenotypic Marker	Function	Expression		
		Monocytes	Macrophages	
			Pro-inflammatory	Pro-resolution
CD11b	Regulator of leukocyte adhesion and migration during an inflammatory response	+	++	+
HLA-DR	Presents peptide antigens to elicit T cell responses	+	++	+
CD80	A co-stimulatory molecule to prime and elicit T cell activation and survival	-	+++	+
CD206	Binds and assists in endocytosis of microbial carbohydrates and endogenous protein	-	+	+++
CD163	Binds to the hemoglobin-haptoglobin complex during the clearance of hemoglobin and cytokine production	-	+	+++

Table 3.1 Receptor expression panel for validating monocyte differentiation into mature macrophages. The table outlines each receptor in the panel and its associated function. The expression of the receptor across monocytes and macrophages in different activated states is also shown.

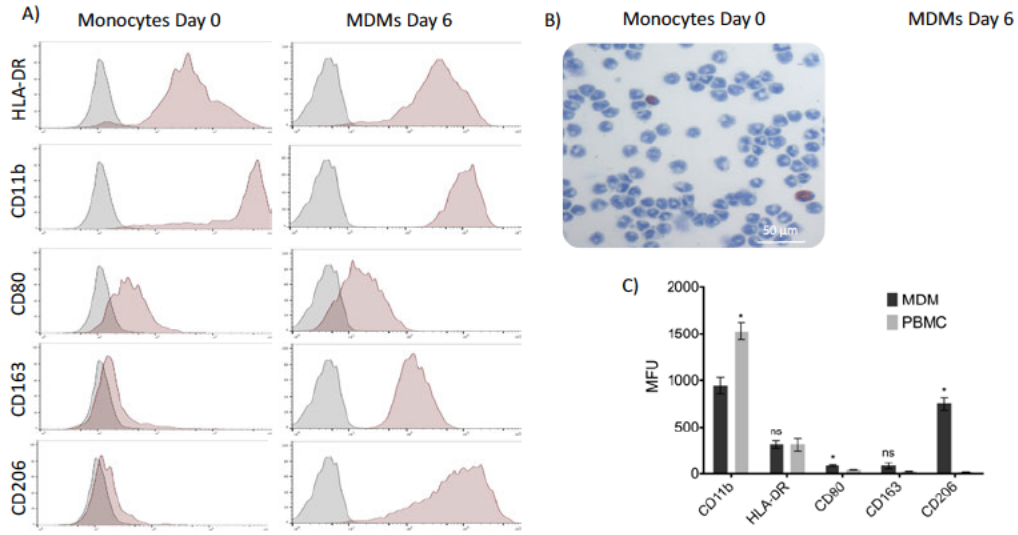

Figure 3.2 Monocyte differentiation into mature macrophages. Freshly isolated human monocytes were plated in media with 5% autologous serum and cultured for six days. A) The differentiation into mature macrophages was assessed by probing for known cell-surface receptors for monocytes and macrophages and the morphology of the cells during culture. B) Morphology of the cells before and after differentiation C) Receptor expression was quantified as mean fluorescence units. Graph shows ±SEM n=3. Analysis between cells for each receptor was made using a paired t test. *= P≤0.05

3.2.1 Typical polarising agents alter cell-surface marker expression on monocyte-derived macrophages

The effect of standard polarising agents on the maturation and differentiation of monocytes was assessed to show that the *in vitro* macrophage phenotype can be dynamic, as expected is the case in macrophage populations. For the final 24 hr of the MDM differentiation process, the cells were treated with a combination of interferon-gamma (IFN) (10 ng/ml) and lipopolysaccharide (LPS) (20 ng/ml) – to yield a pro-inflammatory phenotype – or were treated with interleukin-4 (IL-4) (10 ng/ml), to yield a pro-resolving phenotype. The effect of these polarising agents on cell phenotype was assessed using the same cell-surface receptor panel shown in Figure 3.2. Figure 3.3B shows that CD80, a co-stimulatory molecule expressed more on pro-inflammatory macrophages, was significantly increased following treatment with IFN and LPS [55]. On the other hand, IL-4 treatment significantly increased the expression of CD163, a scavenging receptor associated with pro-resolving

macrophages (Figure 3.3B) [55]. These data demonstrate that MDMs exhibit dynamic phenotypic plasticity when treated with cytokine polarising agents.

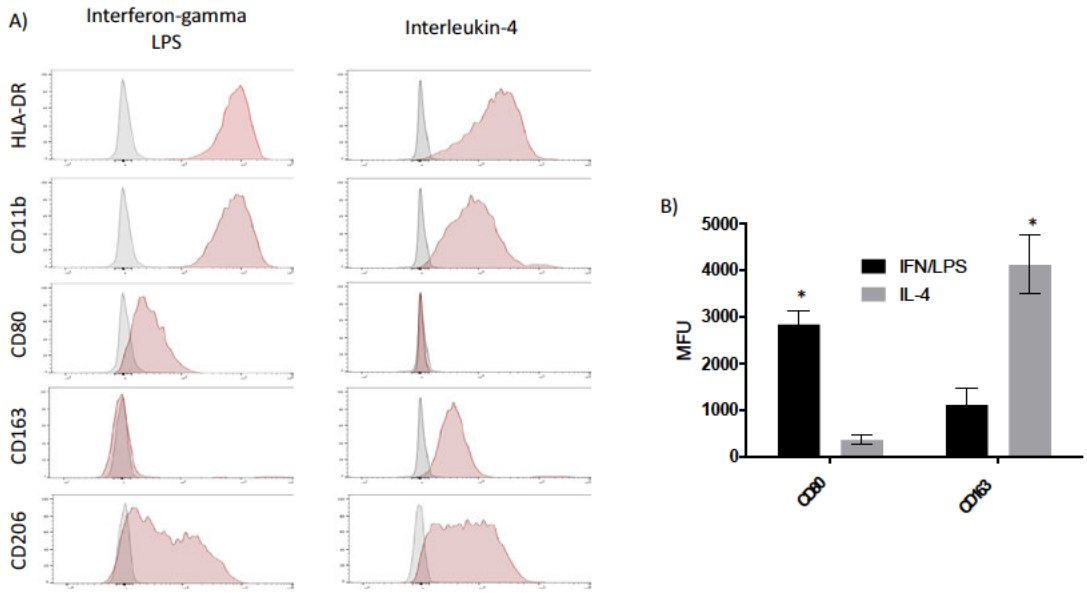

Figure 3.3 The effect of polarising agents on monocyte-derived macrophage receptor expression. Monocyte-derived macrophages were stimulated with either 10 ng/ml interferon-gamma and 20 ng/ml of LPS, or with 10 ng/ml of interleukin-4 for 24 hr. A) The effect these agents had on cell phenotype was assessed by probing for known cell-surface receptors. B) Graph shows receptor expressions that were significantly differed between MDMs of different polarising stimuli. Expression was quantified as mean fluorescence units, ±SEM n=3. Analysis between cells for each receptor was made using a paired t test. *= P≤0.05

3.3 Characterising the phagocytic activity of MDM with biologically relevant targets

3.3.1 Polystyrene microspheres as a phagocytic target causes issues with false-positive phagocytic signal and poor validation with a negative control

The phagocytic capacity of the MDMs was characterised using a flow cytometric-based assay described and characterised in previous studies [164,168]. The assay first used 1 µm polystyrene microspheres labelled with carboxyfluorescein (FAM) as a target. Microspheres can represent inert particles that macrophages are required to clear, particularly alveolar macrophages which encounter inhaled particulates in the lung [177]. To profile phagocytosis, the MDMs were first incubated with different concentrations of microspheres for a 45 min period before being analysed on a flow cytometer. When analysed, the amount of FAM signal from the microspheres in the gated macrophage population was used as a quantifiable measure of phagocytosis. Figure 3.4 shows different microsphere to macrophage ratios and the phagocytic signal shown from each. For each ratio there is a clear subset of macrophages negative for the microsphere fluorescence that can be indicative of non-phagocytic cells. Increasing the microsphere to cell ratio increases the target signal in the macrophage population following the 45 min incubation. Figure 3.4 also shows the amount of microsphere signal in the gated macrophages at 0 min, when no contact time between cell and target had been allowed to take place. This shows the amount of 'coincidence' signal generated for each microsphere to macrophage ratio when analysed by flow cytometry. Any microsphere positive signal at this time point is assumed to represent a false-positive for phagocytosis. This coincidence effect increases in line with the microsphere to macrophage ratio.

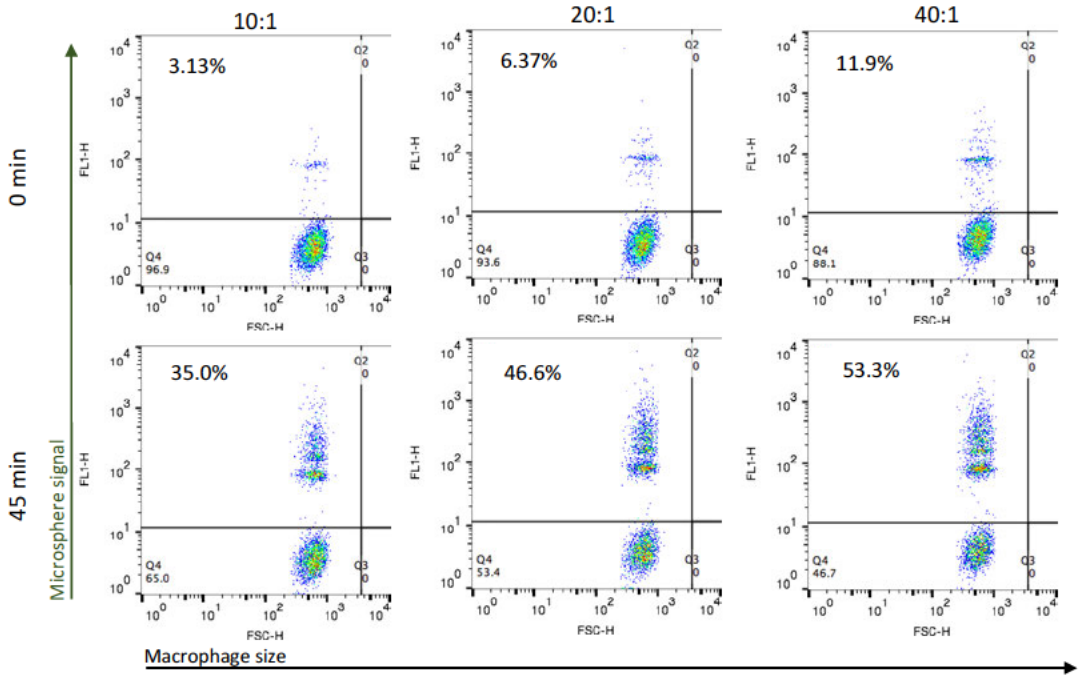

Figure 3.4. The effect of varying polystyrene microsphere to MDM ratios on quantification of phagocytosis. Monocyte-derived macrophages and different concentrations of 1 µm FAM-labelled microspheres were incubated together for 45 min. FAM-microsphere labelled cells were then were then analysed on a BD FACS Calibur, with phagocytosis measured as a percentage of FAM signal in gated macrophages. The microsphere and cell suspensions were analysed at 0 min for each ratio to assess false-positive signal. Representative flow plots from three independent experiments.

To validate that the fluorescent signal associated with MDM was due to phagocytosis of FAM microscpheres, cytochalasin D was used to block polymerisation of actin, a process that is required for phagocytosis [178]. Figure 3.5 shows that Cytochalasin D had no significant impact on the quantification of microsphere phagocytosis.

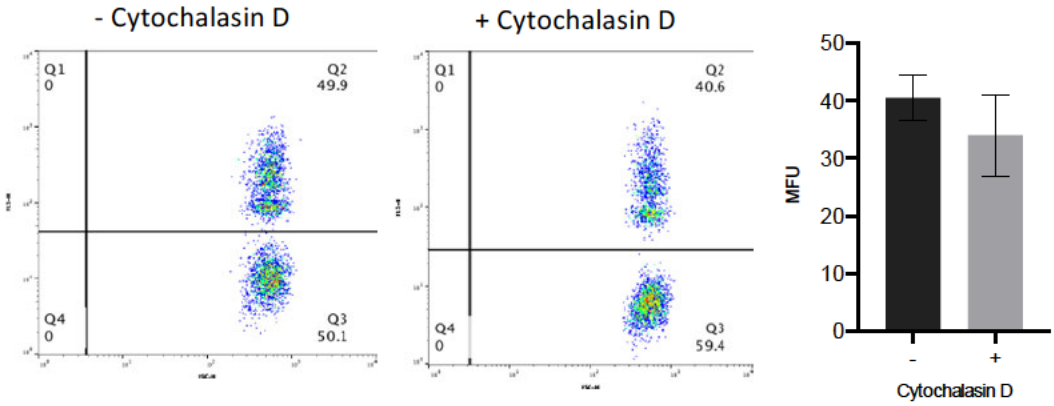

Figure 3.5 The effect of Cytochalasin D as a negative control for macrophage phagocytosis of polystyrene microspheres. Monocyte derived macrophages were incubated with 1 µm FAM-labelled microspheres, at a ratio of 20:1, for 45 min. Microsphere labelled cells were then were then analysed on a BD FACS Calibur, with phagocytosis measured as a percentage of FAM signal in gated macrophages. Cytochalasin D was used as a negative control to validate the assay as a quantifiable measurement of microsphere phagocytosis. Flow cytometry plots are representative of three independent experiments. Graph shows quantification of phagocytosis as the percentage of gated MDM events that were FAM+, +/- cytochalasin D ±SEM n=3.

Corresponding fluorescent microscopy images of MDMs incubated with FAM shown in Figure 3.6 also demonstrate the difficulty of discerning whether or not a microsphere had been internalised by a macrophage, with or without Cytochalasin D being present.

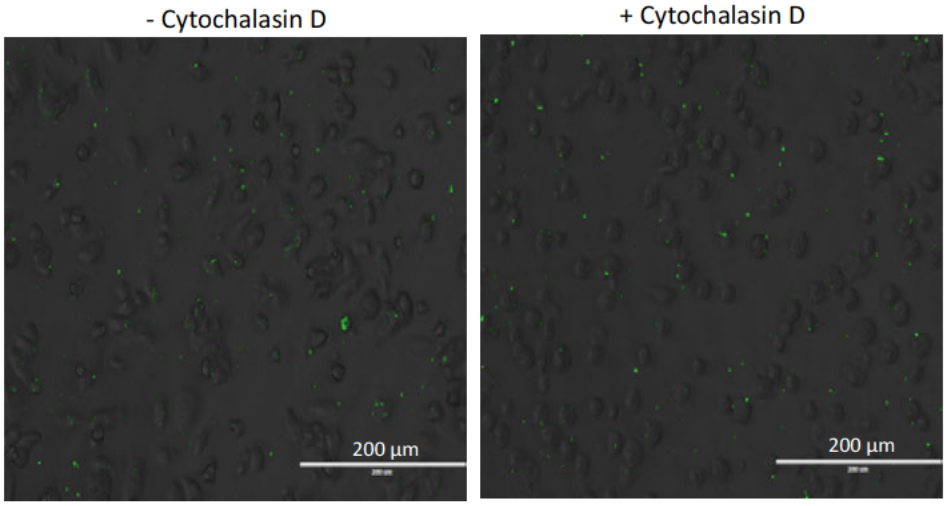

Figure 3.6 The effect of Cytochalasin D as a negative control for imaging macrophage phagocytosis of polystyrene microspheres. Monocyte-derived macrophages were incubated with 1 µm FAM-labelled microspheres, at a ratio of 20:1, for 45 min. Cytochalasin D was used as a negative control to prevent phagocytosis. Images following incubation were taken with an EVOS fluorescent microscope. Images are representative of two independent experiments.

3.3.2 Using bacteria and apoptotic neutrophils align well as biological targets for different types of macrophage phagocytosis

As a more relevant alternative to the use of microspheres, other fluorescently labelled biological targets were considered for the flow cytometric-based profiling of macrophage phagocytosis. The first was fixed *Escherichia coli* (E. coli) labelled with a pHrodo Green ester (Thermofisher). pHrodo is a pH-activated dye that is in a fluorescently quenched state until in an acidic environment. Thus, fluorescence is greatly increased by the emitted dye when a bacterium had entered an acidic environment, such as a mature phagolysosome following phagocytosis [179]. Labelled bacteria were incubated with mature MDMs for 45 min before flow cytometric analysis. The 45 min time-point was chosen to observe more responsive phagocytic activity. Figure 3.7 shows that the labelled bacteria offer a quantifiable measure of phagocytosis in a macrophage population. Cytochalasin D significantly reduced the pHrodo Green signal in the gated macrophage population, supporting the assumption that pHrodo positive signal was a result of phagocytosis (Figure 3.7).

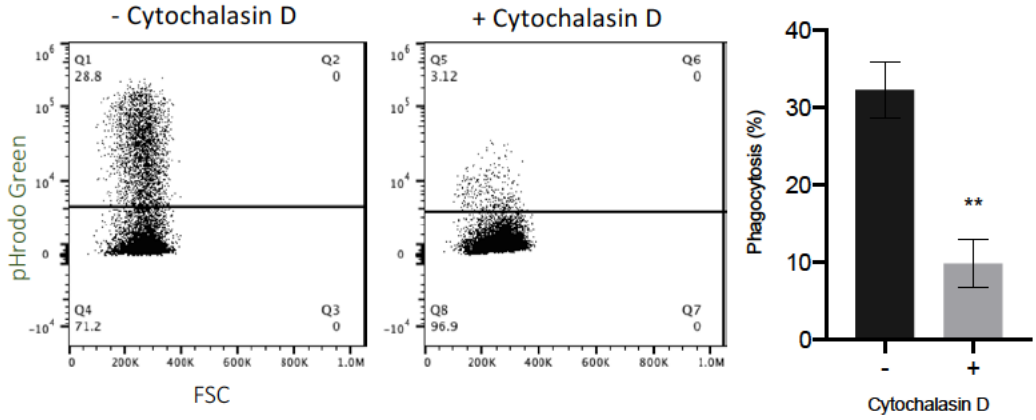

Figure 3.7 Quantifying phagocytosis of bacteria by monocyte-derived macrophages. Monocyte-derived macrophages were incubated with 10 µg/ml of pHrodo Green *E. Coli* Bioparticles. The macrophage population was gated on by size and scatter, then analysed for pHrodo signal as a marker for phagocytosing pHrodo-labelled *E. Coli*. Graph shows quantification of phagocytosis as the percentage of gated macrophage events that were pHrodo+, +/- cytochalasin D ±SEM n=3. Comparison between groups performed with paired t test. **= P≤0.01

Figure 3.8 shows complementary images to this assay, albeit using double concentration of pHrodo-labelled E. coli. The images show the punctate pHrodo

signal within macrophages, which is absent in the presence of Cytochalasin D (Figure 3.8).

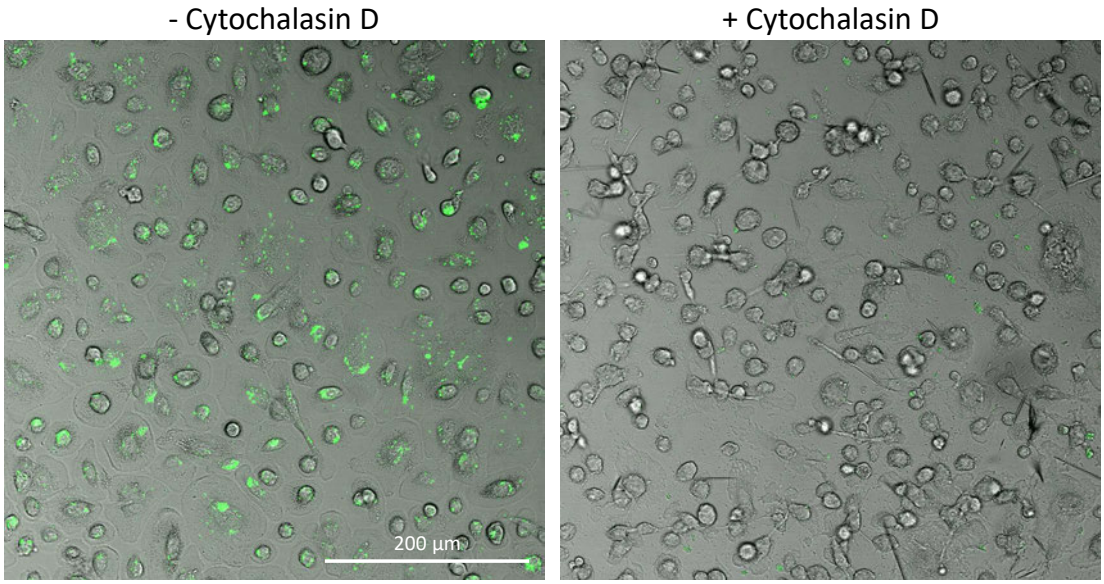

Figure 3.8 The effect of Cytochalasin D as a negative control for imaging macrophage phagocytosis of bacteria. Monocyte-derived macrophages were incubated with *E. Coli* labelled with 20 µg/ml pHrodo Green for 45 min. Cytochalasin D was used as a negative control to prevent phagocytosis. Images following incubation were taken with a CLSM. Images are representative of two independent experiments.

Another biologically relevant target used to profile macrophage phagocytosis was human apoptotic neutrophils, to be used as a relevant target for efferocytosis, a distinct mechanism of internalisation used by macrophages. Human blood neutrophils were cultured for 20 hr to induce apoptosis. While not producing a completely homogenous apoptotic population, this method has been previously used to induce <50% apoptosis in a neutrophil population [171]. The apoptotic neutrophils were then labelled with chloromethyl fluorescein diacetate (CMFDA) cell dye and incubated with mature MDMs at a ratio of 6 neutrophils to one macrophage, following previously established methodology [168]. After co-incubation with apoptotic targets, macrophages (and bound apoptotic cells) were detached with trypsin/EDTA for 5 min at 37 ºC and then analysed by flow cytometry. Two distinct populations of macrophages could be distinguished in terms of levels of fluorescence (Figure 3.9). These corresponded to CMFDA-negative (non-phagocytic) and a CMFDA-positive (phagocytic) MDMs, respectively. Importantly,

using Cytochalasin D to inhibit cytoskeletal activity significantly reduced the CMFDA-positive subset of macrophages, suggesting this population corresponds to phagocytic MDMs (Figure 3.9).

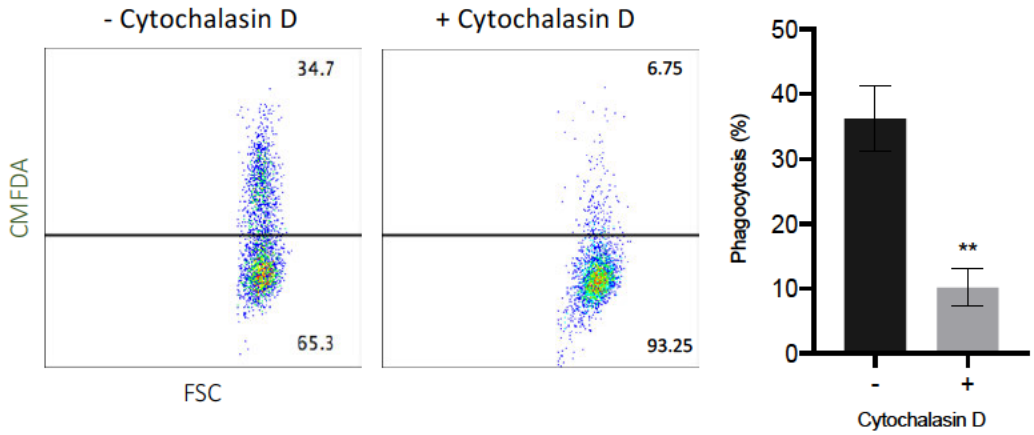

Figure 3.9 Quantifying human monocyte-derived macrophage efferocytosis of apoptotic neutrophils. Monocyte-derived macrophages were incubated for 45 min with apoptotic neutrophils, aged for 20 hr and labelled with chloromethylfluorescein diacetate, at a ratio of 6 neutrophils to 1 macrophage. The gated macrophage was analysed for CMFDA signal as a marker for phagocytosing CMFDA labelled apoptotic neutrophils. Graph shows quantification of phagocytosis as the percentage of gated MDM events that were CMFDA+, +/- cytochalasin D ±SEM n=4. Comparison between groups analysed with paired t test. **= P≤0.01

As neutrophils were the largest (and therefore most easily identifiable) target used in this assay system, an imaging time-series was taken using confocal microscopy to track neutrophil internalisation into a macrophage and capture efferocytosis in real-time. The purpose of this experiment was to gain further understanding of the kinetics of efferocytosis taking place. This could be a useful parameter to understand the different phagocytic activities in health and disease, as well as the effect pharmacological modulators may have on cell activity. The time series was started immediately after adding CMFDA-labelled neutrophils to adherent MDMs. Figure 3.10 shows snapshots of a cropped image during the 45 min time-lapse of two macrophages interacting with neutrophils. The series showed the membrane ruffling of macrophages upon recognition of neutrophils and internalisation of a target (outlined by arrows in Figure 3.10 pointing at neutrophils being internalised).

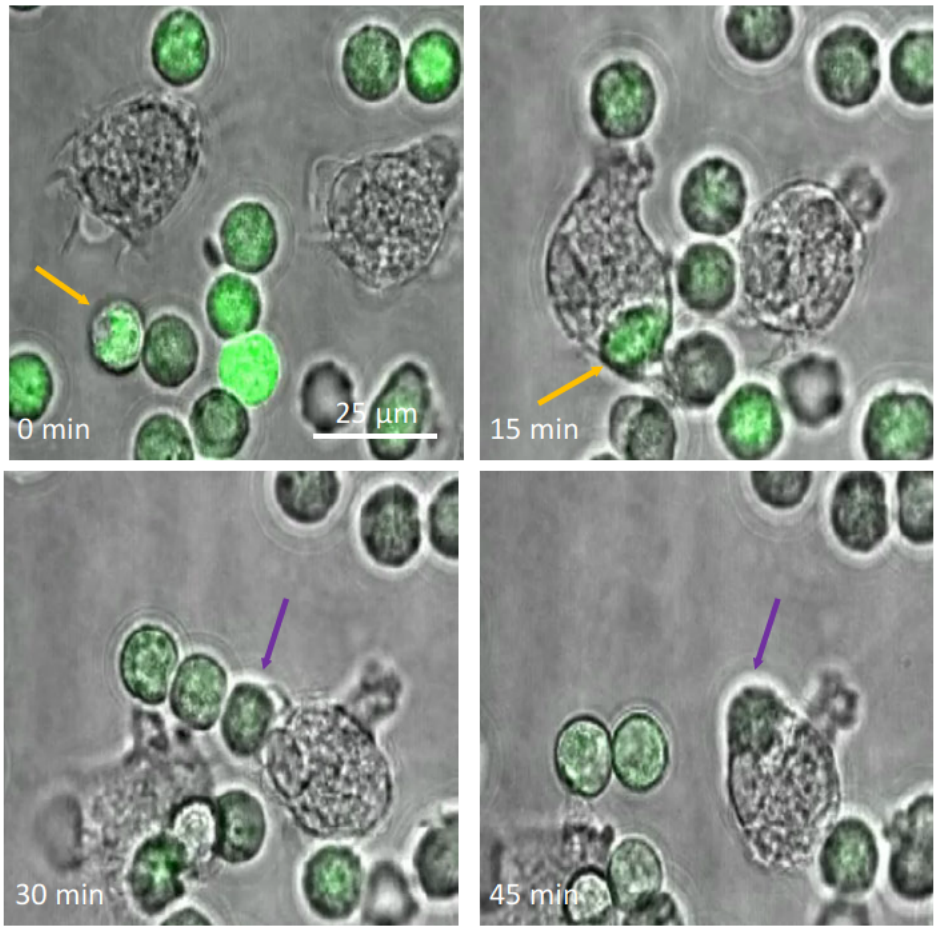

Figure 3.10 Imaging macrophage efferocytosis in real time. A 45 min time-series taken using a CLSM with unlabelled macrophages and apoptotic neutrophils labelled with chloromethylfluorescein diacetate. Coloured arrows highlight specific neutrophils over time that appear to become internalised over the course of the time series. Snapshots of the time-lapse are representative of three independent experiments.

The initial imaging of macrophages phagocytosing neutrophils in real-time revealed drawbacks with the assay setup for live imaging. First, the use of CMFDA-labelled neutrophils at a 6:1 ratio resulted in a field of view that was crowded with fluorescent neutrophil targets. Second, the internalisation of neutrophils by macrophages could be considered to be a subjective observation. This assay was further optimised by labelling apoptotic neutrophils with pHrodo Green STP ester instead. The reason for this is to minimise the fluorescence of unbound targets in the field of view. By using pHrodo Green to label neutrophils, only cells that have been successfully internalised would fluoresce, due to the pH sensitivity of the fluorophore. Figure 3.11 shows an image sequence where pHrodo-labelled neutrophils were incubated with MDM. The

snapshots show an image cropped to a representative macrophage, which is labelled with a red membrane stain. Over time, there is emergence of pHrodo green signal, indicative of the macrophage having internalised a neutrophil and pHrodo fluorescence emitting once inside an acidic phagolysosome (Figure 3.11).

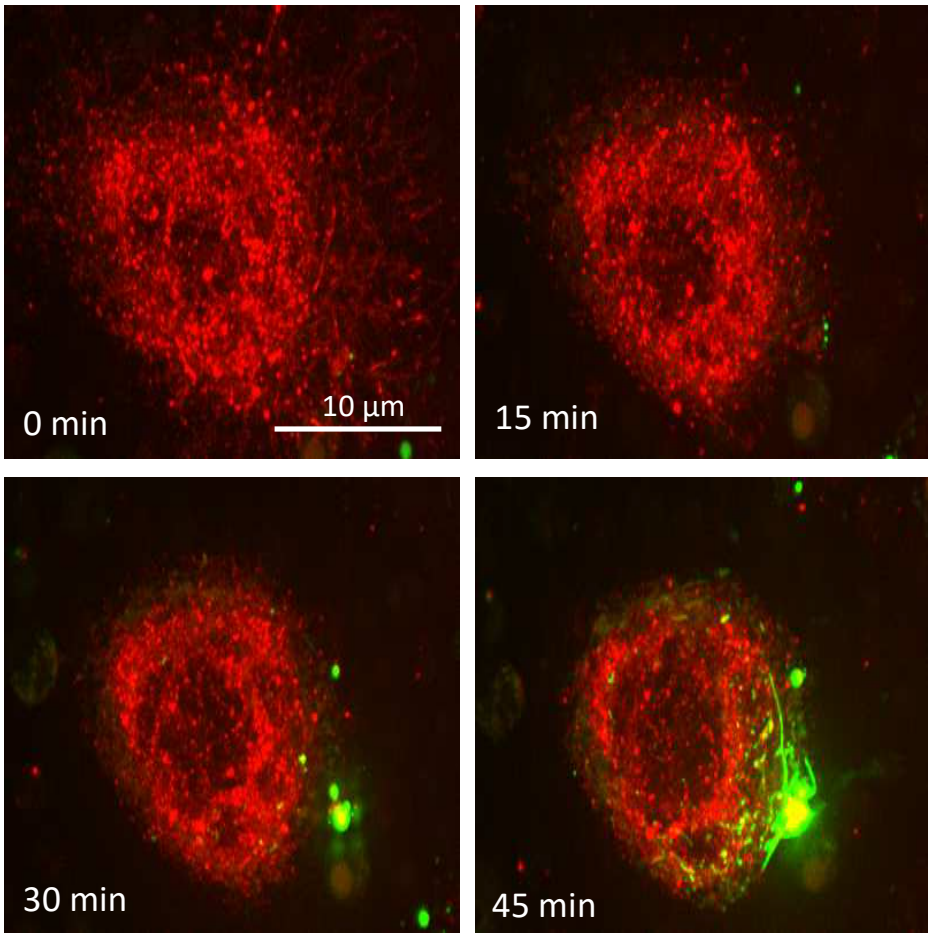

Figure 3.11 Optimising the real-time imaging of macrophage. A 45 min time-series was taken using a SDCM. The snapshots show an image cropped to a macrophage labelled with fuse-it color Red membrane stain incubated with apoptotic neutrophils labelled with pHrodo Green STP ester. The snapshots show the development of pHrodo signal around the macrophage over time. Snapshots of the time-lapse are representative of two independent experiments.

3.3.3 Using flow cytometry to investigate the effect of pharmaceutical manipulation on phagocytic function

Having established assays for quantification of macrophage phagocytosis, I next examined the use of pharmaceutical modulators to macrophage activity. This was to confirm that this *in vitro* assay can effectively quantify the changes to macrophage activity. The glucocorticoid dexamethasone (Dex) was first used to augment efferocytosis in MDMs. Dex is well established as a modulator of macrophage phenotype, driving them to a more pro-resolving state, which includes an increased capacity to clear apoptotic cells [164]. Freshly isolated monocytes were treated with Dex from day 0 of their *in vitro* culture into macrophages. Figure 3.12A shows that, following culture with Dex, the morphology of the MDMs are distinguishable from an untreated population. The Dex-treated cells are smaller in size with a more homogenous, rounded shape (Figure 3.12A). This morphology is a well-defined characteristic appearance of Dex-induced MDM differentiation. The efferocytosis assay outlined in Figure 3.9 was then repeated with the Dex-treated cells. Dex significantly increased internalisation of apoptotic neutrophils by the Dex-treated MDM population confirming augmentation of efferocytic activity in macrophages (Figure 3.12B).

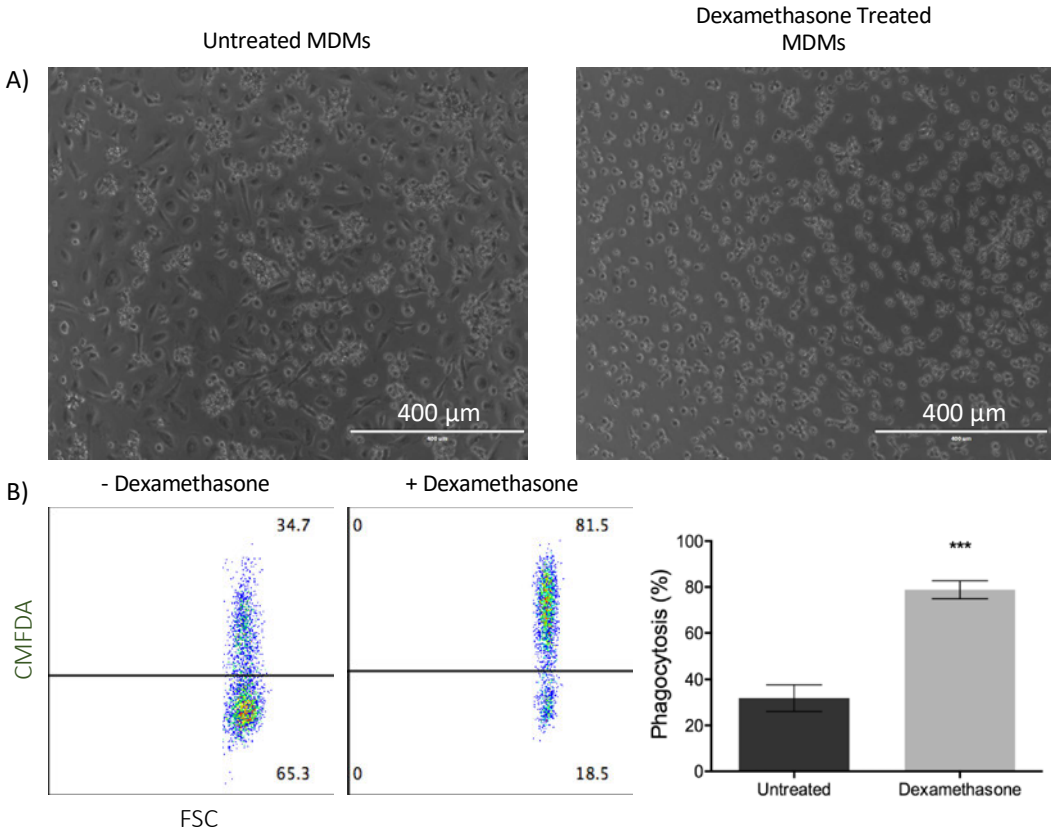

Figure 3.12 Quantifying the effect of dexamethasone on monocyte-derived macrophage efferocytosis. Peripheral blood monocytes were differentiated into macrophages over a 6 day culture, +/- 500 nM dexamethasone from day 0. A) The comparison in morphology of untreated and Dex-treated macrophages, using brightfield images taken with an EVOS fluorescent microscope. B) Flow cytometric analysis of efferocytosis of apoptotic neutrophils, labelled with CMFDA, by macrophages in different Dex treatment conditions. Graph shows the quantification of efferocytosis as the percentage of gated MDM events that were CMFDA+, +/- Dexamethasone ±SEM n=5. Comparison between groups performed with paired t test. ***= P≤0.001

The effect of another known modulator of phagocytic activity, Sulforaphane, was also assessed. Sulforaphane is a compound that acts as an agonist for the transcription factor Nrf2 [101]. The stimulation of Nrf2 has shown to be instrumental in the microbicidal processes that occur in macrophages [100]. Mature human MDMs were treated with sulforaphane for 18 hr prior to performing the same phagocytosis assay shown in Figure 3.7. There was no significant effect by sulforaphane to modulate the macrophage response to clearing E. coli bacteria (Figure 3.13). This suggests that, at least for healthy *in vitro* MDMs, the augmenting effect of sulforaphane on microbial clearance was not achievable.

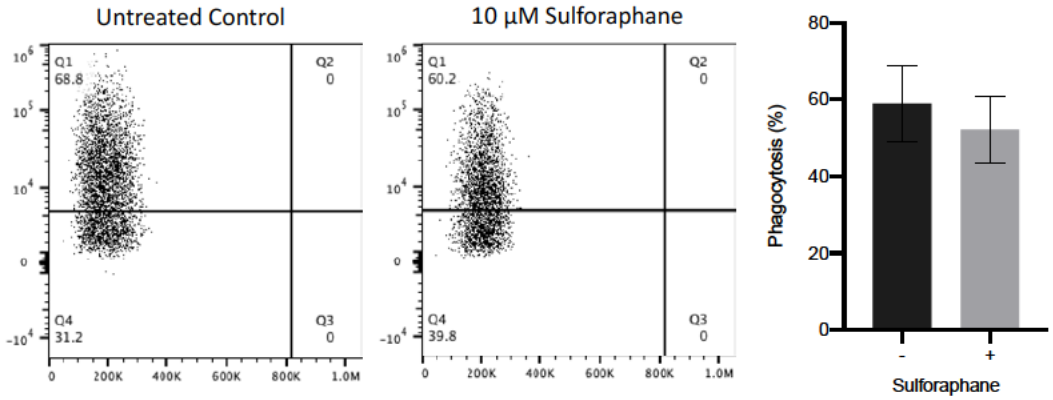

Figure 3.13 Quantifying the effect of sulforaphane on bacterial phagocytosis by monocyte-derived macrophages. Monocyte-derived macrophages were treated with 10 µM Sulforaphane for 18 hr before incubating with 20 µg/ml of pHrodo *E. Coli* Bioparticles for 45 min.. Flow cytometry plots are representative of three independent experiments. Graph shows quantification of phagocytosis as the percentage of gated MDM events that were pHrodo+, +/- Sulforaphane ±SD n=3.

3.4 Discussion

The results presented in this chapter outline studies to optically profile macrophage phagocytic activity. An *in vitro* cell culture model of human monocyte differentiation into macrophages was characterised. These MDMs were used to establish and further characterise assays to profile phagocytic activity. Using a flow cytometry assay to quantify phagocytosis was successful and could be applied to different biological targets and monitor the effects of pharmacological manipulation of macrophage activity.

3.4.1 The human monocyte-derived macrophage model

The choice of using human MDMs for further *in vitro* analysis in this work was to maintain biological relevance to primary human macrophages, in the expectation that the workflow in future chapters would involve profiling macrophages obtained from human patients with COPD. The importance of choosing this model was to work with MDMs from multiple donors that would not be genetically homogenous, as would be the case with a cell line [159]. While this inevitably introduces some variability in experimental results, for example seen as donor variability in how isolated monocytes respond to *in vitro* differentiation – this method would closer reflect differences in primary human macrophages present in patients' lungs *in situ* [180]. To reduce the amount of variability between independent cultures, each monocyte population was enriched by a negative selection technique to reduce the number of lymphocytes present. Lymphocytes produce cytokines (IFN, TNF, IL-1, IL-4 IL-10, IL-13) when in culture with monocytes that can dictate the activation state of mature macrophages [181]. The alternative would be to repeatedly wash lymphocytes away from the adhered monocyte in culture, risking disturbing and detaching a proportion of monocytes. The selection process did remove the vast majority of lymphocytes, which removed the need for washes which resulted in more intact macrophage monolayers at the end of each culture.

Analysis of the cell surface receptor profile for MDM revealed expression of macrophage-specific markers such as: CD80, CD163, and CD206 [182], although there was a degree of variability in expression of some receptors. This became more apparent when quantifying the effects of known polarising agents: IFN γ, LPS, and interleukin-4. Pro-inflammatory stimulants (IFN and LPS) were found to significantly increase CD80 expression when compared to a non-stimulated MDM control. However, in some cultures, CD80 expression was just as high in the "unstimulated" condition following some cultures, epitomising the variability in differentiation of MDMs during *in vitro* culture. It is possible that the levels of other cytokines that may have been present in the autologous serum would influence the activation of mature macrophages to a particular phenotype, without further stimulation [183]. Furthermore, the presence of lymphocytes could also influence the differentiation of monocytes in culture and the ultimate expression of cell-surface receptors [184]. As mentioned, steps had already been taken to reduce the impact of lymphocyte presence in the culture media. Inter-experimental variability between MDM cultures, might be reduced by use of commercially available human AB serum or serum-free media which have shown successful monocyte-macrophage differentiation [185].

3.4.2 A flow-cytometric assay to characterise macrophage phagocytosis of different targets

The use of flow cytometry to quantify uptake of fluorescent targets by macrophages has long been established. The experiments presented in this chapter identified relevant targets for optimal quantification of MDM phagocytosis. These assays were then used to examine the plasticity of macrophage phagocytic activity following pharmacological stimulation.

The use of polystyrene microspheres proved the most challenging target to model the interaction between primary alveolar macrophages and potentially relevant targets [186,77]. In flow cytometric analysis, it became apparent that when MDM and microsphere targets were mixed and analysed immediately there was a positive "coincidence" signal detectable. There are two possible reasons for this coincidence effect: the size and charge of the microspheres. The polystyrene microspheres used were 1 µm in size, smaller than the other targets used in this chapter. Their small size and high macrophage to target ratio may have resulted in particles passing through the flow cell alongside a macrophage. In addition, the charge of the microspheres may have led to rapid binding to the surface of macrophages non-specifically [187]. This may explain the lack of effect of Cytochalasin D , which may prevent phagocytosis, but not binding via blocking actin polymerisation [178]. Others have studied the downstream effect of measuring macrophage phagocytosis with differently sized and charged microspheres [188]. It revealed the importance of considering these factors when using an inert particle as a target for phagocytic assays. For example, they showed that a size of 1 µm was ideal for alveolar microspheres to internalise, though this also required added functional groups (amine or carboxyl) to the microsphere to elicit phagocytosis [188].

In addition to polystyrene microspheres, fluorescently labelled E. coli were used as a target to quantify bacterial phagocytosis using a flow cytometric assay. The use of E. coli was considered one relevant bacterial target for modelling alveolar macrophage interactions with pathogens in lung disease. Previous studies have outlined that defective AMs in COPD show reduced phagocytosis of E. coli [76]. However, one of the most common pathogens associated with defective macrophage phagocytosis and recurring infection in COPD, is *Streptococcus pneumoniae* [189]. Therefore, for future development of this assay, it would be worthwhile to explore labelling of other bacterial species to quantify phagocytosis in different macrophage populations.

Measuring phagocytosis of apoptotic neutrophils (efferocytosis) is important as the clearance of apoptotic material is essential to the resolution of inflammation and maintaining tissue homeostasis [190]. Failure to clear apoptotic cells effectively would lead to an accumulation of necrotic material that would ultimately exacerbate inflammation [191]. In this chapter, I demonstrated the use of CMFDA- and pHrodo-labelled apoptotic neutrophils for quantifying macrophage efferocytosis [168].

3.4.3 Manipulating the phagocytic activity of macrophages

Importantly, I was able to demonstrate a quantifiable effect of treatments to modulate MDM phagocytosis. For example, one of the anti-inflammatory effect of Dex and other synthetic glucocorticoids on macrophages is to promote efferocytosis [164,171]. Dex treatment induced a morphologically homogenous MDM population with a distinct rounded shape, also reported by others [171]. This assay could be used to investigate the effect that Dex has on primary human alveolar macrophages in a diseased state. Defective apoptotic cell clearance exacerbates the pathology of COPD, contributing to the viscous cycle of lung function decline [88]. Therefore, identifying therapeutic strategies to improve apoptotic cell clearance in COPD would be hugely beneficial. Synthetic glucocorticoids like Dex have long been used for their anti-inflammatory properties in inflammatory lung disease. Only one study to date reported limited improvement by Dex on efferocytosis by COPD AMs [192]. Isolating AMs from COPD patients and quantifying the effect dexamethasone has on efferocytosis would shed some more light on this, such as elucidating the underlying mechanisms regulating efferocytosis that become defective. Some studies have shown that the use of macrolide antibiotics, particularly azithromycin, do improve efferocytosis by COPD AMs *in vitro* [193]. This effect was also complemented by a reduction in recurring infections in COPD patients following macrolide treatment. This offers an alternative pharmaceutical approach to apply to the characterisation of augmenting macrophage efferocytosis. It may also offer a potential route to work synergistically with glucocorticoids such as Dex.

The compound sulforaphane was tested for its ability to augment bacterial phagocytosis by MDMs. However, sulforaphane treatment did not increase bacterial internalisation by MDMs in these experiments. Previous studies have shown that sulforaphane was successfully used to improve bacterial clearance by AMs from COPD patients [100]. However, this could be likened to rescuing impaired activity, rather than augmenting phagocytic capacity in otherwise healthy macrophages, which is supported in the same study, which found that sulforaphane had no effect on healthy control macrophages [100]. Sulforaphane has been shown to augment phagocytosis in other *in vitro* macrophage models, however this was using RAW cells as a macrophage model and 2 µm polystyrene beads as phagocytic targets [173]. Besides, the effect sulforaphane had was more pronounced in the absence or lower amounts of serum. This suggests sulforaphane acts to improve phagocytosis of non-opsonised targets Future work from this chapter should explore the effect sulforaphane has on the phagocytosis by human MDMs of bacteria following opsonisation with serum proteins or not.

3.4.4 Limitations and conclusions from this chapter

The work in this chapter establishes an *in vitro* monocyte-derived macrophage model for subsequent studies in this thesis, together with assays to quantify the phagocytic activity of macrophages, as well as their response to pharmacological agents. These studies form the foundation for development of more novel approaches to profiling phagocytic activity in future chapters.

However, there are some limitations to the work in this chapter. Only the human MDM were profiled in this chapter, which will likely differ in phenotype to primary human alveolar macrophages. It would be important to assess phagocytosis of different targets by primary AMs, as well as investigating how they respond to pharmacological manipulation. Although I did not establish an assay for quantitation

of phagocytosis of 1 μM polystyrene microspheres it would be interesting to explore the most appropriate size, charge, and opsonisation state of microsphere would be most effective for quantification of phagocytosis. The time-lapse imaging of neutrophil efferocytosis could also have been extended to use image analysis tools to study the kinetics of macrophage internalisation processes in detail. This system could have been used to further study the impact of pharmacological treatments to manipulate MDM phenotype (e.g. Dex) upon phagocytic activity.

In conclusion, this chapter successfully established the starting point for optically profiling macrophages. The following chapters develop these methods of profiling macrophages, by their phenotype and phagocytic activity, using alternative methods that carry the potential to perform this interrogation of primary human macrophages in the lung, *in situ*.

Chapter Four: A Fluorescent Nanobody for Labelling Human Macrophages via the Mannose Receptor

4.1 Introduction

The mannose receptor (MR) is an endocytic receptor with a broad binding specificity that spans both endogenous and foreign material [194]. It is a member of the C-type lectin family of receptors and was first recognised from its activity in clearing endogenous glycoproteins by alveolar macrophages [195,196]. Targets for the receptor also include sugars present on the surface of microorganisms which are not present on mammalian cells, such as mannose, fucose, and N-acetylglucosamine [197].

When the MR binds to its targets, internalisation occurs in a clatherin-dependent manner [198]. The receptor requires actin polymerisation in order to recycle to and from the cell membrane when shuttling targets from the surface of the cell to the endocytic compartments [194]. This has been determined by downregulating expression of the MR in the presence of cytochalasin D, an inhibitor of actin polymerisation [199]. Once transported inside the cell, acidification in the early endosome is the likely trigger for the MR to dissociate from its target and return to the cell surface [194]. Work to quantify the relative expression of the MR throughout the cell has shown the majority is present in early endosomal compartments [198]. What's more, MR recycling activity occurs even without the presence of ligands to the receptor [198].

A lack of signalling motifs on the cytoplasmic portion of the MR support a hypothesis that the receptor does not directly lead to microbicidal immune cell activation [200]. If the MR is involved in triggering signalling cascades following ligand binding, it would likely require involvement from other receptors. This points to a unique role the receptor plays in clearing microorganisms and debris while preserving inflammatory homeostasis in the microenvironment.

A number of tissue resident macrophages, including alveolar macrophages, are known to highly express the MR [201]. Monocyte-derived macrophages cultured *in vitro* also have a high expression of the MR, while non-differentiated monocytes are negative [202]. Further *in vitro* work has shown that expression of the MR is associated

with polarised states of macrophages. While pro-resolving stimuli, such as IL-10, IL-4 and some corticosteroids increase MR expression, pro-inflammatory stimuli such as interferon-gamma and LPS have a negative effect [196]. This observation suggests that modulation of expression is key to the role of the MR in both innate and adaptive immunity. Evidence of down-regulation by pro-inflammatory stimuli, together with evidence of MR activity increasing antigen uptake and T cell presentation, appears to endow the receptor with a niche role in driving local macrophage activity away from inflammation and instead to promoting a more adaptive immune response to microbes [203].

While it was previously assumed that the main role of the MR was to facilitate phagocytosis of pathogens, there is limited published evidence to support this. Different attempts have been made to 'knock-in' phagocytic activity into non-phagocytic cells through transfection of the MRC1 gene (coding for the MR) with limited success [200]. Given the ability of MR to also recognise a number of glycoproteins, another key function of the receptor likely involves matrix remodelling [203]. This is supported by evidence that MR expression is closely aligned to a macrophage phenotype that exhibits a high scavenging and remodelling capacity [204]. This type of activity includes removal of lysosomal enzymes, myeloperoxidases and tissue plasminogen activator [195].

The MR has been considered a valuable target in work to try and manipulate the function of macrophages *in vivo,* potentially halting or reversing a number of inflammatory diseases. However, the typical routes to polarising macrophages *in vitro* show little translational potential to humans *in vivo*, as pulsing with cytokines would almost certainly have adverse and off-target effects [205]. This has led to investigation of alternative ways of promoting macrophages to shift inflammatory phenotype *in situ* [206,89]. A recent paper demonstrated the use of a nanoparticle system designed to specifically instigate clustering of the macrophage mannose receptor [205]. In a pre-clinical model of mouse bone-marrow-derived macrophages

(BMDM), a gluco-mannan nanoparticle appeared to induce an anti-inflammatory macrophage phenotype – inferred through expression of IL-1 and arginase.

Another approach to target the MR involved its association with the tumour microenvironment and its expression on tumour-associated macrophages (TAM) [207]. In many different tumour types, there is often macrophage infiltration that is associated with tumour progression [208,209]. These TAMs assist in tumour growth by adopting a phenotype that promotes matrix remodelling and angiogenesis [210]. Work by Movahedi et al. found a specific subset of TAMs, which express low levels of MHC II, acting as a highly angiogenic cell type that would assist in tumour growth [211]. The MR is consistently upregulated in MHC II ^{low} macrophages, thus representing a target for identifying TAMs [207]. Movahedi et al. sought to target the mannose receptor by using an antibody-based technique [212]. However, whilst conventional antibody-based approaches are highly specific and the gold standard in targeting cell surface receptors, there are limitations when considering it for *in vivo* use. These drawbacks include likely off-target, Fc-related binding, as well as poor penetration in tissues [213]. One approach to overcome this was to use a camelid nanobody as the targeting ligand. Like human mAb, nanobodies have a high affinity for their target. However, they constitute only the variable fragment of a heavy-chain only antibody and are only a tenth of the size of monoclonal antibodies (around 15 Kda)- so are cleared from the body rapidly when used *in vivo* [214]. Other useful properties of nanobodies include: close identity to the VH_3 domains of human antibodies, thus having low immunogenicity; being highly soluble and stable in extreme pH and temperature ranges [215]. The small size and single-binding domain allow nanobodies to overcome the challenges usually present with antibody targeting, making them better equipped for tissue penetration and target specificity for *in vivo* applications [215]. Movahedi et al. developed a camelid nanobody specific to an extracellular domains of the MR [216]. Their work demonstrates use of this nanobody as a radiolabel and fluorescent label to identify MHC II ^{low} TAMs [212].

The draw of the MR as a target for tracking TAMs present at cancer sites led to the commercialisation of a receptor-binding pharmaceutical, Tilmanocept. This synthetic tracer is made up of multiple units of mannose bound to other sugars that can serve as binding sites for radiotracer labelling [217]. Tilmanocept was designed to specifically label TAMs in the tumour microenvironment. The efficacy of this probe has been shown through phase 3 clinical trials, while complementary *in vitro* work validate its mannose receptor specificity towards human MR-positive macrophages [218].

In addition to serving as a marker for TAMs, the MR has been used as a target for tracking macrophage involvement in atherosclerosis, particularly with respect to their involvement in plaque instability [219]. Building on previous work showing that the mannose receptor is highly expressed by macrophages associated with vulnerable plaques (which could indicate high risk of thrombosis), a near infra-red optical imaging agent was developed by Kim et al. to label macrophages during atheroma, to be imaged using optical coherence tomography (OCT) [220]. The probe described in their work was composed of mannosamine (an MR ligand) connected to maleimide via a PEG linker and conjugated to either a Cy 5.5 or Cy 7 fluorophore. This probe showed successful labelling of macrophages when imaged with an OCT system [219].

Looking beyond using the MR as a proxy for only detecting the presence of macrophages, additional studies have involved quantifying the expression of the receptor as a way to monitor the response of macrophages to different therapies for treatment of inflammatory disease. One example involves methods to manipulate macrophage cell activity to alleviate the pathology of chronic obstructive pulmonary disease (COPD). During COPD, there is dysregulated apoptosis and macrophage dysfunction in the airways [77]. Alveolar macrophages show defective clearance of apoptotic cells during COPD, while there is a net increase of apoptotic material and secondary necrosis that exacerbates the inflammatory response [191,221]. Therefore,

efferocytosis is postulated to be a key process to manipulate in order to improve lung function for COPD patients [88,222]. Low doses of macrolide antibiotics such as azithromycin have shown clinical benefits with inducing anti-inflammatory responses [223]. Azithromycin has also been shown to improve the efferocytosis function of AMs [224]. In one study, azithromycin increased MR expression by 50% *in vitro*, while using an MR blocking antibody reduced the phagocytic capacity of AMs by 60% [107]. This shows the potential to use expression of the MR as a proxy for macrophage phenotype, including the restoration of cell activity that was lost in disease.

The hypothesis for this chapter was a fluorescent nanobody probe can selectively label mature human macrophages via the mannose receptor and profile their inflammatory phenotype. As it is the first iteration of a MR-nanobody probe developed by our group, the aims of this chapter focus on the early biological characterization of the MR-nanobody: determine the cell and target specificity as well as mechanisms of labelling.

4.2 Use of an MR-Nanobody to selectively label macrophages

A mannose receptor-specific nanobody which has been previously described was acquired for the purposes of developing a macrophage-specific optical probe [216]. The nanobody is from camelid origin, developed through immunisation with commercially available extracellular domains of the human mannose receptor. The nanobody was subsequently isolated from a phage display library. Four fluorophores of sulphonated Cyanine 5 (SCy5) were conjugated to the nanobody scaffold to yield a far-red fluorescent MR-nanobody (Fig 4.1A), synthesised by Gavin Birch (Bradley Group, University of Edinburgh).

The MR-nanobody construct was first assessed with viable human monocyte-derived macrophages to determine cellular labelling. Using confocal microscopy as shown in Figure 4.1, MR-nanobody labelled MDMs in a concentration dependent manner. Using 50 nM of MR-nanobody provided a significantly higher signal than other concentrations, with a good signal to noise ratio (Figure 4.1D). As a result, the 50 nM concentration was considered the most appropriate for further experiments. This live-cell imaging was performed without a wash step (Figure 4.1D).

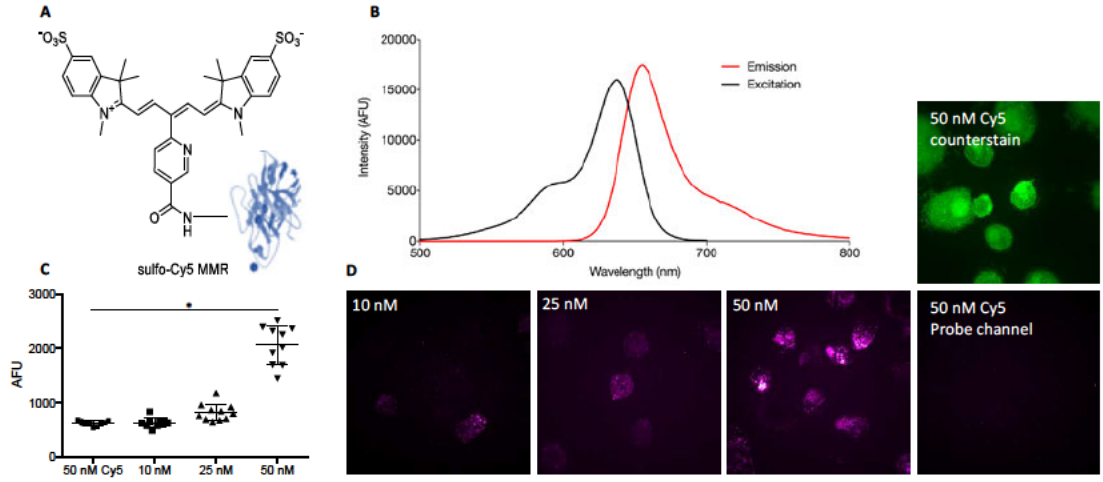

Figure 4.1 A) Chemical scaffold of novel mannose receptor (MR) targeting nanobody probe conjugated to sulphonated Cyanine 5 fluorophores. B) excitation/emission spectra of the MR Nanobody; excitation max: 636 nm, emission max: 674. C) Fluorescence quantification of human monocyte-derived macrophages imaged with a bench-top confocal microscope with increasing concentrations of MR Nanobody probe and Free Cyanine 5 dye control. Error bars represent the standard deviation of MR-nanobody signal from 10 MDMs cells across three independent experiments. Analysis performed using multiple paired t tests between concentrations. *= P≤0.05 D) Representative images of three independent experiments. The counterstain image for the Cy5 control is included to show cells were in the field of view.

4.2.1 MR-Nanobody shows specificity towards differentiated monocyte-derived macrophages

The cell-type specificity of the probe was then further assessed by comparing labelling of MDMs with their precursor cells: purified peripheral blood monocytes (PBMC). PBMC cells do not express the mannose receptor until they are differentiated into mature macrophages [202]. As shown in Figure 4.2 confocal microscopic analysis revealed that freshly isolated human monocytes were not labelled by the MR-nanobody. In contrast, following a 6-day differentiation into macrophages, the probe signal becomes apparent. Figure 4.2 also shows flow cytometric analysis of MR-nanobody labelling for the two cell types, compared to equimolar amounts of a free Cy5 dye control. The representative flow histogram for MR-Nanobody and monocytes show that there is a stronger signal from the probe compared to the control. This signal appears stronger in the flow histogram representing labelling of mature macrophages.

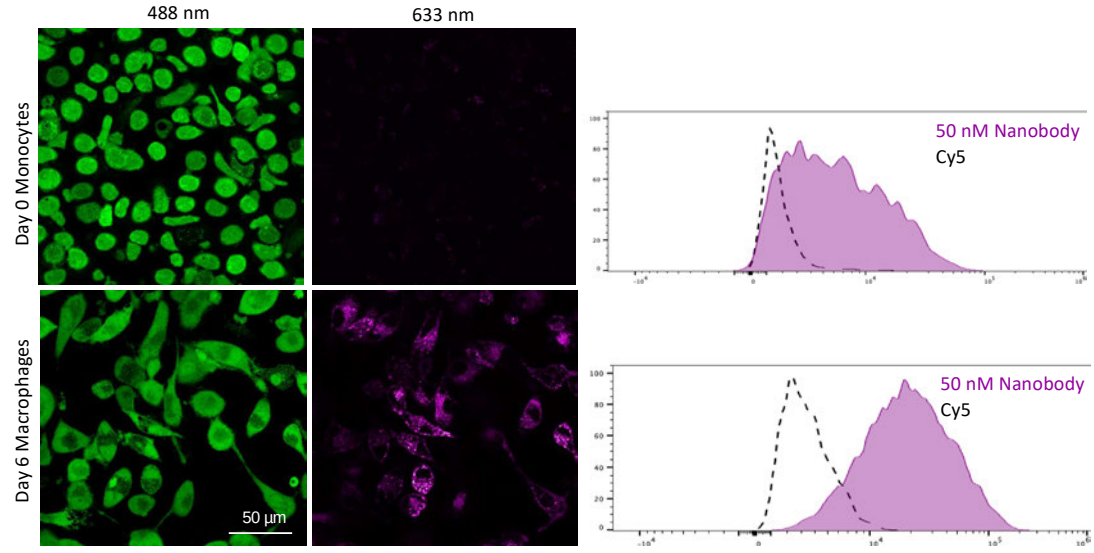

Figure 4.2 MR Nanobody selectively labels differentiated macrophages. 488 nm imaging panels represent cell labelling with Cell Tracker CMFDA as a counterstain. 633 nm imaging panels represent labelling by the MR-nanobody. Peripheral blood monocytes show minimal labelling signal when imaged. Differentiated monocyte-derived macrophages after 6 days of culture show greater fluorescent labelling. Plots to the right represent complimentary flow histogram analysis of MR Nanobody labelling for each cell type. Dotted lines represent 50 nM Cy5 dye control and solid plots represent MR-nanobody labelling. Images were taken by a CLSM and are representative of repeated FOV from three experimental repeats.

This analysis was repeated with a positive control antibody for mannose receptor labelling. An CD206 monoclonal antibody (BD Biosciences), conjugated to a PE fluorophore, as used in chapter three to determine mannose receptor expression (Figure 3.2). Figure 4.3 shows that, with the commercial anti-CD206 antibody, the staining pattern is similar to that of the MR-Nanobody. There was minimal labelling of monocytes when imaged with confocal microscopy, which was increased with differentiated macrophages. The representative flow histograms in Figure 4.3 show that for monocytes, there was minimal signal from the anti-CD206 antibody when compared to a PE isotype control. CD206 antibody binding was increased markedly with differentiated macrophages. The confocal imaging of MR-nanobody labelling of macrophages displays a similar staining pattern to that of the anti-CD206 antibody, with punctate labelling throughout the cell. This observation suggests that the majority of the MR-nanobody labelling appears within cells, rather than the cell surface. This could be representative of early endosomal compartmental labelling, where the majority of the mannose receptor would be expected to be expressed.

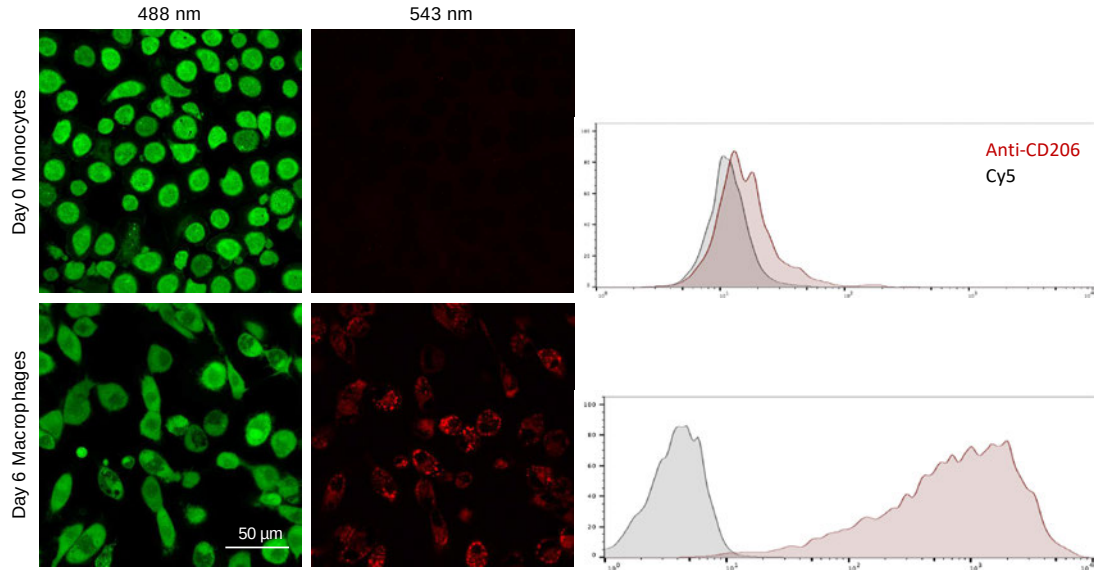

Figure 4.3 Anti-CD206 IgG monoclonal antibody selectively labels mature macrophages. Peripheral blood monocytes show no fluorescence labelling. Differentiated monocyte-derived macrophages after 6 days of culture exhibit fluorescent labelling. CMFDA dye was used to counterstain cells. Images were taken by a CLSM and are representative of repeated FOV from two experimental repeats. Flow cytometry histograms show labelling of anti-MR antibody (red) in comparison to an isotype control (grey).

4.2.2 MR-Nanobody labels broncho-alveolar lavage cells

The potential of the MR-nanobody to label a more biologically relevant primary human macrophage population, rather than *in vitro* MDMs, was also assessed. Broncho-alveolar lavage (BAL) samples were collected from aged patients (with suspected idiopathic pulmonary fibrosis) undergoing routine bronchoscopy at the Royal Infirmary of Edinburgh. Figure 4.4 shows the cellular cytospin of the BAL sample revealing that, as would be expected in a BAL sample, over 90% of the cells present had a morphology consistent with that of an alveolar macrophage (large cytoplasm and single nucleus). These BAL cells were labelled with both the MR-nanobody and PE anti-CD206 monoclonal as a positive control for mannose receptor labelling and examined by immunofluorescence microscopy. Figure 4.4 shows that the MR-nanobody labelled the cells in the BAL sample. The staining pattern shown from confocal microscopy revealed similarities between the MR-nanobody and the anti-CD206 monoclonal.

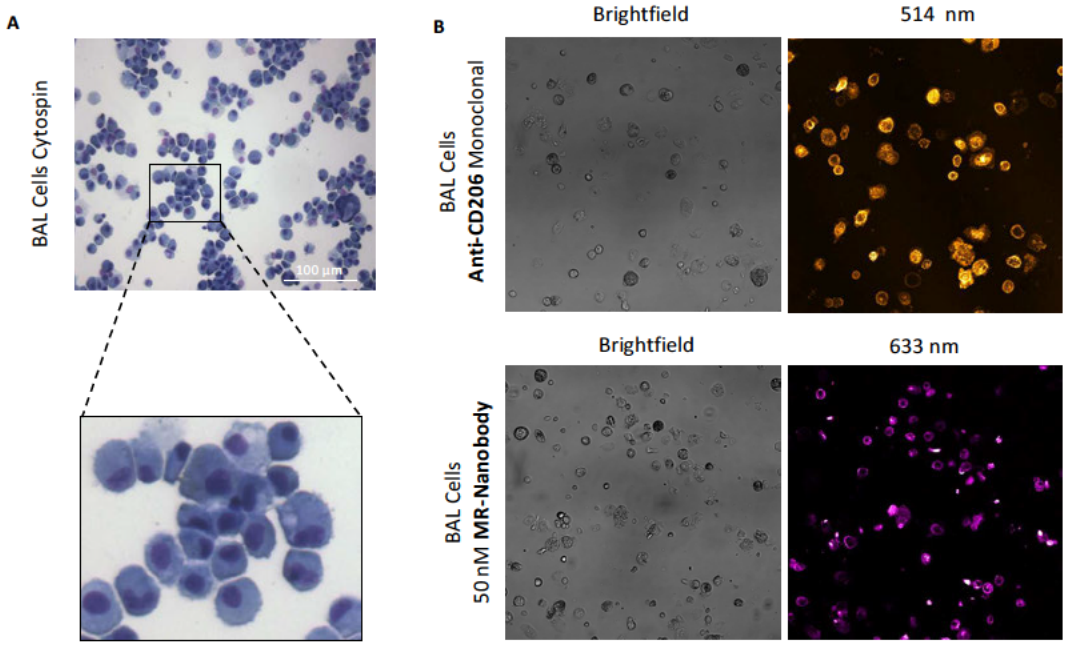

Figure 4.4 MR Nanobody labels cells from human broncho-alveolar lavage. A) Cell morphology from cytospin shows >90% of cells exhibit alveolar macrophage morphology. B) Representative images how MR-Nanobody and an PE anti-CD206 monoclonal antibody labels primary human broncho-alveolar lavage cells.

4.2.3 Localisation of MR-Nanobody labelling to the cytoplasm of macrophages

In order to examine if the MR-nanobody was internalised by macrophages, the same labelling protocol was repeated: human MDM were incubated with the MR-nanobody at 37 ºC for 20 min and then imaged using a spinning disc confocal microscope (SDCM). This imaging system allows for rapid, live cell imaging with minimal photobleaching and the capacity to acquire a detailed z stack of images taken at different depths of focus through live cells. The imaging data was then analysed using Imaris (Bitplane) image analysis software to render a 3D iso-surface of macrophages in the field of view. The isosurface was created by using Cell Tracker Green CMFDA dye, that allows the visualisation of the entire cell. Using this isosurface, it was possible to localise the MR-nanobody labelling relative to the cell isosurface. Figure 4.5 shows that the majority of nanobody labelling is localised to punctate regions throughout the cytoplasm of a cell. This shows that, not only is the probe mostly internalised by macrophages, it may become compartmentalised once inside.

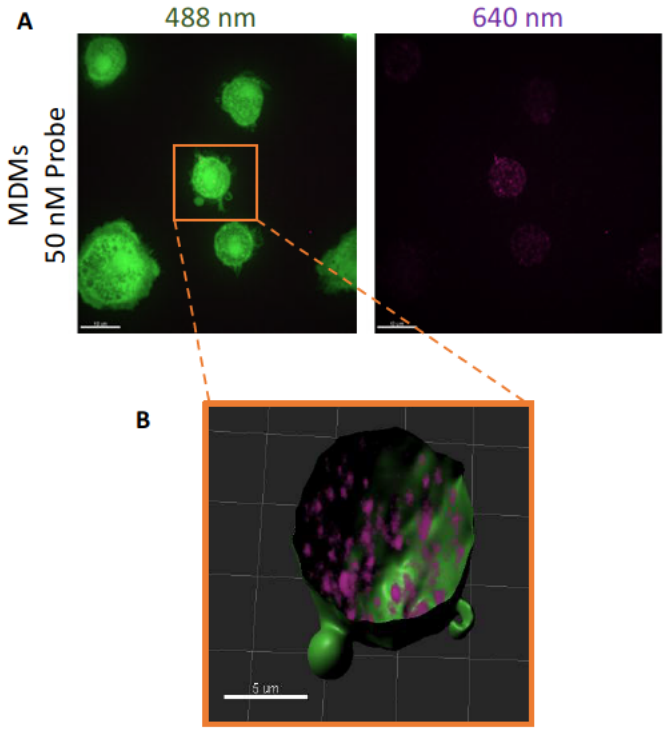

Figure 4.5 Localisation of the MR nanobody during live cell labelling. A) Human monocyte-derived macrophages were incubated with the MR-nanobody and imaged using a spinning disc confocal microscope to create a z stack of ~95 optical planes. Cell-tracker Green dye was used to label the entire cell in order to create an isosurface, allowing for more detailed spatial analysis of where the probe is localised. B) using Imaris image analysis software showed the majority of probe labelling inside the cell. Representative confocal images of three independent experiments.

4.2.4 MR-Nanobody initially labels the cell surface of macrophages

The SDCM system was also used to examine the early labelling kinetics of the MR-nanobody to determine how soon labelling became apparent together with localisation of the signal within the cell (as seen after 20 min of incubation shown in previous figures). An imaging time-course was performed with live human MDM cells and the MR-nanobody. Figure 4.6 shows that by 10 min there is clear labelling of cells, localised to the membrane, as shown by the ring-like staining pattern around the positive cells.

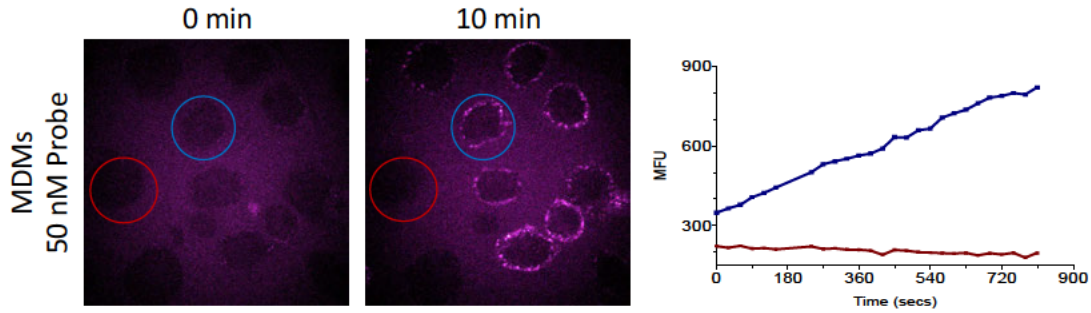

Figure 4.6 Labelling kinetics of MR nanobody. Using Spinning Disc Confocal Microscopy (SDCM) with live human Monocyte-derived Macrophages (MDMs), 100 nM of MR-nanobody was introduced and a time-course was set to track the initial labelling kinetics of the probe. Images show labelling of probe at 0 min and 10 min. Graph shows dynamic changes in labelling signal of two highlighted cells in the FOV. Representative confocal image time-lapse of two independent experiments.

4.2.5 Inhibiting cytoskeletal actin polymerisation reduces MR-nanobody labelling

Active forms of endocytosis, including receptor-mediated internalisation, requires the involvement of the actin cytoskeleton of cells. Therefore, the effect of cytochalasin D – a known inhibitor of actin polymerisation – on MR-nanobody labelling of macrophages was assessed. Figure 4.7 shows that using cytochalasin D to block actin polymerisation significantly reduces the extent of labelling of the probe. This suggests that the MR-nanobody requires cytoskeletal activity for efficient labelling of cells.

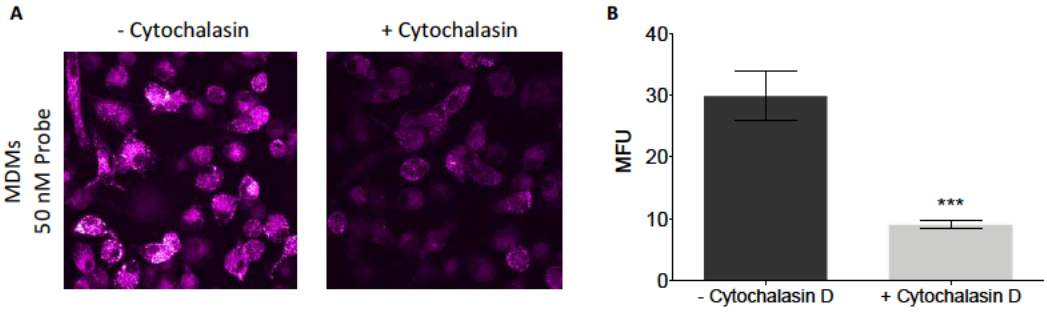

Figure 4.7 Cytochalasin D has a negative effect on MR-nanobody labelling. Human MDMs were labelled with MR nanobody with or without 10 µg/ml of Cytochalasin D. Representative CLSM images show a weakening of probe labelling in the presence of Cytochalasin D and quantification of the MFU for cells in the field of view show a significantly negative effect on probe signal. Graph bars represent mean fluorescence (±SEM) of cells from three independent experiments. Analysis with paired t-test; *** = p>0.001

4.2.6 MR-Nanobody shows no off-target labelling of lung epithelial cells but off-target labelling of human granulocytes

Further cell-type specificity assessments were carried with other cell types representative of those that would be found in the alveolar space. This is important for the characterisation of the MR-nanobody as a potential imaging probe to be used *in vivo*, to demonstrate its labelling is specific to macrophages. The human carcinoma A549 cell line was used as a model to monitor how the MR-nanobody interacts with human alveolar epithelial cells. Figure 4.8 shows that the MR-nanobody does not label the A549 cells, when assessed using confocal microscopy.

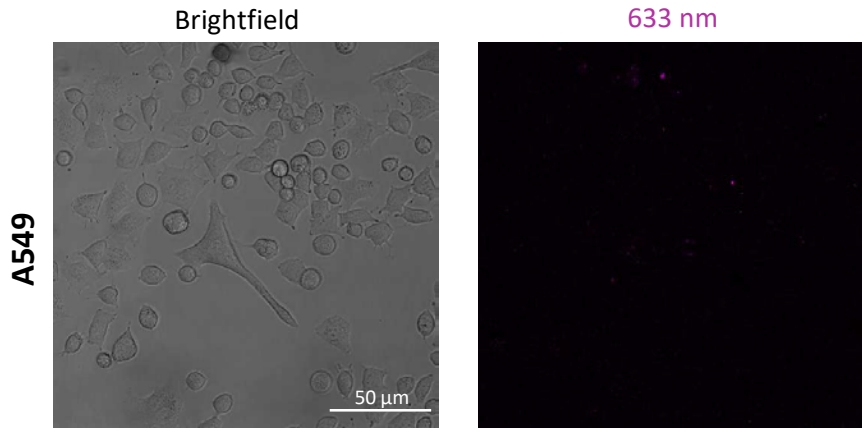

Figure 4.8 MR Nanobody shows no off-target labelling of a alveolar epithelial cell line. Representative images show that MR Nanobody does not label A549 cell line. The 633 nm image shows the MR-Nanobody fluorescent channel. Representative confocal images from two experimental repeats.

I next examined labelling of other immune cell types by using human polymorphonuclear (PMN) cells, freshly isolated from whole blood to assess MR-

nanobody. Figure 4.9 shows that a proportion of PMN cells are labelled by the MR-nanobody. Further to this, equimolar amounts of Cyanine 5 dye also labels PMN cells, a labelling characteristic not shared by macrophages (macrophages could not be labelled with free dye alone). A specific morphological appearance of the positive PMN cells appears to align with labelling, whether from the MR-nanobody or free Cy5 dye alone. This appearance is flatter and more granular than cells that are left unlabelled, which have a more rounded appearance.

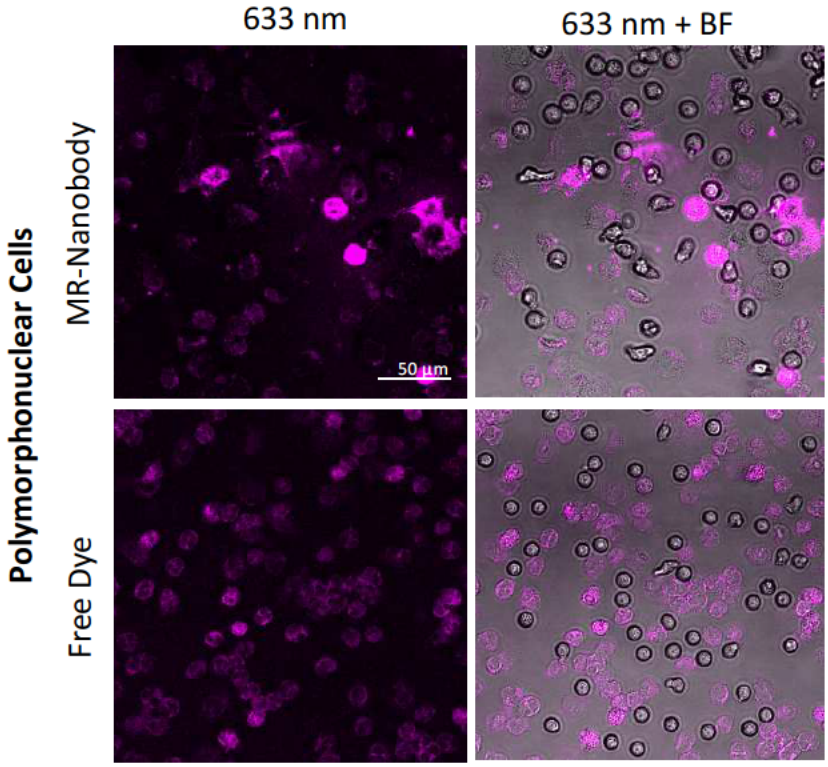

Figure 4.9 MR Nanobody shows some off-target labelling of activated peripheral blood granulocytes. Quiescent granulocytes do not exhibit labelling. Free sulphonated Cy5 dye also labels activated granulocytes. The 633 nm image shows the MR-Nanobody fluorescent channel. Images were taken by a CLSM and are representative of repeated FOV from two experimental repeats.

4.2.7 MR-Nanobody labelling does not differentiate between macrophage polarised states

The expression of the MR has been suggested to align to certain macrophage phenotypes, or represent a marker to track the manipulation of their phenotype away from an inflammatory state [196]. In chapter three, receptor expression profiling of macrophages following different polarising stimulants did not significantly alter expression of the mannose receptor (CD206) (Figure 3.3). While it could be expected that the MR-nanobody would yield the same result, it would still be worthwhile to assess MR-nanobody labelling of polarised macrophages, as a nanobody ligand may be a more sensitive indicator of altered receptor recycling activity. MDMs were polarised into different activated states: a pro-inflammatory phenotype through interferon-gamma (IFN) and lipopolysaccharide (LPS) stimulation, or an anti-inflammatory phenotype through interleukin-4 stimulation. Figure 4.10 shows that, from flow cytometric analysis, the labelling of the MR-nanobody showed little difference between either of the polarised macrophage phenotypes when compared with an untreated control MDM population. This observation was supported by confocal imaging that shows similar labelling patterns by the MR-nanobody of the different macrophage populations.

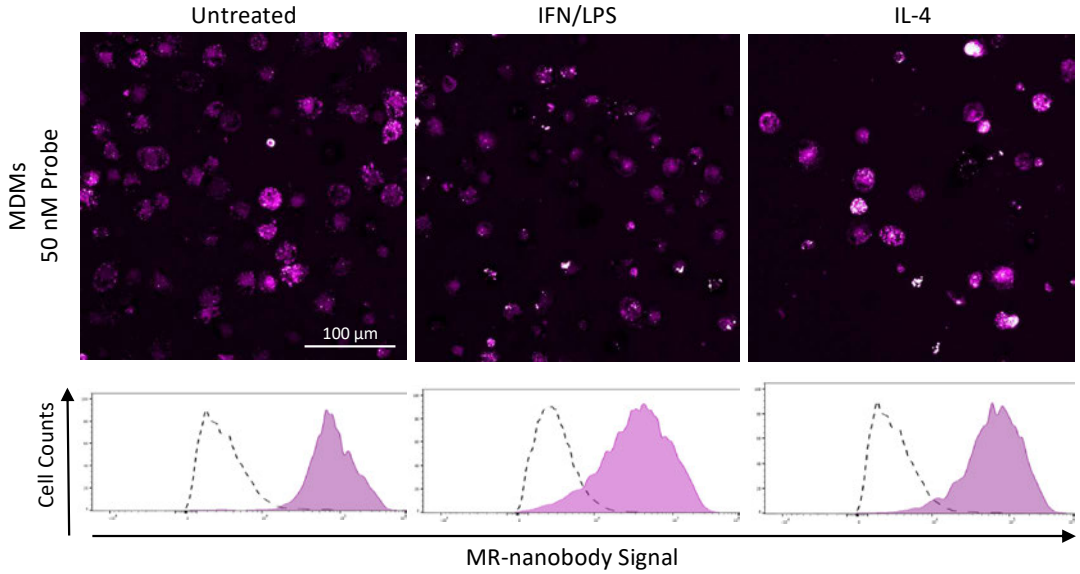

Figure 4.10 MR nanobody labelling of polarised human monocyte-derived macrophages (MDMs). Human MDMs were polarised into a pro-inflammatory state (20 ng/ml IFN-g, 10 ng/ml LPS for 25 hr) or into an anti-

inflammatory state (20 ng/ml IL-4 for 24 hr). The labelling characteristics of the MR-nanobody on these polarised states was compared to an untreated control using (A) CLSM and (B) flow cytometric analysis. Representative images and histograms of two independent experiments.

4.2.8 Excess mannan in the cell media does not competitively inhibit MR-Nanobody labelling

Following on from examination of the cell-type specificity of the MR-nanobody, it was necessary to determine that specific labelling of macrophages previously shown was due to the specific interaction between the MR-nanobody and its proposed target, the MR. The first approach taken to determine this was to assess whether competitive inhibition of the ligand-MR interaction would act to prevent MR-nanobody labelling. Figure 4.11 shows flow cytometric determination of MR-nanobody labelling of MDMs with and without excess amounts of mannan (a known ligand for the mannose receptor, previously used to determine target specificity of other mannose receptor probes) [218]. There was no significant reduction of MR-nanobody labelling when excess amounts of mannan were present (quantification not shown). Rather, there was a slight increase in MR-nanobody labelling in the presence of mannan (Figure 4.11).

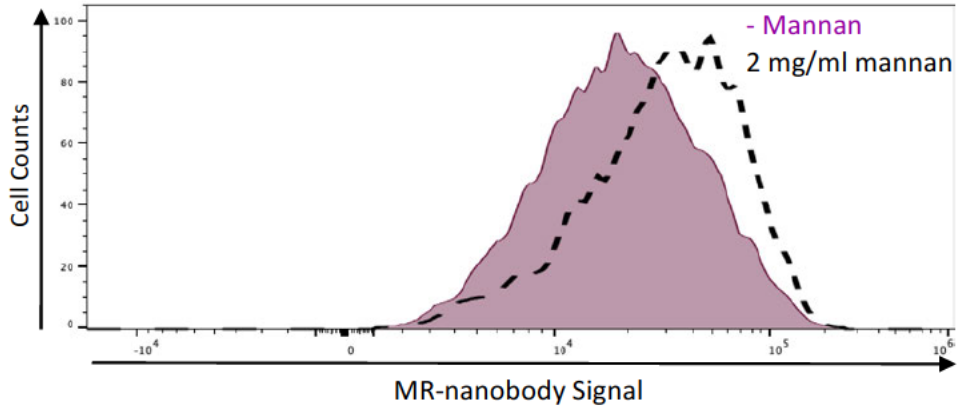

Figure 4.11 MR Nanobody signal is not knocked down by presence of mannan. 2 mg/ml of mannan was added to the cell media 30 min before and during MR nanobody labelling of human MDMs. This form of competitive inhibition had no effects on the MR nanobody signal in the cell population when analysed using flow cytometry. Flow histogram representative of two independent experiments.

4.2.9 Transfecting the mannose receptor into a negative cell type does not confer MR-nanobody labelling

An alternative method of determining target specificity of the MR-nanobody would be to 'knock in' expression of the receptor into a negative cell line – via a transfection – and assess whether this aligns with labelling of the MR-nanobody probe. To do this, the Chinese Hamster Ovary (CHO) cell line was transfected with an expression plasmid containing the human MRC1 gene (Origene, MI, USA) using a transient lipofectamine-based transfection technique. Figure 4.12 shows that, following transfection, the CHO cell population showed expression of the mannose receptor when analysed with an anti-CD206 monoclonal antibody together with flow cytometry. In contrast, no-plasmid "control" population of CHO cells showed no expression of the receptor. However, it was not possible to show labelling of the MR-transfected CHO cells with the MR-nanobody (compared to a Cy5 dye only control) using flow cytometry.

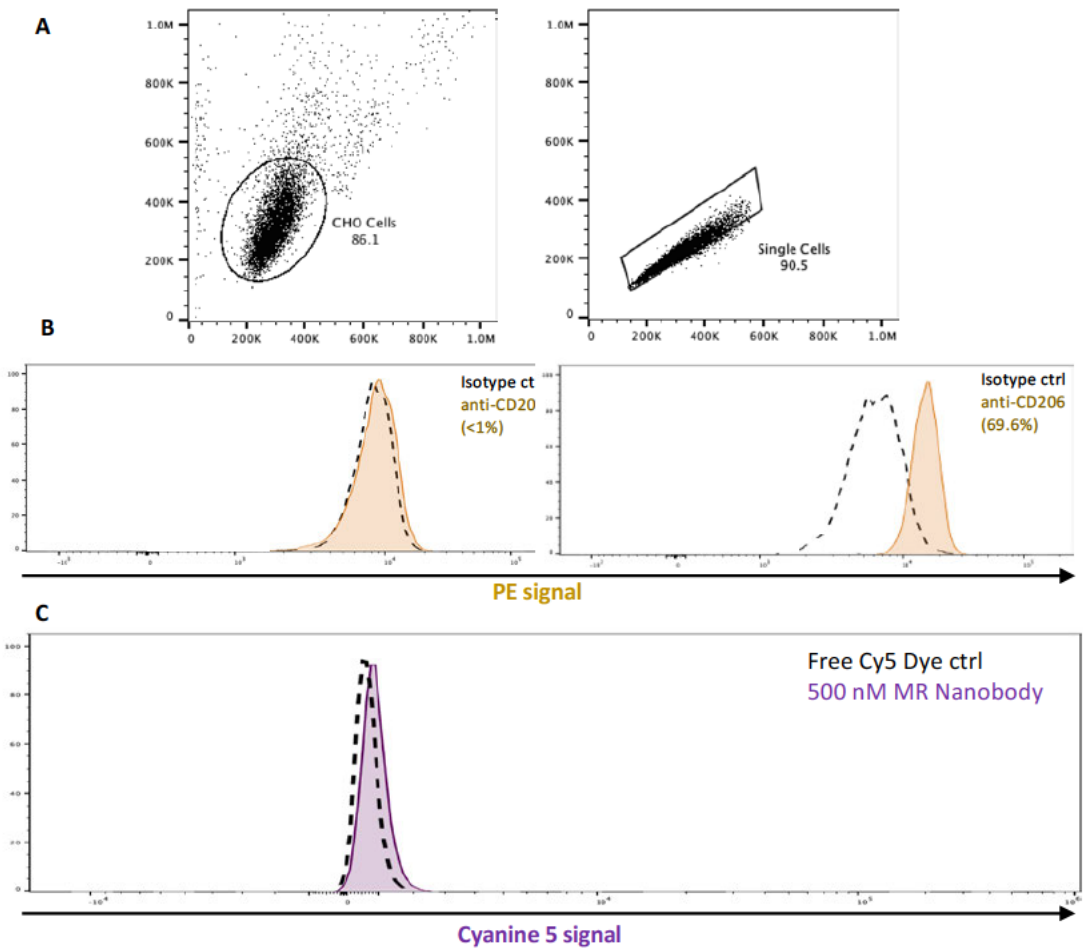

Figure 4.12 Transfection of the mannose receptor into a negative cell line does not confer labelling of the MR Nanobody probe. Chinese Hamster Ovary (CHO) cells were transfected with the MRC1 gene to knock in expression of the mannose receptor and then analysed by flow cytometry for CD206 expression and labelling by the MR nanobody. A) Gating strategy of the flow cytometric analysis. B) Flow cytometric analysis showed that 69.6% of the transfected population were positive for CD206 expression compared to an isotype control. C) Despite expression of CD206, MR nanobody (500 nM) failed to label transfected cells any more than equimolar amounts of free Cy5 dye. Flow histograms representative of two independent experiments, performed 72 and 120 hr post-transfection

4.3 Discussion

The results of this chapter showed the early biological characterisation of a fluorescently labelled nanobody construct intended to specifically target the macrophage mannose receptor. The MR-nanobody construct demonstrated cell-type specificity towards macrophages, with a similar staining pattern to that of commercial monoclonal antibodies for the same mannose receptor target. This demonstrates the potential of this novel probe construct: a macrophage-specific probe that features biochemical properties – attributed to the nanobody – that would allow safe use in a clinical setting. Characterisation of this probe will lay the foundation of carrying out macrophage receptor phenotyping in humans, *in situ*, for the benefit of experimental medicine.

4.3.1 Cell-type specificity of the MR-nanobody

At nanomolar concentrations, the MR-nanobody specifically labelled human monocyte-derived macrophages, with a high signal to noise ratio, despite no wash step. The high affinity of the MR-nanobody for macrophages would be of critical importance for labelling cells in the alveolar space in humans, *in vivo*, which represents a far more complex environment than an *in vitro* situation.

In addition, the MR-nanobody also labelled primary human bronchoalveolar macrophages, demonstrating the potential to label macrophages *in situ*. Previous work has demonstrated relatively high expression of the mannose receptor on AM highlighting its potential for targeting AMs *in vivo* [225].

The MR-nanobody did not show differential labelling of MDM polarised into different inflammatory phenotypes, even though receptor profiles of the MDM demonstrated that polarisation had been induced (see chapter 3, Figure 3.3). Similarly, the expression of MR was not altered on polarised MDM populations. This

observation is antithetical to previous reports of modulating the mannose receptor expression on macrophages *in vitro* [196]. Others have found that stimulating macrophages with IL-4 elicited a higher expression of the mannose receptor, while the reverse occurred when stimulating with interferon gamma [226,227]. It is possible these different results could be due to differences between mouse ([3, 24,25]) and human cells (this study). In addition, it is possible that there is some variability of human macrophage phenotypes following in *vitro* cytokine stimulation.

The MR-nanobody appeared to specifically label MDMs, but not their monocyte precursors. This observation is consistent with data shown in Chapter 3 (Figure 3.2) and the work of others, that the mannose receptor was only expressed on MDM.[202]. It was worth noting some technical discrepancies in MR-nanobody labelling of monocytes. While confocal microscopy analysis revealed minimal signal with monocytes, flow cytometry analysis showed low level MR-nanobody labelling. Thus, flow and confocal data could lead to different conclusions about the level of off-target labelling of this probe. One explanation for this is the differences in sensitivity between the two optical systems (flow cytometry and confocal imaging). The flow cytometric analysis may be detecting MR-nanobody binding to monocytes that would not be seen on an imaging system. Monocytes are capable of fluid-phase pinocytosis and therefore a proportion of this population could non-specifically internalise the MR-nanobody – though to a much less degree as the more activate internalisation processes happening with mature macrophages [225].

The cell-type specificity aspect of this work uncovered what appeared to be off-target labelling by the MR-nanobody when incubated with human neutrophils when imaged with confocal microscopy. The labelled cells were morphologically distinct from those that were negative, with a stretched, flattened morphology characteristic of an activated neutrophil [228]. This observation may reveal an issue with using a fluorescent probe in the presence of activated neutrophils which exhibit altered surface charge and increased membrane porosity. The activated neutrophils

also stained when incubated with Cy5 fluorophore alone, possibly due to the Cy5 dye "sticking" to the activated cell membrane. It could also be that activated neutrophils increase fluid-phase pinocytosis, accumulating fluorophore inside the cell non-specifically [229]. As each MR-nanobody probe has multiple cyanine 5 fluorophore units attached, accumulation of probe inside the cell would yield a much higher signal than that of free dye. It would be important to assess the effects of blocking neutrophil pinocytosis in order to test this hypothesis. This could be achieved by blocking the activity of PI3 kinase within the cell (such as Wortmannin) or using micropinocytosis blockers such as Dynasore (an inhibitor of dynamin activity), to show the effect this has on the off-target labelling of the MR-nanobody [230, 231]. It could then be possible to delineate the different routes the probe takes when labelling neutrophils and macrophages, testing whether the route of internalisation with neutrophils is non-specific, while a more active process governs uptake of the probe by macrophages.

4.3.2 Target specificity of the MR-nanobody

Work in this chapter also sought to define the target specificity of the MR-nanobody. The MR-nanobody binds to an epitope on the extracellular domain of the mannose receptor. Characterisation of the MR-nanobody probe should show that conjugation of a fluorophore - cyanine 5 or any other alternative fluorophore in future iterations - does not interrupt epitope binding of the nanobody. The initial attempt at determining target specificity was to competitively inhibit the MR-nanobody from binding to the mannose receptor. To do this, the probe was incubated with human MDMs in the presence of excess mannan – a known ligand for the mannose receptor. This form of competitive inhibition has been used previously to validate the target specificity of other mannose receptor probes [218]. However, excess mannan did not diminish MR-nanobody labelling of MDMs. One reason for this could be the nature of ligand-receptor interactions and the different binding routes taken by mannose and the MR-nanobody when interacting with the receptor. The extracellular domain

on the mannose receptor the nanobody binds to has not been reported, therefore it could bind independently of the carbohydrate-recognition domains that recognise mannan [232]. There are several extracellular domains on the mannose receptor, including the cysteine-rich domain or the fibronectin domains that may contain the epitope that the nanobody binds to [200]. It should also be noted that the excess mannan in this competition assay may actually have had the reverse effect on the MR-nanobody. Preliminary data, based on two experimental repeats, suggested that excess mannan slightly increased the levels of MR-nanobody labelling. This could in fact be a functional response of increased mannose receptor activity in the presence of a ligand. Previous studies have found that the majority of this endocytic receptor exists within the cell, in endosomal compartments [196]. The recycling capacity of the receptor can dynamically change in response to ligand binding [233]. Therefore, having excess mannan in the cell media may stimulate a higher proportion of receptors being present on the cell surface – with a greater number of epitopes for the MR-nanobody to bind to.

Further target specificity analysis using CHO cells that had been transfected with the mannose receptor expression revealed that despite positive staining with a CD206 mAb post-transfection, the MR-nanobody was unable to label the transfected CHO cells. Although one conclusion would be that the MR-nanobody is not target specific, it would be important to demonstrate that the transfected receptor retained structural integrity, complete with epitope for MR-nanobody binding [234]. In addition, the functional capabilities of the transfected receptor could be explored: this could be achieved through fluorescently labelling mannosylated compounds to show if the receptor is functionally active for internalising a target [233].

4.3.3 Characterisation of mannose receptor probes

As outlined previously in this chapter, the mannose receptor has already been established as an imaging target for probes to specifically label macrophages – some even using the same nanobody-based targeting ligand [216]. As this chapter seeks to add to our understanding of probing macrophage heterogeneity using the mannose receptor, it is worthwhile to consider the similarities and differences with how this work validated the MR-nanobody and approaches taken by others. The most prominent example of an MR-targeting probe is Tilmanocept, a radiolabelled probe to target macrophages via the mannose receptor [218]. Rather than using an antibody-based ligand, Tilmanocept uses mannose sugars to target the receptor. The *in vitro* characterisation for Tilmanocept used a similar model to that used in this body of work: human monocyte-derived macrophages cultured in autologous serum [218]. The primary function of Tilmanocept is to label tumour-associated macrophages present in lymph nodes. Taking a similar approach to work in this chapter, flow cytometry was used to demonstrate the cell-type specificity of a cyanine 3 labelled Tilmanocept. Validation of Tilmanocept *in vitro* used mannan competition as a way to determine target specificity of the probe towards the mannose receptor [218]. Unlike the MR-nanobody described in this chapter, fluorescently labelled Tilmanocept was blocked from labelling human MDMs in the presence of the concentration of mannan used in my study. The authors also used 'knock down' of the mannose receptor via siRNA to show that macrophages require MR expression for Tilmanocept labelling, while transfection of the MRC1 gene into HEK cells showed Tilmanocept labelling increased when 'knocking in' the mannose receptor [218]. In their initial *in vitro* validation of a fluorescently conjugated MR-nanobody [216], Movahedi et al. used isolated macrophages from mouse models of lung and breast carcinoma. Using the nanobody ligand conjugated to commercial fluorophores (AlexaFlour488 and 647), they showed cell-type specificity towards a specific subset of tumour-associated macrophages that were MHC II ^{low}, while all other myeloid cells in a tumour sample – including granulocytes – were negative for labelling [216]. They also sought to determine target specificity of the nanobody by using an MR-

knockout mouse model to show mannose receptor expression was required for the nanobody to label. In addition, they also used a control nanobody structure with no affinity for macrophages, to show that nanobody binding to the macrophages was a specific process [216].

4.3.4 Limitations of the work in this chapter and conclusion

The work in this chapter describes studies to characterise a novel approach to optically profiling macrophages and validate its potential for specifically targeting macrophages via the mannose receptor. Ultimately there were some limitations to how confidently that assessment could be made.

First, it would have been useful to have additional controls in place to determine the target specificity of the MR-nanobody. Use of macrophages lacking mannose receptor expression would have confirmed whether the MR-nanobody labelling required the MR or another pathway. Acquiring another, non-specific, nanobody construct and carrying out the same fluorophore conjugation would aid in discerning if macrophages non-specifically internalise these compounds or whether labelling represents an active process.

Second, it was not possible to explore if the choice of fluorophore had an impact on the function of the probe. The MR-nanobody described in this chapter was conjugated to four far-red cyanine 5 (sulphonated) dyes. Alternative fluorophores across the visible spectrum possess a variety of properties: they can vary in their size, their charge properties, and their solubility. This can lead to significant consequences in terms of probe function. In the context of using a nanobody – a compound only 15 kDa in size – the size of the fluorophore conjugated to the fragment could significantly impact on its ability to bind to its epitope [235]. For example, the fluorophore nitrobenzodioxazole (NBD) has been popularised for use in imaging probes due to its small size [236,237]. One drawback of using NBD is its

limited spectral properties, often emitting only in the "green" window of the visible spectrum. One reason this fluorophore was not initially considered for labelling the MR-nanobody is due to this emission, as it would overlap significantly autofluorescent tissue of the human lung [131]. However, recent work has looked to expand the spectral characteristics of small fluorophores, such as NBD, which may align well with future iteration of the MR-nanobody [238].

Work in this chapter showed that not only the MR-nanobody probe, but also free cyanine 5 dye in solution would 'stick' to polymorphonuclear cells. Therefore, interchanging the fluorophore on the MR-nanobody could shed more light on its non-specific labelling of neutrophils and possibly its ability to bind to the mannose receptor.

Despite these limitations, this chapter presents the MR-nanobody, with a far-red fluorescence, as a novel probe that shows cell-type specificity towards macrophages. The work shows that labelling mostly occurs through internalisation by cells in an active process. It also shows that primary human alveolar macrophages can be labelled by this probe. This chapter lays the foundation for using a fluorescent nanobody to target macrophages in the human lung, to be used in combination with optical systems capable of carrying out cellular imaging of alveolar macrophages *in situ.*

Chapter Five: Imaging Macrophage Phagocytosis Using Optical Endo-microscopy and Spectral Ratio Imaging

5.1 Introduction

5.1.1 Novel markers for non-invasive profiling of macrophage phenotype and activity

The traditional methods of profiling macrophage phenotypes – whether they align to pro-inflammatory or pro-resolving states – have typically involved quantifying the expression of known markers to activated phenotypes [55]. Some of these are outlined in chapter three, such as cell surface receptors indicating pro-inflammatory phenotypes (CD80) or pro-resolving phenotypes (CD163). Other approaches can also include quantifying cell products such as iNOS and Arg1, or gene expression [239]. A challenge in experimental medicine is how the phenotype of macrophages could be profiled while the cells are still *in situ*. Chapter four presents a novel fluorescent nanobody that targets the mannose receptor, which is associated with certain macrophage phenotypes, with the potential to be used *in situ* [216]. This still involves the use of an exogenous probe to identify macrophages based on cell-surface marker expression. However, there are other endogenous markers on macrophages that could allow for even more minimally invasive methods of profiling.

The metabolic state of macrophages – whether their main form of energy production is via aerobic glycolysis or oxidative phosphorylation – can align with what activated state the cells are in [240]. Pro-inflammatory macrophages favour aerobic glycolysis, while anti-inflammatory cells favour oxidative phosphorylation [241]. A key molecule involved in both forms of energy production is the coenzyme NADH, which is present in different forms depending on the metabolic activity of the cell [242]. During glycolysis, NADH is unbound in the cytoplasm of the cell; during oxidative phosphorylation, NADH is bound to mitochondrial shuttles [243]. NADH is an inherently autofluorescent molecule, which can serve as a maker for label-free imaging of macrophages [244]. More importantly, the binding state of NADH dictates

the measurable fluorescence lifetime of the molecule, providing a quantifiable, label-free way to determine a macrophage's polarised state [243,245]. Studies have demonstrated the potential of using fluorescence-lifetime imaging microscopy (FLIM) as a quantifiable method of determining the metabolic state of macrophages, *in vitro* following polarisation [243]. One study showed that different FLIM signatures aligned with other markers for polarised states, such as iNOS production following IFN and LPS stimulation, or Arginase production following stimulation by IL-13 and IL-4 [243]. However, it is necessary to note this work was using an *in vitro* model of mouse bone-marrow derived macrophages in extreme polarised states, which may not reflect how human macrophage phenotypes would present *in vivo*.

Other methods of interrogating macrophage phenotypes using endogenous markers, label-free, have been used in the context of the tumour microenvironment. It has previously been established that characterisation of macrophage phenotypes surrounding a tumour has a close relationship with a patient's clinical outcome, even the potential efficacy of some treatments [246,247]. One study used hyperspectral imaging (HSI) as a label-free way to classify known macrophage phenotypes [248]. Using a combination of imaging and spectroscopy, HSI provides complete spectral information for every pixel of an image [68]. Their aim was to provide a fingerprint of macrophage phenotypes based on morphological and spectral detail from polarised human macrophages *in vitro*, using visible light and NIR reflectance [248]. Analysis of the different spectra revealed tangible differences between macrophage polarised states, though variability in data between human donors exemplified the challenge of aligning this system for translational purposes.

As more evidence suggests that the plasticity of macrophages, including those in the alveolar space, may complicate the intended results of therapies, it is becoming increasingly important to understand exactly how these cells respond to drugs *in situ* [249]. This is because it would be difficult to account for all the factors that contribute to macrophage plasticity in their native environment, such as the alveolar space.

This requires imaging systems in place that are capable of carrying out this form of interrogation.

5.1.2 Potential of *in situ* profiling of human AMs

Despite advances in the profiling of macrophage activity, there remains a challenge to effectively profile these cells *in situ.* AMs exemplify this as it is difficult to access the distal region of the alveolar space where they reside [250]. Therefore, it has not been possible to profile alveolar macrophage activity while they are still in their native environment. However, there are now imaging systems available that can overcome this challenge. Developments in optical microendoscopy (OEM) has led to widefield and confocal fluorescence-based imaging systems [131,130]. These systems use fibre imaging bundles small enough to access and image the distal regions of the human lung [129,127]. In a clinical context, this form of imaging can be incorporated into routine bronchoscopy and may provide further structural and molecular information about a patient's lung pathology [131]. The autofluorescence of elastin in lung tissue means the structure of the lung is readily imaged with fluorescence-based systems and can direct the fibre-imaging bundles to the alveolar space for interrogation [131]. OEM presents an opportunity to align these systems - capable of directly imaging inside the alveolar space - with imaging of alveolar macrophages *in situ*. Moreover, using fluorescence means there is scope to perform multiplex imaging; to image in a range of colour wavelengths, with potential to specifically label cells to detect over the autofluorescence of lung tissue as well as distinguish between cell types.

5.1.3 Autofluorescent challenge of imaging AMs

However, there lies a challenge to using fluorescent microscopy in the alveolar space. This environment already presents large amounts of autofluorescence from the lung tissue, but also from resident cells. Evidence shows that AMs in particular can be highly autofluorescent [251,252]. Autofluorescence from macrophages can derive from NADH within the cell, but also other co-enzymes such as riboflavin and flavin [253,254]. This characteristic has long been used to isolate alveolar macrophages using flow cytometry [255]. Autofluorescence appears to be exacerbated in AMs from a smoker [251]. It has previously been shown that the tar component of cigarette smoke, which is highly autofluorescent, is a likely contributor to the high amount of macrophage autofluorescence [256]. Having this amount of autofluorescence in the lung can limit the use of exogenous fluorescent probes to effectively carry out molecular imaging in this region [257]. While there are methods to minimise cellular autofluorescence *in vitro*, such as use of crystal violet as a quencher, this would not be feasible in the context of profiling macrophages *in situ* [258].

The ability to interrogate the activity of COPD AMs from a smoker *in situ* would be of high value in the context of experimental medicine. It could be used to confirm phagocytic defects of these cells *in situ*, even monitor the effects of potential therapies targeting the cells without removing them from the alveolar space. Previous studies *in vitro* have shown that smoking exacerbates the phagocytic defect of alveolar macrophages during COPD [83,222]. Therefore, routes to overcome the challenge of smoker's macrophage autofluorescence would have to be explored to effectively profile these cells *in situ.* There has recently been described a novel OEM system that incorporates multispectral unmixing capabilities [147]. It has already been used to image inside the human alveolar space, spectrally unmixing autofluorescent lung tissue and fluorescent probes to detect bacteria. It is possible this system may be used to mitigate the autofluorescence of alveolar macrophages in the lung and spectrally separate this autofluorescence from exogenous fluorophores introduced to this space [147].

The hypothesis for this chapter is that optical endomicroscopy combined with spectral ratio imaging can image autofluorescent alveolar macrophages label-free and profile their phagocytic activity using labelled targets. The aims were to: characterise imaging of labelled macrophages using an OEM imaging system and develop an assay to validate use of a fluorescent and spectroscopy-based imaging setup to profile phagocytosis of highly autofluorescent alveolar macrophages from smoker's with COPD.

5.2 Profiling phagocytosis with OEM

The work in chapter three described standard techniques to profile the phagocytic activity of macrophages. While it showed to be an effective method of quantifying phagocytosis and any modulators to activity, the flow-cytometric technique is still limited to profiling cells *in vitro*; it can't be used to profile AMs in their native environment. This chapter will outline the preliminary work undertaken to explore how macrophage phagocytosis may be profiled *in situ*, using novel OEM imaging systems.

5.2.1 Using wide-field fibre-based endomicroscopy to image phagocytosis

A three colour, widefield OEM imaging platform – named Versicolour - has been previously described and characterised for the application of imaging the alveolar space [130]. For the initial work to show this system could also profile the phagocytic activity of macrophages, the same assay described in chapter three was carried out. This involved incubating MDMs with apoptotic neutrophils, labelled with pHrodo Green STP ester. In order to visualise all macrophages in the field of view, Syto 61 Red nuclear stain was used to label the macrophages. The pH sensitivity of the pHrodo dye was used as a marker for acidification of a phagolysosome (therefore phagocytosis taking place) and cytochalasin D was again used as a negative control for phagocytic activity. Versicolour has a 470 nm blue LED and a 625 nm red LED to excite pHrodo Green and Syto 61, respectively. The distal end of the imaging fibre bundle (connected to Versicolour) was touched against the surface of the culture plate wells the macrophages were adhered to. Figure 5.1 shows representative images using Versicolour following a 45 min incubation between the macrophages and apoptotic neutrophils. Without cytochalasin D present, there are a number of red-labelled macrophages that also exhibit green fluorescence, indicative of pHrodo Green signal (Figure 5.1A). This green fluorescence is knocked down in the presence of cytochalasin D (Figure 5.1B). This shows that Versicolour, a widefield OEM system

capable of imaging in the alveolar space, is able to differentiate phagocytic macrophages from non-phagocytic using the pH-sensitive pHrodo Green dye as a marker for target internalisation.

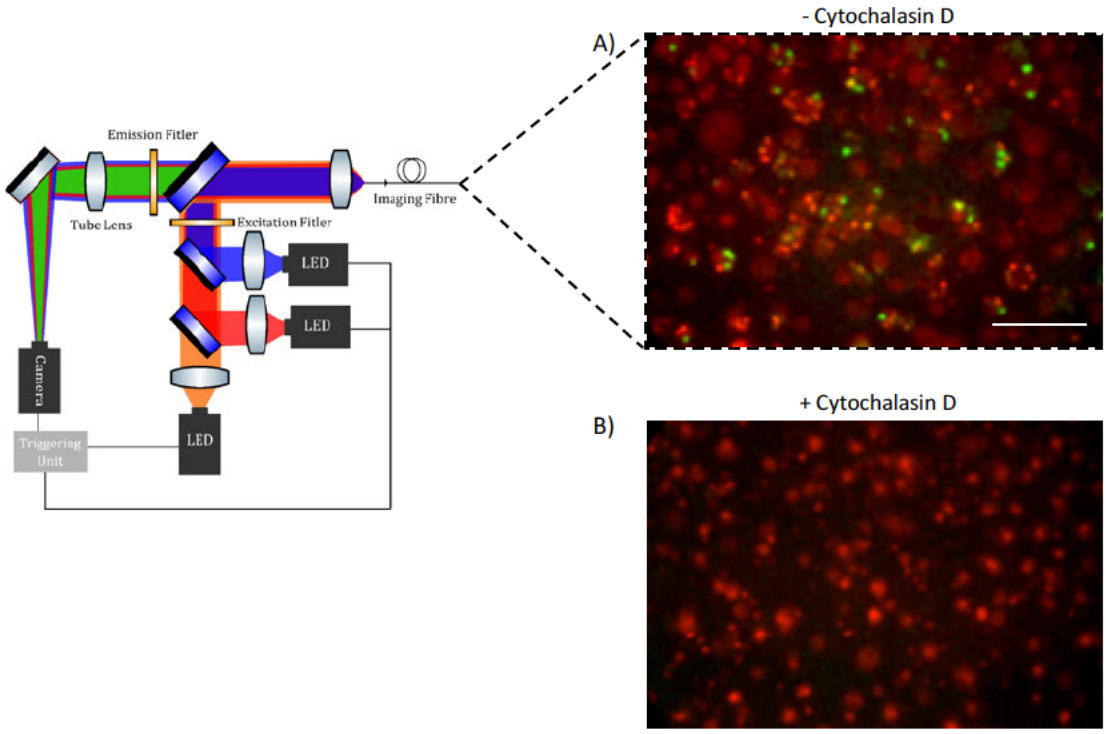

Figure 5.1 Imaging macrophage phagocytosis with OEM. Monocyte-derived macrophages were labelled with Syto 64 Red nuclear stain and incubated for 45 min with apoptotic neutrophils, aged for 20 hr and labelled with pHrodo Green STP Ester. The OEM imaging was performed with Versicolour, a widefield fibre-based imaging system developed by the Proteus Group, University of Edinburgh. Snapshots are representative of imaging videos taken with the distal end of the imaging fibre, of red labelled macrophages adhered to the bottom of the wells of tissue-culture plates. Each snapshot represents the amount of visible pHrodo Green signal +/- 5 µg/ml Cytochalasin D. Images are representative of three independent experiments. Scale bars (white) = 100 µm.

5.3 Spectral Ratio imaging in combination with OEM to image autofluorescent AMs of COPD smokers

While Figure 5.1 shows that it is possible to profile phagocytosis of macrophages using OEM and a pH-sensitive dye, there would in fact be challenges associated with using this technique to profile primary human AMs. More specifically, AMs of current smokers with COPD. These macrophages have previously shown to be highly autofluorescent, with a broad emission profile that would interfere with fluorescent

imaging of phagocytic targets [259]. Any fluorescent imaging in the alveolar space is exacerbated further by the inherent autofluorescence of lung tissue, namely the elastin and collagen structures [131]. The AMs of COPD smokers in particular are often defective in their phagocytic function and are an attractive target for designing therapies to restore activity [83,224]. Therefore, it would be worthwhile to overcome the autofluorescent challenge posed by these macrophages, in order to identify those which also exhibit pHrodo fluorescence as well as their own autofluorescence. This would aid in efforts made in experimental medicine to profile these cells *in situ*.

5.3.1 A novel imaging system combining spectral ratio and OEM

A novel OEM imaging system has been designed and characterised to overcome the autofluorescent challenges faced when imaging in the alveolar space [147]. This system was developed and built by Helen Parker (University of Edinburgh) who has collaborated on work in this chapter to apply the profiling of phagocytosis to her imaging setup. The setup is described in Figure 5.2, with some similarities and differences to the Versicolour widefield OEM. Both systems incorporate an imaging fibre to capture fluorescence and LED excitation sources. However, the spectral ratio (SR) system only uses one colour, a blue 470 nm LED. The SR system also differs from Versicolour by incorporating an 'optical chopper' and a dichroic mirror that splits emitted fluorescent light at 605 nm wavelength. This means that all fluorescent light that is emitted following excitation by the 470 nm LED is split into two channels: the short channel - incorporating all light under 605 nm - and long channel - incorporating light over 605 nm. While many fluorescent objects will be spectrally similar when excited with the same light source, they will have different intensities across the short channel and long channels defined by the SR system. The relative intensities in both channels for a fluorescent object can be transformed into a single spectral ratio value that can be assigned to a false-colour scale. Mapping different spectral ratio values across a new colour scale can enhance the contrast between spectrally similar fluorescent sources [147].

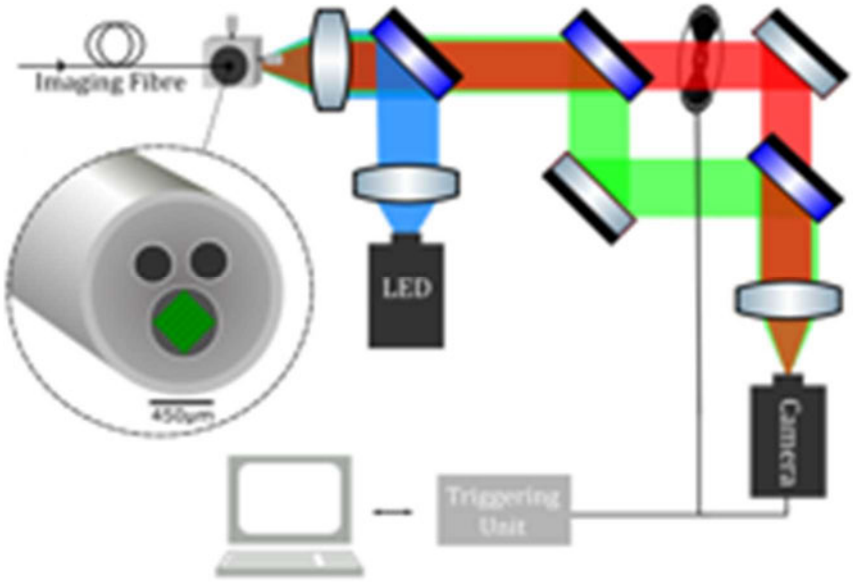

Figure 5.2 A spectral ratio OEM imaging system, developed by Helen Parker, University of Edinburgh. A bespoke imaging fibre is coupled to a blue 470 nm LED via a dichroic mirror. Any emitted fluorescent is passed up from the distal end of the imaging fibre to a second dichroic mirror at 605 nm. Emitted light over 605 nm is passed through an optical chopper and recombined with another dichroic mirror onto a monochromatic camera. A PC is used to control a triggering unit with outputs to the camera and the chopper. Schematic and description adapted with permission from Helen Parker.

This technique has the potential to enhance the contrast between spectrally similar objects in the human lung, namely lung tissue and AMs. Figure 5.3A shows the fluorescent emission spectra overlay of each. The emission of AMs is an average of three populations of macrophages isolated from BAL of COPD patients. The lung tissue emission was taken from the boundary tissue of lung cancer resections. The emission plots show their autofluorescence is similar, both peaking at ~550 nm . The AM emission maintains a slightly higher intensity across the higher wavelengths compared to lung tissue autofluorescence. Figure 5.3B shows what the spectral ratio value of each would be if their intensities were divided into short and long channels at different wavelength cut-offs. The plot shows that the higher the cut-off wavelength, the more distinct their spectral ratio values would be. The cut-off wavelength in the SR system is 605 nm. At this cut-off, the spectral ratio value of lung tissue would be ~2.5 (arbitrary units), while the macrophage value would be ~5.

Therefore, if these values were assigned to a false-colour image scale, they would appear as distinct colours.

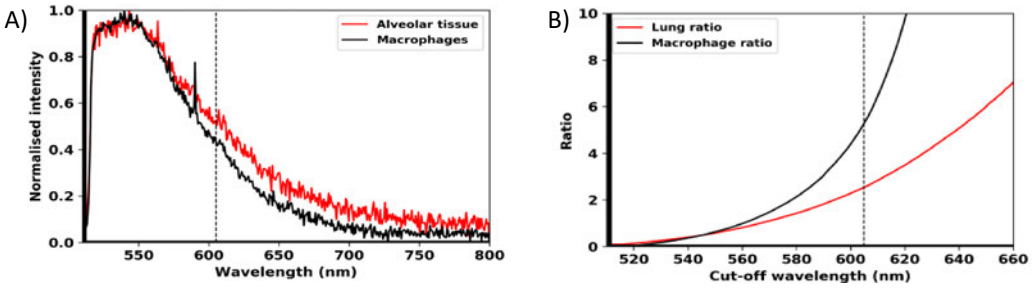

Figure 5.3 Emission spectra of alveolar macrophage and lung tissue autofluorescence. Human alveolar macrophages were freshly isolated from broncho-alveolar lavage fluid and their autofluorescent spectrum was measured using an imaging fibre connected to a commercial spectrometer, exciting at 470 nm. A) The macrophage spectrum was overlaid with the autofluorescent emission spectrum of human lung tissue. The normalised intensity of the two spectra differ at the cut off wavelength of 605 nm (shown on the dotted line). B) The spectral ratio values generated from their emission spectra result in different values for macrophages and lung tissue across a range of wavelengths. At the defined cut-off wavelength of 605 nm, lung spectral ratio value is ~2.5; macrophage spectral ratio value is ~5. The autofluorescence emission of macrophages and lung tissue are representative of emission measurements taken from three independent patient cells. The plot in panel B has been created by Helen Parker.

Figure 5.4 shows how the application of SR works in practice, when imaging the alveolar space of a whole *ex vivo* human lung model. It shows how lung tissue and AMs present when using single-colour fluorescence imaging (Figure 5.4A), then how they can be distinguished when applying SR values and a new colour scale (Figure 5.4B). This demonstrates the potential use of SR imaging to image highly autofluorescent AMs in a COPD lung and differentiate them from other autofluorescence in the region.

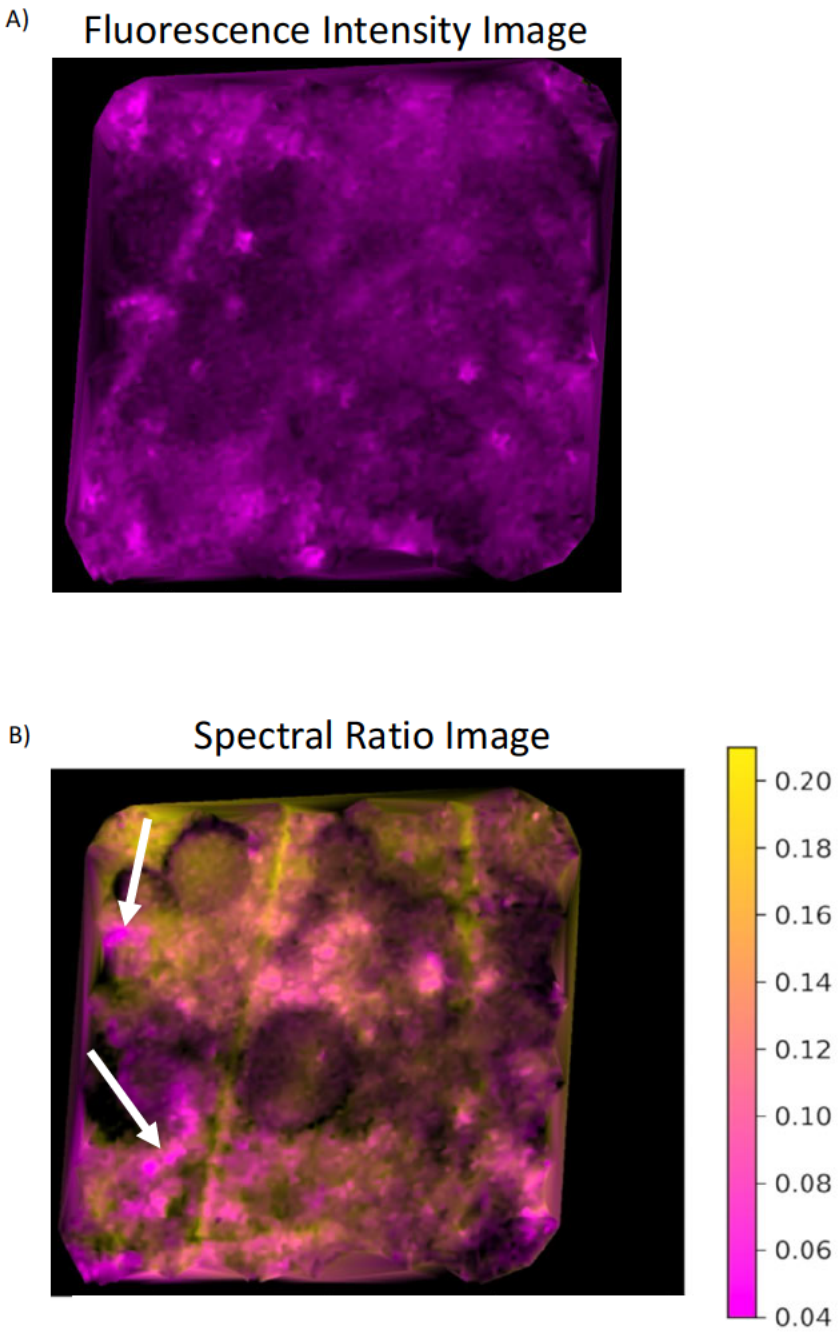

Figure 5.4 Application of spectral ratio imaging to OEM imaging in the alveolar space. A novel OEM imaging system using spectral ratio colour scaling was used with a whole human *ex vivo* lung model. A) Standard fluorescence intensity imaging of the alveolar space from single colour excitation elicits single colour fluorescence. B) Utilising transforming the fluorescence intensities of objects in the FOV to a spectral ratio value and mapping them to a colour scale (shown to the right of the image) enhances the contrast between spectrally similar sources. Arrows show identifiable autofluorescent AMs (pink) against lung tissue (yellow). Imaging performed and images provided by Helen Parker.

5.3.2 Applying spectral ratio OEM with assays to profile phagocytosis of MDMs

Having established the potential for spectral ratio imaging to discern macrophage autofluorescence from lung tissue autofluorescence. The progression of this work was to show that phagocytic macrophages could be identified in a population via internalisation of pHrodo Green-labelled targets. The amount of AM autofluorescence however would cause issues with identifying pHrodo signal within a cell. Therefore, the application of pHrodo emission to the SR setup was considered. Figure 5.5A shows an overlay of pHrodo Green emission, compared to AMs and lung tissue autofluorescence. There is a distinct shape to pHrodo Green emission compared to AMs and lung tissue. While their emission peaks are similar, pHrodo emission intensity is noticeably lower in higher wavelengths. This suggests that, as pHrodo emission intensity is distinct at the cut-off wavelength of 605 nm, a unique spectral ratio value would be applied to pHrodo. Figure 5.5 also shows the relative visibility of pHrodo signal against either AMs Figure 5.5B or lung tissue when factoring each of their SR values (Figure 5.5C) (with a relative visibility value of 1 being indistinguishable). These plots show that it would be possible to multiplex the three emissions of pHrodo, macrophages and lung tissue into separate colours on an SR scale. In principle, this would mean AMs could be identified label-free by their autofluorescence, while any phagocytic cells would present as a different colour as a result of pHrodo Green signal.

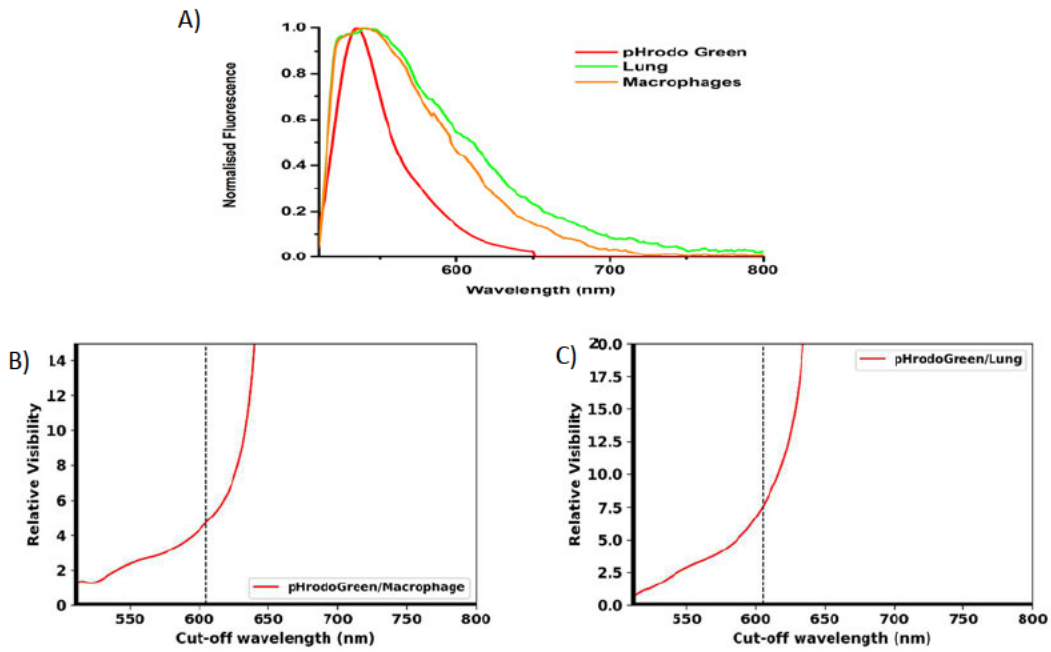

Figure 5.5 Incorporating pHrodo Green emission into spectral ratio imaging. A) The emission profile of pHrodo Green (red), compared to human alveolar macrophages (orange) and lung tissue (green). B) The relative visibility of pHrodo Green as a spectral ratio value compared to alveolar macrophages across a range of potential cut-off wavelengths. the defined cut-off wavelength of 605 nm marked by dotted line. C) The relative visibility of pHrodo Green as a spectral ratio value compared to lung tissue across a range of potential cut-off wavelengths. the defined cut-off wavelength of 605 nm marked by dotted line. Plots in panels B) and C) were created by Helen Parker.

The first step was to apply the SR system to a previously established phagocytosis assay. MDMs were left unlabelled and incubated with apoptotic neutrophils labelled with pHrodo Green. This is a repeat of the assay shown in Figure 5.1 with the Versicolour system. Again, cytochalasin D was used as a negative control for phagocytosis. Figure 5.6 shows the initial imaging of MDMs and apoptotic neutrophils with the SR system. In the absence of cytochalasin D, there is punctate yellow spots in regions of the field of view, while the rest of the image displays fluorescent noise in a pink colour. In the presence of cytochalasin D, the yellow spots are eliminated, leaving just the colour of the noise. This indicates the yellow signal seen represented the spectral ratio value of pHrodo and internalised neutrophils. However, it was not possible to identify all macrophages in the field of view, as the autofluorescence of MDMs is likely not bright enough to be detected by the SR system (Figure 5.6). Therefore, it was not possible to demonstrate the ability of the SR system to distinguish between phagocytic and non-phagocytic macrophages in

a field of view using MDMs. It did, however, help to show that this spectral ratio system can readily image pHrodo signal and provide insight into how that labelling would look in phagocytic cells using this imaging setup.

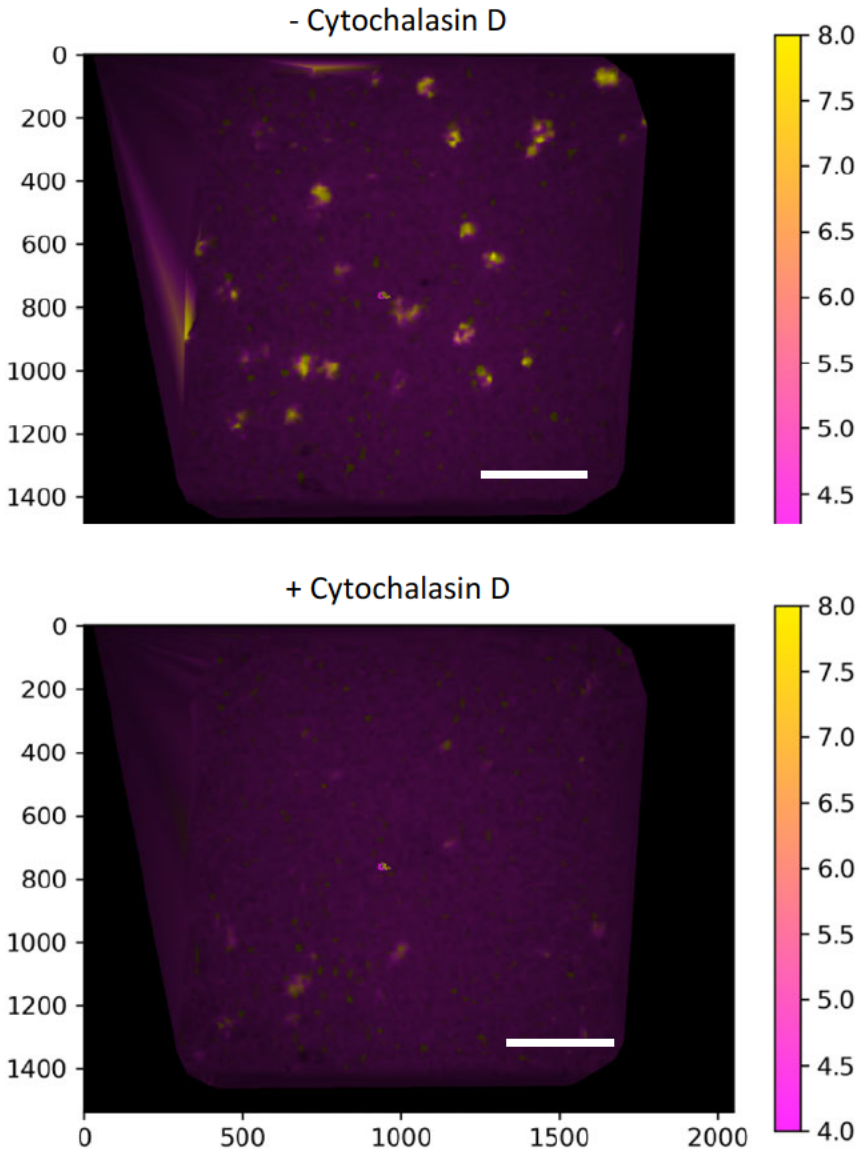

Figure 5.6 Spectral ratio OEM of human monocyte-derived macrophage phagocytosis. Monocyte-derived macrophages were incubated with 10 µg/ml of *E. Coli* pHrodo Green bioparticles for 45 min to allow phagocytosis to take place. Cytochalasin D was used as a negative control for phagocytosis. The MDMs were then imaged with a spectral ratio OEM following incubation. The spectral ratio values in the field of view are represented in a coloured scale bar shown to the right of each image. Representative images of two independent experiments.

5.3.3 Profiling phagocytosis of AMs from a COPD smoker using spectral ratio OEM

The next stage in this workflow was to show that the spectral ratio system can profile the phagocytic activity of highly autofluorescent AMs from a COPD smoker. AMs were isolated from a BAL of a smoker with COPD and adhered to the bottom wells of tissue culture plates. The macrophages were then incubated with apoptotic neutrophils labelled with pHrodo green, with cytochalasin D used as the negative control. Figure 5.7 shows the imaging of macrophages with and without cytochalasin D. There is predominantly one coloured signal shown in the field of view. Based on the low spectral ratio value (corresponding to more red coloured fluorescence) and size of the signal objects, this appears to be the autofluorescence of the AMs. The range of colours is limited in both images, regardless of the presence of cytochalasin D. The histograms below each image also portray the range of spectral ratio values, further indicating there is only one source of signal (from the AM autofluorescence). This means there does not appear to be any pHrodo signal present in the cytochalasin D^- condition (Figure 5.7). Therefore, while the SR system could identify alveolar macrophages, label-free, based on autofluorescence, it was not possible to differentiate phagocytic cells due to a lack of pHrodo signal. It is possible that the phagocytic function of these cells was defective to the point where no cells were phagocytically active during this assay.

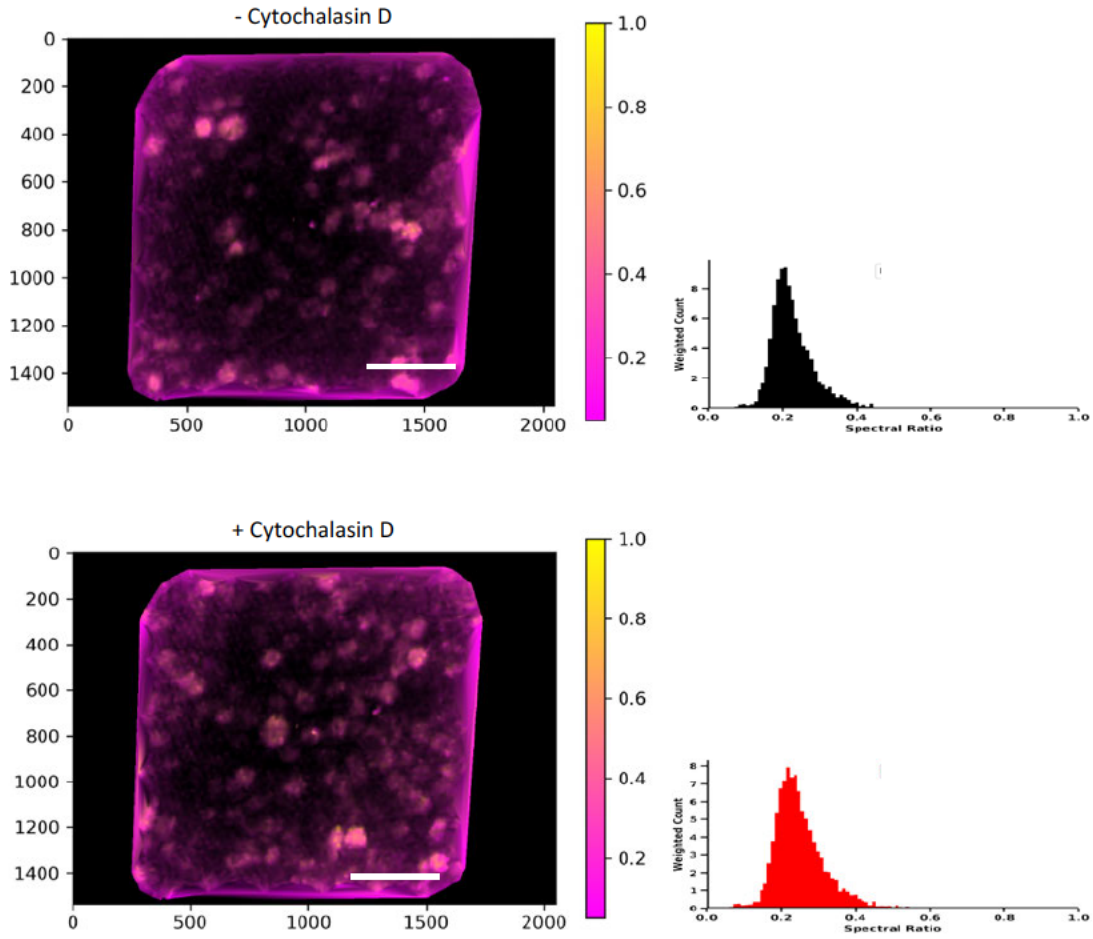

Figure 5.7 Spectral ratio OEM of primary human alveolar macrophages from a smoker with COPD. Alveolar macrophages were isolated from a broncho-alveolar lavage and incubated with 10 µg/ml of *E. Coli* pHrodo Green bioparticles for 45 min to allow phagocytosis to take place. Cytochalasin D was used as a negative control for phagocytosis. The spectral ratio values in the field of view are represented in a coloured scale bar shown to the right of each image. Histograms below each snapshot portrays the range of spectral ratio values in the field of view. Representative images of two independent experiments. Scale bars (white) = 100 µm.

5.3.4 Using a cell dye to mimic macrophage autofluorescence in MDMs for validation of spectral ratio profiling of phagocytosis

The previous assays showed that, while it is possible to image pHrodo signal inside MDMs using the SR system, it was not possible to show that the system can identify this signal amongst spectrally similar cell autofluorescence, as MDM autofluorescence was too weak to be imaged. The SR system could readily image smoker's AMs, though it could not identify pHrodo signal, possibly due to the phagocytic defect often associated with these cells [221,83]. Therefore, an 'in-between'

model was considered to aid in validating the SR system. This involved labelling healthy MDMs, already established as phagocytic, with a dye that would mimic the fluorescence emission of alveolar macrophages. The dye used was Syto 81 Orange nuclear dye. This dye was chosen because it can be excited to the same extent as pHrodo Green using the 470 nm excitation source (Figure 5.8A). Similar to AM autofluorescence, the emission spectrum of Syto 81 is noticeably broader than pHrodo green, with higher intensity at higher wavelengths, particularly at the 605 nm cut-off used by the SR system (Figure 5.8A). This would mean that Syto 81 could be excited similarly to pHrodo with the spectral ratio system yet yield a different spectral ratio value. MDMs were labelled with Syto 81 then incubated with apoptotic neutrophils labelled with pHrodo Green. Figure 5.8B shows the imaging of MDMs alone, using their Syto 81 label to be identified. Though the resolution is poor, there is fluorescent signal shown from the cells. Figure 5.8C shows imaging with labelled MDMs following incubation with labelled apoptotic neutrophils. There are differences to the colour profile in this image. In addition to the pink colour, representing the spectral ratio value of the Syto 81-labelled macrophages, there is yellow signal indicating spectral ratio values of pHrodo Green (as the yellow values represent fluorescent signal of lower wavelengths). This indicates it is possible to identify all the macrophages in a field of view and discern which are phagocytic.

The application of cytochalasin D was once again used as the established negative control for this phagocytosis assay. Figure 5.9 shows the comparison in spectral ratio imaging of Syto 81-labelled macrophages together with pHrodo-labelled neutrophils. Despite the presence of cytochalasin D, there is still a combination of spectral ratio value colours in the image. As previous work in this thesis has repeatedly validated cytochalasin D as a block on phagocytosis and subsequent pHrodo signalling, it would have to be inferred that the yellow signalling seen in the images may not actually be the result of pHrodo signal.

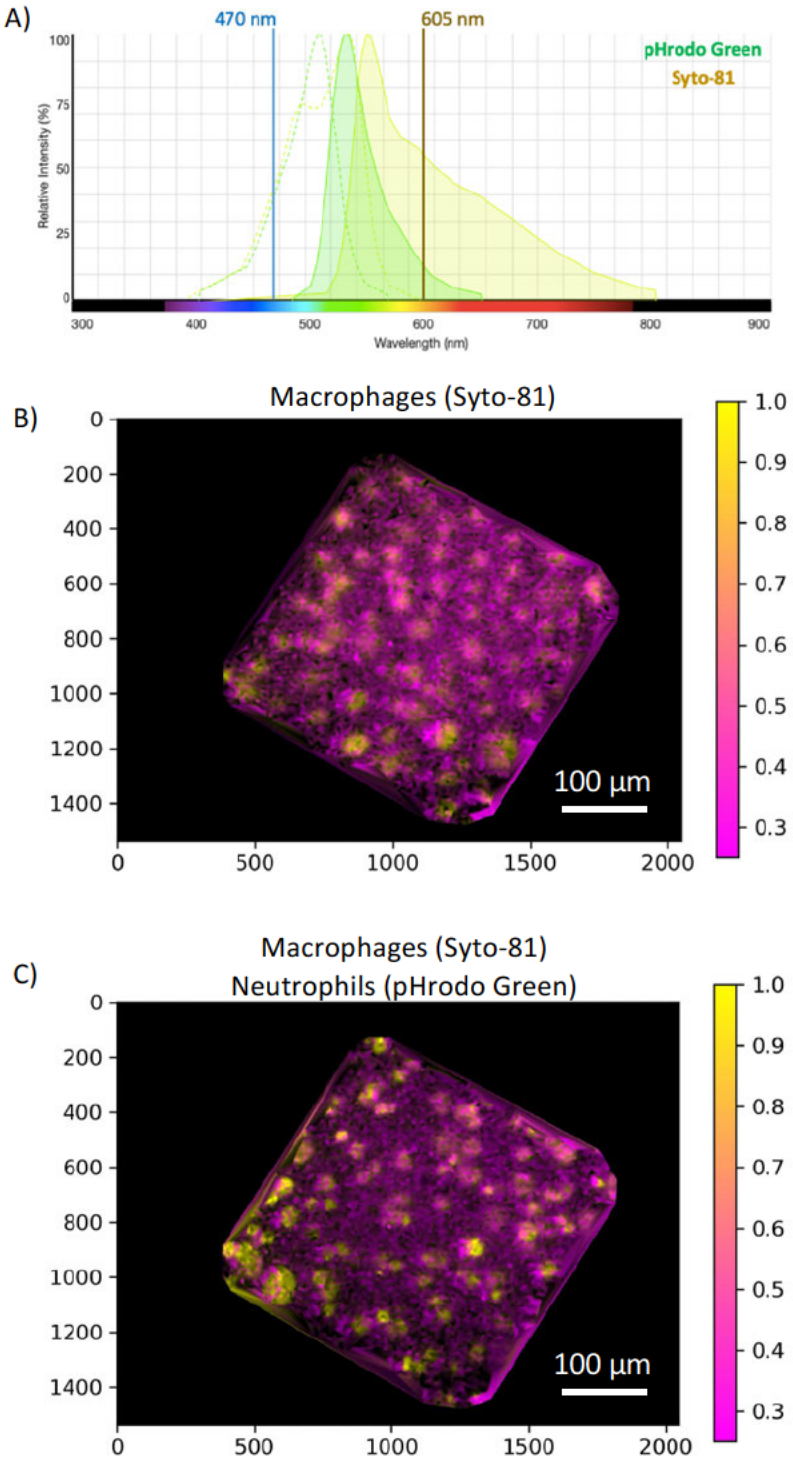

Figure 5.8 Spectral ratio OEM of labelled Monocyte-derived macrophages as a model for alveolar macrophage autofluorescence. A) The excitation/emission spectra of pHrodo Green (green) and Syto 81 (yellow). Each fluorophore would excite at 470 nm with equivalent intensity. Syto 81 has a higher relative intensity of emission at wavelengths over 605 nm. B) Monocyte-derived macrophages were labelled with Syto 81 Orange nuclear dye and imaged with the spectral ratio system to determine the spectral ratio characteristics of the labelled cells C) Monocyte-derived macrophages were incubated with 10 µg/ml of *E. Coli* pHrodo Green bioparticles for 45 min to allow phagocytosis to take place. The MDMs were then imaged with a spectral ratio OEM following incubation. The spectral ratio values in the field of view are represented in a coloured scale bar shown to the right of each image. Representative images of two independent experiments.

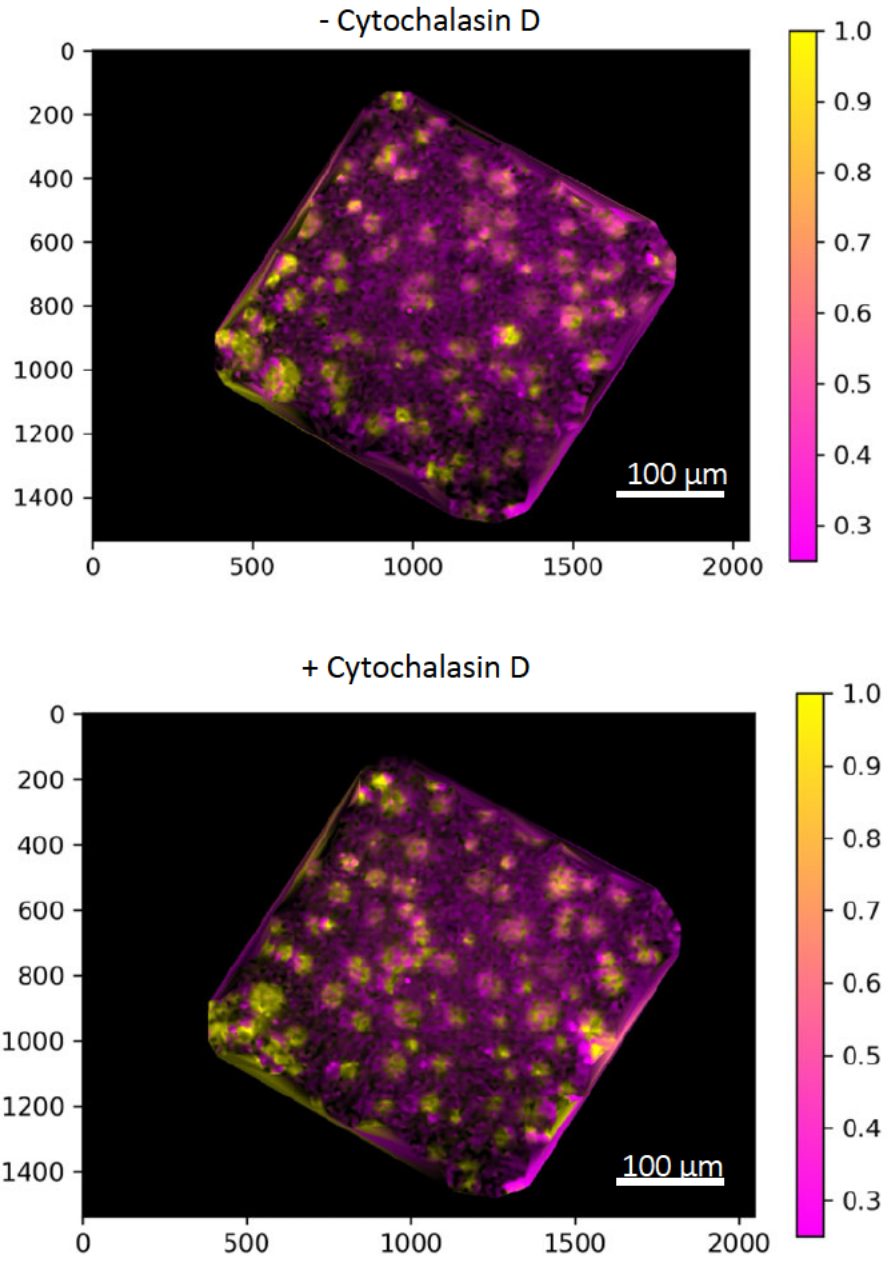

Figure 5.9 Effect of cytochalasin D on Spectral ratio OEM of labelled Monocyte-derived macrophages. Monocyte-derived macrophages were incubated with 10 µg/ml of *E. Coli* pHrodo Green bioparticles for 45 min to allow phagocytosis to take place. Cytochalasin D was used as a negative control for phagocytosis. The MDMs were then imaged with a spectral ratio OEM following incubation. The spectral ratio values in the field of view are represented in a coloured scale bar shown to the right of each image. Representative images of two independent experiments.

5.4 Discussion

The work described in this chapter sought to provide early proof of concept for profiling human macrophage activity *in situ.* A three-colour OEM was used to image labelled MDMs, even detecting pHrodo-labelled neutrophils within macrophages as a marker of phagocytic activity. A similar OEM setup, with multispectral acquisition properties was used to explore potential techniques to overcome autofluorescence in human lung when profiling macrophages in this space.

5.4.1 Imaging macrophages using OEM

The three-colour imaging capabilities of Versicolour allow for multiplexing of probes to fluorescently label different targets. This could mean specifically labelling different cell types in the alveolar space. There are already probes developed by our group to label activated neutrophils and live bacteria using OEM in the whole lung model [136,134,135]. Using versicolour to show the capability to perform cellular imaging with an *in situ* imaging system – and coupling that with a imaging fibre that has a capillary channel to deliver fluorescent probes – opens up new possibilities of studying cellular interactions in the lung. A green neutrophil activation probe previously reported could be used in conjunction with the MR-nanobody described in chapter four of this thesis to study macrophage-neutrophil interactions in the alveolar space [136]. Probes to specifically label bacteria in the human lung, also developed by the Proteus group, could be coupled with the MR-probe to further study host-pathogen interactions [135,134].

5.4.2 Validation of spectral ratio OEM imaging of autofluorescent macrophages

This chapter begins to establish a new application for the novel SR imaging system. It has already been characterised with distinguishing labelled bacteria from human lung tissue [147]. The work in this chapter sought to apply this technique to primary human macrophages and a labelled phagocytic target. Modelling of the emission spectra of human macrophages, pHrodo Green as the phagocytic marker, and human lung tissue with each of their SR values showed the potential of spectrally unmixing these largely overlapping fluorescent sources.

However, a key challenge emerged when attempting to validate the SR imaging system: using phagocytic cells that were also autofluorescent enough to be imaged label-free. It was possible to validate the system image pHrodo signal (inferred as being inside a macrophage), or primary alveolar macrophages via autofluorescence, but it was not possible to image both simultaneously. There was either an issue with detecting cellular autofluorescence of healthy MDMs – previously established as being phagocytic – or difficulty detecting phagocytosis in highly autofluorescent primary macrophages that likely had a phagocytic defect. One workaround for this was to label the healthy MDMs with a cell dye that had similar spectral properties to primary macrophage autofluorescence. Another option could have been to isolate a subset of healthy MDMs that exhibited higher amounts of autofluorescence. One study has explored optimising MDM culture conditions to isolate this subset [252]. Their rationale was that *in vitro* MDMs typically display a phenotype that makes them very adherent to the surfaces they grow on. However, the non-adherent cells in an MDM population that remained viable, displayed higher amounts of autofluorescence. These cells also shared microscopic characteristics of alveolar macrophages, such as a much more granular cytoplasm [252,255]. This suggests a potential avenue to explore for working with viable, autofluorescent macrophages that can be more representative of AM autofluorescence.

The emission spectra of smoker's macrophages align with a study also looking at the spectral characteristics of these cells [259]. The emission spectra of lung macrophages from several patients followed a similar pattern: peaking at 550nm but having a broad spectrum that stretched to 700 nm [259]. This spectrum is similar to that of tobacco tar components [259]. This same study also found that this high level of autofluorescence was resistant to photobleaching, and non-fluorescent macrophages could become autofluorescent when exposed to serum from a smoker in culture [259].

While the use of Syto 81 helped image non-phagocytic MDMs and show a range of spectral ratio values in the field of view, the image data when using cytochalasin D made it difficult to determine if the range of values included pHrodo signal. Addition of pHrodo-labelled apoptotic neutrophils did result in a change in spectral ratio values (and ultimately the false-colouring) of the macrophages in the field of view. However, this was unchanged in the presence of cytochalasin D. Cytochalasin D has been well established throughout this thesis as a negative control for phagocytosis, validated by knock-down of pHrodo Green signal in macrophages. However, this effect was not repeated using the spectral ratio system with Syto 82-labelled MDMs. This could be because cytochalasin D may have an effect on the spectral properties of the MDMs. Another, more likely, reason is cytochalasin D had an impact on the fluorescence of Syto 81, ultimately changing its spectral ratio value. Alternative controls for phagocytosis could be used, such as placing the cells at 4 °C, to determine if cytochalasin D had an impact on the spectral ratio values of the MDMs.

5.4.3 Alternative OEM systems for in situ profiling of human macrophages

The challenge the SR system sought to overcome was the abundance of autofluorescence present in the alveolar space. This signal would interfere with specific labelling of macrophages and/or introducing labelled phagocytic targets to profile their activity. While it was not possible in the scope of this thesis, there are alternative OEM systems, also capable of imaging in the alveolar space *in situ*, that could take a different approach to mitigating autofluorescence. A novel two-colour OEM system has been developed by our group to utilise fluorescent lifetime, rather than intensity, as a form of imaging [260]. Fluorescence lifetime imaging microscopy (FLIM) has been well established and used in clinical settings to distinguish between spectrally similar fluorescent sources [261,246]. Rather than intensity, FLIM systems incorporate sensors that measure the decay of fluorescence – usually over a nanosecond timeframe – from fluorescent sources following excitation [260]. This property is unique to different fluorophores or and endogenous fluorescent proteins [262]. A fibre-based OEM system has already been used to image human lung tissue and distinguish endogenous fluorescence from fluorescent probes labelling live bacteria [260]. The ability to distinguish between macrophage activated states using FLIM has been previously described [243]. For the purpose of profiling phagocytic activity, it is likely that the autofluorescence of AMs would have a different FLIM signature to labels of phagocytic targets, such as pHrodo. Fluorescence lifetime is an environmentally sensitive property, which is altered in different conditions, such as changes to pH [263]. It is feasible that, depending on the sensitivity of a detector for changes in lifetime, the FLIM signature of human macrophages may dynamically change following phagocytosis. This may open up an entirely label-free method of profiling phagocytosis and would be worthwhile to explore.

5.4.4 Limitations and conclusions to this chapter

While this chapter did take an entirely novel approach to profiling macrophages, there were notable limitations that, if addressed, would progress this work closer to becoming a valuable tool in experimental medicine. First, the use of MDMs proved difficult when validating the spectral ratio system for profiling highly autofluorescent macrophages. The MDMs exhibited minimal amounts of autofluorescence. There was limited success in using Syto 81 to mimic AM autofluorescence. A more biologically relevant model should have been explored, such as isolated more fluorescent subset of MDMs, or instilling cigarette smoke products into the MDM culture [252,259]. However, it would have to be determined if each of these methods has any impact on the phagocytic ability of MDMs, which is the prerequisite for using them as a model for this assay. Given the effect smoking appears to have on alveolar macrophage phagocytosis, instilling the products of cigarette smoke to MDMs may give the same effect. The second limitation to this workflow was the isolation of primary human AMs. There were noticeable variations in cell numbers and viability between BAL samples. This was determined as being the result of each lavage procedure not always being carried out in optimal conditions for subsequent isolation of cells. This led to inconclusive assays as the AMs were either too low in number or not viable following adherence to a culture dish. Third, the *in vitro* assay for validating OEM imaging could have been optimised further. The imaging was carried out in the wells of tissue culture plates, where the macrophages were adhered. The transparent plastic dishes contributed to some reflected light during the OEM imaging, particularly when using the spectral ratio system, causing a lot of noise in the eventual images.

Nonetheless, the work in this chapter describes the first use of OEM in the context of imaging dynamic biological events. It demonstrates the potential of using these types of imaging systems in the application of profiling macrophage activity. The

development of these assays and ultimate progression into a whole lung model would demonstrate the use this application could have in experimental medicine. Being able to profile alveolar macrophages *in situ*, in real-time can advance our understanding of how these cells may respond to therapies designed to alter their activity.

Chapter Six: Summary and Future Directions

6.1 Summary of Thesis chapters

The work in this thesis has concentrated on advancing methodologies aimed at profiling macrophages into translational assay systems. The work first established *in vitro* systems to profile human monocyte-derived macrophages, before progressing these systems to use methods that could be applied to studies in experimental medicine. The approaches taken involved characterisation of a mannose receptor fluorescent nanobody to selectively label macrophages and using optical endomicroscopy platforms to profile macrophage phagocytic activity. The findings from each chapter are briefly summarised below.

6.1.1 Chapter three summary

The purpose of the work in chapter three was to establish an *in vitro* system to differentiate human peripheral blood monocytes into macrophages. Assays using bench-top optical systems (flow cytometry and confocal microscopy) were used to establish the surface receptor phenotype and phagocytic activity of the MDMs. This model was to be used throughout the rest of the work in this thesis to explore novel ways to translate profiling of human macrophage phenotype and activity.

• The differentiation of peripheral blood monocytes into macrophages was determined by cell morphological changes and changes to the receptor profile. Notably, differentiated macrophages expressed CD80, CD163 and CD206 (the mannose receptor) while their monocyte precursors did not

• The MDMs demonstrated plasticity in their surface receptor expression following polarisation with IFNγ, LPS and IL-4. Notably, polarisation with IFNγ and LPS increased expression of pro-inflammatory marker CD80, while IL-4 polarisation increased expression of pro-resolution marker CD163

• The use of fluorescent polystyrene microspheres as a phagocytic target for the MDMs, caused a coincidence effect signal when the MDMs were analysed using flow cytometry. Using cytochalasin D as a negative control for phagocytosis showed little effect of reducing the microsphere signal in MDMs

• The use of fluorescently labelled E. coli and apoptotic neutrophils served as more biologically relevant and effective targets for a phagocytic assay system. Using flow cytometry, it was possible to quantify phagocytic cells in the MDM population and block the phagocytic signal using cytochalasin D

• A time-series of a macrophage and apoptotic neutrophil co-culture using confocal microscopy and a heated stage allowed for the study of macrophage/target interactions in real time. This system was developed further by using spinning disc confocal microscopy and labelling apoptotic neutrophil targets with a pH sensitive dye for easier tracking of phagocytic activity

• The flow cytometry phagocytosis assay system was used to track the modulation of phagocytic activity of macrophages by pharmacological agents. The glucocorticoid Dexamethasone augmenting efferocytosis of apoptotic neutrophils, while the Nrf-2 agonist sulforaphane did not increase phagocytosis of bacteria

6.1.2 Chapter four summary

Chapter four sought to develop profiling of macrophages based on receptor expression, by using a fluorescent nanobody targeting the MR that could be used for *in vivo* studies.

• The MR-nanobody, following conjugation to sulphonated Cyanine 5 dyes, was able to label MDMs with a high signal to noise ratio, using nanomolar amounts of nanobody with no wash step required

• The staining pattern of the MR-nanobody when imaged with confocal microscopy was similar to a commercial anti-CD206 mAb

• The MR-nanobody could selectively label MDMs over monocytes and A549 cells (acting as a alveolar epithelial cell model) but showed off-target labelling of human neutrophils, albeit a subset of neutrophils that may be activated or even necrotic

• The MR-nanobody labelled primary human alveolar macrophages from a broncho-alveolar lavage sample, demonstrating potential use to label AMs *in vivo*

• Stimulating MDMs with IFNγ, LPS and IL-4 did not alter the labelling characteristics of the MR-nanobody, suggesting it could not differentiate between polarised macrophages

• Studies into the labelling characteristics of the MR-nanobody showed that it initially labelled the membrane of macrophages, before being internalised into the cytoplasm. Cytochalasin D reduced the amount of labelling by the MR-nanobody

• Using excess mannan as a known MR ligand did not block MR-nanobody labelling and provided inconclusive results about the target specificity of the MR-nanobody

• The MRC1 gene, coding for the MR, was successfully transfected into CHO cells, as determined by flow cytometric labelling with a anti-CD206 mAb, but this did not prompt labelling by the MR-nanobody following transfection

6.1.3 Chapter five summary

Chapter five focussed on the application of novel OEM platforms, designed to image in the alveolar space *in situ,* to profiling the phagocytic activity of macrophages. This

involved two systems: one using standard fluorescence intensity imaging to image phagocytic macrophages, and another utilising a greater detail of spectral analysis to image autofluorescent alveolar macrophages.

• Versicolour, a fluorescence widefield OEM platform developed by the Proteus group (University of Edinburgh), was able to perform two-colour imaging of labelled MDMs and identify phagocytic cells based on fluorescence of separately labelled apoptotic neutrophils. Phagocytic cells were identified by fluorescence of pH-sensitive pHrodo labelling of apoptotic neutrophils, the signal for which was blocked by cytochalasin D.

• A novel OEM platform was developed by Helen Parker (University of Edinburgh) to enhance the contrast of spectrally similar objects via spectral ratio imaging: calculating specific spectral ratio values of objects determined by unique fluorescence emission profiles

• The SR system could differentiate between the autofluorescence of alveolar macrophages and lung tissue by assigning different SR values due to distinct fluorescence emission spectra

• The SR system could image phagocytic MDMs in an *in vitro* assay system, through detecting pHrodo signal of internalised E. coli. This signal was validated as indicative of phagocytosis due to blocking with cytochalasin D.

• The SR system could image human alveolar macrophages in an *in vitro* setting based solely of autofluorescence but could not identify phagocytic cells due to a lack of pHrodo signal from phagocytic targets.

• Using Syto-81 nucleic acid stain labelling of MDMs to model AM autofluorescence, the SR system showed potential to differentiate between phagocytic and non-

phagocytic macrophages even with spectrally similar fluorescence signals of Syto 81 and pHrodo Green. However, cytochalasin D was not able to block what was assumed to be pHrodo signal, thereby not validating successful profiling of phagocytic cells.

6.2 Limitations and Future Directions

6.2.1 Modelling and profiling alveolar macrophages

A prominent challenge for *in vitro* studying of macrophage phenotype activity is using a representative model for the macrophage subset that is the focus of the work- in the case of this thesis it was the alveolar macrophage. As discussed in more detail in chapter three, there is a great deal of heterogeneity in the phenotypes of different macrophage populations. The cell surface receptor expression profile of AMs is likely unique to that population and may not be clearly reflected by *in vitro* monocyte-derived macrophages or differentiated monocytic cell lines. Had it been possible to acquire more broncho-alveolar samples during this study, I would have sought to characterise in more detail the receptor expression profile of AMs. As these AMs would likely be from COPD patients, receptor profiling would therefore reflect AM receptor expression in COPD pathology. This would have helped validate the choice of receptor targets for probes to label AMs during COPD, as well as provide greater detail of phagocytic receptor expression on COPD AMs.

One challenge of profiling primary AMs *in vitro* is the high levels of autofluorescence from these cells. When using optical imaging platforms to profile cell phenotype and activity, the AM autofluorescence can impede the use of fluorescent mAb to label surface receptors, or labelled targets for phagocytic activity. The purpose of some of the work in chapter five was to demonstrate how spectral ratio imaging can mitigate AM autofluorescence with *in situ* imaging systems, however optical systems with similar properties would be required for more detailed studies *in vitro*. There are now

spectral flow cytometry systems that would suit these studies. Spectral flow cytometry takes advantage of multispectral and hyperspectral analysis of cells, gaining a detailed spectral profile on a single cell basis. These systems can define the spectral fingerprint of an autofluorescent AM and increase the detection of fluorescent mAb, other probes, or labelled phagocytic targets. These *in vitro* systems would improve understanding of COPD AM phagocytic activity. By mitigating AM autofluorescence in the detection of phagocytic targets, more detailed studies on the phagocytic defect of COPD AMs could be performed, including their response to pharmacological manipulation *in vitro.*

Alternative bench-top imaging platforms are also available to mitigate AM autofluorescence, such as confocal microscopes which utilise fluorescence lifetime as well as intensity. One such system has been in development by the Proteus Group (University of Edinburgh) which encompasses an inverted microscope with a heated stage. The use of FLIM has become an attractive modality in the study of macrophages [243,245]. This bench-top FLIM platform would allow dynamic FLIM imaging of macrophage phagocytosis for the first time. This could open up new avenues for profiling macrophages based on their optical fingerprint (fluorescence intensity, spectroscopy, fluorescence lifetime).

6.2.2 Use of macrophage probes for *in vivo* use

The study of potential receptor probes to be used *in vivo* for AMs would also require detailed analysis of the receptor profiles of AMs during COPD, in order to validate target expression for the probe. In the context of this thesis, the level of MR expression on COPD AMs was not established (though the MR-nanobody did label isolated COPD AMs). The suitability of the MR, or any other receptor as a probe

target, should be evaluated in line with the ultimate purpose of a macrophage probe. For example, the mannose receptor is a suitable target to selectively label macrophages over other cell types, though may not provide further phenotypic information. In the literature, the MR is often considered a marker for macrophages in an anti-inflammatory state. However, from my studies of MDMs *in vitro*, the expression of the MR remained heterogenous following MDM differentiation with distinct polarising agents or pharmacological treatment. This indicated that the MR may not be the most suitable receptor probe target for profiling the activated state of a macrophage.

Another consideration not explored in the work in chapter four was the effect on macrophage function probe labelling had. The MR-nanobody selectively labelled macrophages and appeared to be actively internalised by the cells. Further work should focus on if the MR-nanobody altered the phenotype or function of labelled macrophages. This should include evaluating changes to receptor expression, cell viability, and phagocytic activity following MR-nanobody labelling.

The end purpose of *in vivo* macrophage probes was to be used with OEM platforms for *in situ* labelling of macrophages. Therefore, the imaging characteristics of the MR-nanobody or other candidate probes with OEM platforms would be required. For example, the limit of detection (LoD) for the concentration of probe used in *in vitro* systems, using sensitive optical detection methods such as flow cytometry and confocal microscopy, may not align with the LoD of OEM platforms. In addition, the labelling characteristics with OEM platforms and the MR-nanobody should be carried out with model systems more relevant to the alveolar space. This could involve imaging labelled macrophages on *ex vivo* lung tissue, or in perfused whole lung models that have been established by the Proteus Group.

6.2.3 OEM to profile macrophages *in situ*

While the use of OEM platforms to perform *in situ* profiling of macrophages can be a great asset to methods of experimental medicine, some limitations may hinder the development of these studies. A notable limitation is the small field of view (FOV) created by the bespoke imaging fibre bundles that allow for *in situ* imaging. Due to size restrictions, the total FOV in these bundles is ~450 µm across. This would ultimately provide a limited area to profile macrophage activity in the alveolar space, resulting in a likely unrepresentative population of cells and an increased chance of missing important events such as phagocytosis. As this technology progresses, there will be approaches taken to overcome this limited FOV. Incorporating operator-controlled distal tip steering of the fibre imaging bundle will provide greater control of regional exploration in the alveolar space. This could allow mosaicking of multiple FOV to generate a more representative picture of an AM population.

As OEM platforms become paired with optical probes or phagocytic targets to profile macrophages *in situ*, effective quantification of these fluorescence-based assays would be required to provide objective information of macrophage activity. The development of machine learning algorithms to detect labelled bacteria in the human lung following OEM imaging has been previously described [264]. Similar approaches would be required with the profiling of macrophages in the alveolar space to extract a detailed optical fingerprint of macrophage activity in this space.

As has been described in chapter five of this thesis, the main challenge of optical imaging in the human lung *in situ* is the high amounts of autofluorescence - from lung tissue and AMs – that could interfere with detection of optical probes and labelled phagocytic targets. The potential of the SR system described in chapter five and in a published study represents the ability to mitigate this autofluorescence in the lung and carry out multiplexed imaging of multiple fluorophores, even when they are spectrally similar. Given more time, I would have expanded the work in chapter five to demonstrate the multiplexing capabilities of the SR system,

performing imaging on human lung tissue, combined with autofluorescent cells with the MR-nanobody or phagocytic targets. This would show it is possible to overcome the multiplexing limitations of optical imaging in the alveolar space. Building on this, the work would progress onto using a perfused whole lung model to demonstrate the ability to perform real time profiling of macrophage phenotype and phagocytic activity *in situ* using a model system as biologically relevant as it can be to image in a live human lung. Such an assay system would be of high value to monitoring the response of AMs to pharmacological stimulation while still in the 3D alveolar space, rather than in a highly controlled *in vitro* setting.

6.3 Conclusion

The work in this thesis has provided the foundation to profiling macrophages in the human lung. Taking forward optical assay systems, designed to profile the receptor expression of macrophages and their phagocytic activity, and combining them with optical probes and imaging platforms capable of performing *in situ* imaging, it will be possible to expand understanding of macrophage activity in the human lung. These methodologies could ultimately become an influential approach of experimental medicine to profile AMs *in situ* and monitor pharmaceutical effects on their activity.

References

1. Tracy, R. P. The five cardinal signs of inflammation: Calor, dolor, rubor, tumor… and penuria (apologies to Aulus Cornelius Celsus, de medicina, c. A.D. 25). *Journals Gerontol. - Ser. A Biol. Sci. Med. Sci.* (2006). doi:10.1093/gerona/61.10.1051
2. Doherty, D. E., Downey, G. P., Worthen, G. S., Haslett, C. & Henson, P. M. Monocyte retention and migration in pulmonary inflammation. Requirement

for neutrophils. *Lab. Investig.* (1988).

3. Lee, W. L., Harrison, R. E. & Grinstein, S. Phagocytosis by neutrophils. *Microbes Infect.* (2003). doi:10.1016/j.micinf.2003.09.014
4. Geissmann, F., Manz, M. G., Jung, S., Sieweke, M. H., Merad, M. & Ley, K. Development of monocytes, macrophages, and dendritic cells. *Science* **327,** 656–61 (2010).
5. Akira, S., Uematsu, S. & Takeuchi, O. Pathogen recognition and innate immunity. *Cell* (2006). doi:10.1016/j.cell.2006.02.015
6. Sica, A. & Mantovani, A. Macrophage plasticity and polarization: In vivo veritas. *J. Clin. Invest.* (2012). doi:10.1172/JCI59643
7. Meagher, L. C., Savill, J. S., Baker, a, Fuller, R. W. & Haslett, C. Phagocytosis of apoptotic neutrophils does not induce macrophage release of thromboxane B2. *J. Leukoc. Biol.* **52,** 269–273 (1992).
8. Savill, J. S., Wyllie, A. H., Henson, J. E., Walport, M. J., Henson, P. M. & Haslett, C. Macrophage phagocytosis of aging neutrophils in inflammation. Programmed cell death in the neutrophil leads to its recognition by macrophages. *J. Clin. Invest.* **83,** 865–875 (1989).
9. Ahn, G. O., Tseng, D., Liao, C. H., Dorie, M. J., Czechowicz, A. & Brown, J. M. Inhibition of Mac-1 (CD11b/CD18) enhances tumor response to radiation by reducing myeloid cell recruitment. *Proc. Natl. Acad. Sci. U. S. A.* (2010). doi:10.1073/pnas.0911378107
10. Fadok, V. A., Bratton, D. L., Konowal, A., Freed, P. W., Westcott, J. Y. & Henson, P. M. Macrophages that have ingested apoptotic cells in vitro inhibit proinflammatory cytokine production through autocrine/paracrine mechanisms involving TGF-β, PGE2, and PAF. *J. Clin. Invest.* (1998). doi:10.1172/JCI1112
11. Voll, R. E., Herrmann, M., Roth, E. A., Stach, C., Kalden, J. R. & Girkontaite, I. Immunosuppressive effects of apoptotic cells [9]. *Nature* (1997). doi:10.1038/37022
12. Auffray, C., Sieweke, M. H. & Geissmann, F. Blood Monocytes: Development,

Heterogeneity, and Relationship with Dendritic Cells. *Annu. Rev. Immunol.* (2009). doi:10.1146/annurev.immunol.021908.132557

13. Davies, L. C., Jenkins, S. J., Allen, J. E. & Taylor, P. R. Tissue-resident macrophages. *Nat. Immunol.* (2013). doi:10.1038/ni.2705
14. Hashimoto, D., Chow, A., Noizat, C., Teo, P., Beasley, M. B., Leboeuf, M., Becker, C. D., See, P., Price, J., Lucas, D., Greter, M., Mortha, A., Boyer, S. W., Forsberg, E. C., Tanaka, M., van Rooijen, N., García-Sastre, A., Stanley, E. R., Ginhoux, F., Frenette, P. S. & Merad, M. Tissue-resident macrophages self-maintain locally throughout adult life with minimal contribution from circulating monocytes. *Immunity* (2013). doi:10.1016/j.immuni.2013.04.004
15. Mills, C. D., Kincaid, K., Alt, J. M., Heilman, M. J. & Hill, A. M. M-1/M-2 Macrophages and the Th1/Th2 Paradigm. *J. Immunol.* (2000). doi:10.4049/jimmunol.164.12.6166
16. Italiani, P. & Boraschi, D. From monocytes to M1/M2 macrophages: Phenotypical vs. functional differentiation. *Front. Immunol.* **5,** 1–22 (2014).
17. Gordon, S. Alternative activation of macrophages. *Nat. Rev. Immunol.* **3,** 23–35 (2003).
18. Pesce, J. T., Ramalingam, T. R., Mentink-Kane, M. M., Wilson, M. S., Kasmi, K. C. E., Smith, A. M., Thompson, R. W., Cheever, A. W., Murray, P. J. & Wynn, T. A. Arginase-1-expressing macrophages suppress Th2 cytokine-driven inflammation and fibrosis. *PLoS Pathog.* (2009). doi:10.1371/journal.ppat.1000371
19. Förstermann, U. & Sessa, W. C. Nitric oxide synthases: Regulation and function. *Eur. Heart J.* (2012). doi:10.1093/eurheartj/ehr304
20. Pettersen, J. S., Fuentes-Duculan, J., Suárez-Farĩas, M., Pierson, K. C., Pitts-Kiefer, A., Fan, L., Belkin, D. A., Wang, C. Q. F., Bhuvanendran, S., Johnson-Huang, L. M., Bluth, M. J., Krueger, J. G., Lowes, M. A. & Carucci, J. A. Tumor-associated macrophages in the cutaneous SCC microenvironment are heterogeneously activated. *J. Invest. Dermatol.* (2011). doi:10.1038/jid.2011.9
21. Vogel, D. Y. S., Vereyken, E. J. F., Glim, J. E., Heijnen, P. D. A. M., Moeton, M.,

van der Valk, P., Amor, S., Teunissen, C. E., van Horssen, J. & Dijkstra, C. D. Macrophages in inflammatory multiple sclerosis lesions have an intermediate activation status. *J. Neuroinflammation* (2013). doi:10.1186/1742-2094-10-35

22. Ponzoni, M., Pastorino, F., Di Paolo, D., Perri, P. & Brignole, C. Targeting macrophages as a potential therapeutic intervention: Impact on inflammatory diseases and cancer. *Int. J. Mol. Sci.* **19,** (2018).
23. Arora, S., Dev, K., Agarwal, B., Das, P. & Syed, M. A. Macrophages: Their role, activation and polarization in pulmonary diseases. *Immunobiology* **223,** 383–396 (2018).
24. Rabinovitch, M. Professional and non-professional phagocytes: an introduction. *Trends Cell Biol.* (1995). doi:10.1016/S0962-8924(00)88955-2
25. Mechnikov, I. I. Immunity in infective diseases. *Rev. Infect. Dis.* (1988). doi:10.1093/clinids/10.1.223
26. Mills, C. M1 and M2 Macrophages: Oracles of Health and Disease. *Crit. Rev. Immunol.* **32,** 463–488 (2013).
27. Gordon, S. Phagocytosis: An Immunobiologic Process. *Immunity* **44,** 463–475 (2016).
28. Ghisletti, S., Barozzi, I., Mietton, F., Polletti, S., De Santa, F., Venturini, E., Gregory, L., Lonie, L., Chew, A., Wei, C. L., Ragoussis, J. & Natoli, G. Identification and Characterization of Enhancers Controlling the Inflammatory Gene Expression Program in Macrophages. *Immunity* (2010). doi:10.1016/j.immuni.2010.02.008
29. Janeway, C. A. The immune system evolved to discriminate infectious nonself from noninfectious self. *Immunol. Today* (1992). doi:10.1016/0167-5699(92)90198-G
30. Kawai, T. & Akira, S. Toll-like Receptors and Their Crosstalk with Other Innate Receptors in Infection and Immunity. *Immunity* (2011). doi:10.1016/j.immuni.2011.05.006
31. Herre, J., Marshall, A. S. J., Caron, E., Edwards, A. D., Williams, D. L., Schweighoffer, E., Tybulewicz, V., Reis E Sousa, C., Gordon, S. & Brown, G. D.

Dectin-1 uses novel mechanisms for yeast phagocytosis in macrophages. *Blood* (2004). doi:10.1182/blood-2004-03-1140

32. Peiser, L., Gough, P. J., Kodama, T. & Gordon, S. Macrophage class A scavenger receptor-mediated phagocytosis of Escherichia coli: Role of cell heterogeneity, microbial strain, and culture conditions in vitro. *Infect. Immun.* (2000). doi:10.1128/IAI.68.4.1953-1963.2000
33. Dahl, M., Bauer, A. K., Arredouani, M., Soininen, R., Tryggvason, K., Kleeberger, S. R. & Kobzik, L. Protection against inhaled oxidants through scavenging of oxidized lipids by macrophage receptors MARCO and SR-AI/II. *J. Clin. Invest.* (2007). doi:10.1172/JCI29968
34. Flannagan, R. S., Jaumouillé, V. & Grinstein, S. The Cell Biology of Phagocytosis. *Annu. Rev. Pathol. Mech. Dis.* **7,** 61–98 (2012).
35. Bruhns, P., Iannascoli, B., England, P., Mancardi, D. A., Fernandez, N., Jorieux, S. & Daëron, M. Specificity and affinity of human Fcγ receptors and their polymorphic variants for human IgG subclasses. *Blood* (2009). doi:10.1182/blood-2008-09-179754
36. Nagata, S., Suzuki, J., Segawa, K. & Fujii, T. Exposure of phosphatidylserine on the cell surface. *Cell Death Differ.* (2016). doi:10.1038/cdd.2016.7
37. Kobayashi, N., Karisola, P., Peña-Cruz, V., Dorfman, D. M., Jinushi, M., Umetsu, S. E., Butte, M. J., Nagumo, H., Chernova, I., Zhu, B., Sharpe, A. H., Ito, S., Dranoff, G., Kaplan, G. G., Casasnovas, J. M., Umetsu, D. T., DeKruyff, R. H. & Freeman, G. J. TIM-1 and TIM-4 Glycoproteins Bind Phosphatidylserine and Mediate Uptake of Apoptotic Cells. *Immunity* (2007). doi:10.1016/j.immuni.2007.11.011
38. Park, S. Y., Jung, M. Y., Kim, H. J., Lee, S. J., Kim, S. Y., Lee, B. H., Kwon, T. H., Park, R. W. & Kim, I. S. Rapid cell corpse clearance by stabilin-2, a membrane phosphatidylserine receptor. *Cell Death Differ.* (2008). doi:10.1038/sj.cdd.4402242
39. Park, D., Tosello-Trampont, A. C., Elliott, M. R., Lu, M., Haney, L. B., Ma, Z., Klibanov, A. L., Mandell, J. W. & Ravichandran, K. S. BAI1 is an engulfment

receptor for apoptotic cells upstream of the ELMO/Dock180/Rac module. *Nature* (2007). doi:10.1038/nature06329

40. Anderson, H. A., Maylock, C. A., Williams, J. A., Paweletz, C. P., Shu, H. & Shacter, E. Serum-derived protein S binds to phosphatidylserine and stimulates the phagocytosis of apoptotic cells. *Nat. Immunol.* (2003). doi:10.1038/ni871
41. Kitano, M., Nakaya, M., Nakamura, T., Nagata, S. & Matsuda, M. Imaging of Rab5 activity identifies essential regulators for phagosome maturation. *Nature* (2008). doi:10.1038/nature06857
42. Russell, D. G. Mycobacterium tuberculosis and the intimate discourse of a chronic infection. *Immunol. Rev.* (2011). doi:10.1111/j.1600-065X.2010.00984.x
43. Jankowski, A., Scott, C. C. & Grinstein, S. Determinants of the phagosomal pH in neutrophils. *J. Biol. Chem.* (2002). doi:10.1074/jbc.M110059200
44. Lambrecht, B. N. Alveolar Macrophage in the Driver's Seat. *Immunity* **24,** 366–368 (2006).
45. THEPEN, T., KRAAL, G. & HOLT, P. G. The Role of Alveolar Macrophages in Regulation of Lung Inflammation. *Ann. N. Y. Acad. Sci.* **725,** 200–206 (1994).
46. van Furth, R. & Cohn, Z. A. The origin and kinetics of mononuclear phagocytes. *J. Exp. Med.* (1968). doi:10.1084/jem.128.3.415
47. Guilliams, M., De Kleer, I., Henri, S., Post, S., Vanhoutte, L., De Prijck, S., Deswarte, K., Malissen, B., Hammad, H. & Lambrecht, B. N. Alveolar macrophages develop from fetal monocytes that differentiate into long-lived cells in the first week of life via GM-CSF. *J. Exp. Med.* **210,** 1977–1992 (2013).
48. Maus, U. A., Janzen, S., Wall, G., Srivastava, M., Blackwell, T. S., Christman, J. W., Seeger, W., Welte, T. & Lohmeyer, J. Resident alveolar macrophages are replaced by recruited monocytes in response to endotoxin-induced lung inflammation. *Am. J. Respir. Cell Mol. Biol.* (2006). doi:10.1165/rcmb.2005-0241OC
49. Marques, L. J., Teschler, H., Guzman, J. & Costabel, U. Smoker's lung

transplanted to a nonsmoker: Long-term detection of smoker's macrophages. *Am. J. Respir. Crit. Care Med.* (1997). doi:10.1164/ajrccm.156.5.9611052

50. Shibata, Y., Berclaz, P. Y., Chroneos, Z. C., Yoshida, M., Whitsett, J. A. & Trapnell, B. C. GM-CSF regulates alveolar macrophage differentiation and innate immunity in the lung through PU.1. *Immunity* **15,** 557–567 (2001).

51. Guilliams, M., De Kleer, I., Henri, S., Post, S., Vanhoutte, L., De Prijck, S., Deswarte, K., Malissen, B., Hammad, H. & Lambrecht, B. N. Alveolar macrophages develop from fetal monocytes that differentiate into long-lived cells in the first week of life via GM-CSF. *J. Exp. Med.* (2013). doi:10.1084/jem.20131199

52. Chen, B. D. M., Mueller, M. & Chou, T. H. Role of granulocyte/macrophage colony-stimulating factor in the regulation of murine alveolar macrophage proliferation and differentiation. *J. Immunol.* (1988).

53. Schneider, C., Nobs, S. P., Kurrer, M., Rehrauer, H., Thiele, C. & Kopf, M. Induction of the nuclear receptor PPAR-γ 3 by the cytokine GM-CSF is critical for the differentiation of fetal monocytes into alveolar macrophages. *Nat. Immunol.* (2014). doi:10.1038/ni.3005

54. Gautiar, E. L., Shay, T., Miller, J., Greter, M., Jakubzick, C., Ivanov, S., Helft, J., Chow, A., Elpek, K. G., Gordonov, S., Mazloom, A. R., Ma'Ayan, A., Chua, W. J., Hansen, T. H., Turley, S. J., Merad, M., Randolph, G. J., Best, A. J., Knell, J., Goldrath, A., Brown, B., Jojic, V., Koller, D., Cohen, N., Brenner, M., Regev, A., Fletcher, A., Bellemare-Pelletier, A., Malhotra, D., Jianu, R., Laidlaw, D., Collins, J., Narayan, K., Sylvia, K., Kang, J., Gazit, R., Garrison, B. S., Rossi, D. J., Kim, F., Rao, T. N., Wagers, A., Shinton, S. A., Hardy, R. R., Monach, P., Bezman, N. A., Sun, J. C., Kim, C. C., Lanier, L. L., Heng, T., Kreslavsky, T., Painter, M., Ericson, J., Davis, S., Mathis, D. & Benoist, C. Gene-expression profiles and transcriptional regulatory pathways that underlie the identity and diversity of mouse tissue macrophages. *Nat. Immunol.* (2012). doi:10.1038/ni.2419

55. Murray, P. J., Allen, J. E., Biswas, S. K., Fisher, E. A., Gilroy, D. W., Goerdt, S., Gordon, S., Hamilton, J. A., Ivashkiv, L. B., Lawrence, T., Locati, M., Mantovani, A., Martinez, F. O., Mege, J. L., Mosser, D. M., Natoli, G., Saeij, J. P., Schultze, J. L., Shirey, K. A., Sica, A., Suttles, J., Udalova, I., vanGinderachter, J. A., Vogel, S. N. & Wynn, T. A. Macrophage Activation and Polarization: Nomenclature and Experimental Guidelines. *Immunity* **41,** 14–20 (2014).

56. Thepen, T., Van Rooijen, N. & Kraal, G. Alveolar macrophage elimination in vivo is associated with an increase in pulmonary immune response in mice. *J. Exp. Med.* (1989). doi:10.1084/jem.170.2.499

57. Blumenthal, R. L., Campbell, D. E., Hwang, P., DeKruyff, R. H., Frankel, L. R. & Umetsu, D. T. Human alveolar macrophages induce functional inactivation in antigen-specific CD4 T cells. *J. Allergy Clin. Immunol.* (2001). doi:10.1067/mai.2001.112845

58. Lyons, C. R., Ball, E. J., Toews, G. B., Weissler, J. C., Stastny, P. & Lipscomb, M. F. Inability of human alveolar macrophages to stimulate resting T cells correlates with decreased antigen-specific T cell-macrophage binding. *J. Immunol.* (1986).

59. Hoidal, J. R., Schmeling, D. & Peterson, P. K. Phagocytosis, Bacterial Killing, and Metabolism by Purified Human Lung Phagocytes. *J. Infect. Dis.* (1981). doi:10.1093/infdis/144.1.61

60. Joshi, N., Walter, J. M. & Misharin, A. V. Alveolar Macrophages. *Cell. Immunol.* **330,** 86–90 (2018).

61. MacLean, J. a, Xia, W., Pinto, C. E., Zhao, L., Liu, H. W. & Kradin, R. L. Sequestration of inhaled particulate antigens by lung phagocytes. A mechanism for the effective inhibition of pulmonary cell-mediated immunity. *Am. J. Pathol.* **148,** 657–666 (1996).

62. Hussell, T. & Bell, T. J. Alveolar macrophages: plasticity in a tissue-specific context. *Nat. Rev. Immunol.* **14,** 81–93 (2014).

63. Powers, K. A., Szászi, K., Khadaroo, R. G., Tawadros, P. S., Marshall, J. C.,

Kapus, A. & Rotstein, O. D. Oxidative stress generated by hemorrhagic shock recruits Toll-like receptor 4 to the plasma membrane in macrophages. *J. Cell Biol.* (2006). doi:10.1084/jem.20060943

64. Maris, N. A., Dessing, M. C., de Vos, A. F., Bresser, P., van der Zee, J. S., Jansen, H. M., Spek, C. A. & van der Poll, T. Toll-like receptor mRNA levels in alveolar macrophages after inhalation of endotoxin. *Eur. Respir. J.* (2006). doi:10.1183/09031936.06.00010806

65. Laskin, D. L., Malaviya, R. & Laskin, J. D. in *Comp. Biol. Norm. Lung Second Ed.* (2015). doi:10.1016/B978-0-12-404577-4.00032-1

66. Steinmüller, C., Franke-Ullmann, G., Lohmann-Matthes, M. L. & Emmendörffer, A. Local activation of nonspecific defense against a respiratory model infection by application of interferon-γ: Comparison between rat alveolar and interstitial lung macrophages. *Am. J. Respir. Cell Mol. Biol.* (2000). doi:10.1165/ajrcmb.22.4.3336

67. Murray, C. J. L. & Lopez, A. D. Measuring the global burden of disease. *N. Engl. J. Med.* (2013). doi:10.1056/NEJMra1201534

68. Lu, G. & Fei, B. Medical hyperspectral imaging: a review. *J. Biomed. Opt.* (2014). doi:10.1117/1.jbo.19.1.010901

69. Vestbo, J., Hurd, S. S., Agustí, A. G., Jones, P. W., Vogelmeier, C., Anzueto, A., Barnes, P. J., Fabbri, L. M., Martinez, F. J., Nishimura, M., Stockley, R. A., Sin, D. D. & Rodriguez-Roisin, R. Global strategy for the diagnosis, management, and prevention of chronic obstructive pulmonary disease GOLD executive summary. *Am. J. Respir. Crit. Care Med.* (2013). doi:10.1164/rccm.201204-0596PP

70. Shapiro, S. D. The macrophage in chronic obstructive pulmonary disease. in *Am. J. Respir. Crit. Care Med.* (1999).

71. Stefano, A. D. I., Capelli, A., Lusuardi, M., Balbo, P., Donner, C. F., Saetta, M., Ce, M., Lm, F., Cf, D. & Severity, S. M. Severity of Airflow Limitation Is Associated with Severity of Airway Inflammtion in Smokers. *Am. J. Respir. Crit. Care Med.* **158,** 1277–1285 (1998).

72. Barnes, P. J. Alveolar Macrophages as Orchestrators of COPD. *COPD J. Chronic Obstr. Pulm. Dis.* **1,** 59–70 (2004).

73. Traves, S. L., Culpitt, S. V., Russell, R. E. K., Barnes, P. J. & Donnelly, L. E. Increased levels of the chemokines GROα and MCP-1 in sputum samples from patients with COPD. *Thorax* (2002). doi:10.1136/thorax.57.7.590

74. Tomita, K., Caramori, G., Lim, S., Ito, K., Hanazawa, T., Oates, T., Chiselita, I., Jazrawi, E., Fan Chung, K., Barnes, P. J. & Adcock, I. M. Increased p21CIP1/WAF1 and B cell lymphoma leukemia-xL expression and reduced apoptosis in alveolar macrophages from smokers. *Am. J. Respir. Crit. Care Med.* (2002). doi:10.1164/rccm.2104010

75. Berenson, C. S., Kruzel, R. L., Eberhardt, E. & Sethi, S. Phagocytic Dysfunction of Human Alveolar Macrophages and Severity of Chronic Obstructive Pulmonary Disease. **208,** (2013).

76. Taylor, A. E., Finney-Hayward, T. K., Quint, J. K., Thomas, C. M. R., Tudhope, S. J., Wedzicha, J. A., Barnes, P. J. & Donnelly, L. E. Defective macrophage phagocytosis of bacteria in COPD. *Eur. Respir. J.* **35,** 1039–1047 (2010).

77. Hodge, S., Hodge, G., Scicchitano, R., Reynolds, P. N. & Holmes, M. Alveolar macrophages from subjects with chronic obstructive pulmonary disease are deficient in their ability to phagocytose apoptotic airway epithelial cells. *Immunol. Cell Biol.* **81,** 289–296 (2003).

78. Martí-Lliteras, P., Regueiro, V., Morey, P., Hood, D. W., Saus, C., Sauleda, J., Agustí, A. G. N., Bengoechea, J. A. & Garmendia, J. Nontypeable Haemophilus influenzae clearance by alveolar macrophages is impaired by exposure to cigarette smoke. *Infect. Immun.* (2009). doi:10.1128/IAI.00305-09

79. Blander, J. M. & Medzhitov, R. Regulation of Phagosome Maturation by Signals from Toll-Like Receptors. *Science (80-.).* (2004). doi:10.1126/science.1096158

80. Todt, J. C., Freeman, C. M., Brown, J. P., Sonstein, J., Ames, T. M., McCubbrey, A. L., Martinez, F. J., Chensue, S. W., Beck, J. M. & Curtis, J. L. Smoking decreases the response of human lung macrophages to double-stranded RNA

by reducing TLR3 expression. *Respir. Res.* (2013). doi:10.1186/1465-9921-14-33

81. Pons, A. R., Noguera, A., Blanquer, D., Sauleda, J., Pons, J. & Agustí, A. G. N. Phenotypic characterisation of alveolar macrophages and peripheral blood monocytes in COPD. *Eur. Respir. J.* (2005). doi:10.1183/09031936.05.00062304
82. Kunz, L. I. Z., Lapperre, T. S., Snoeck-Stroband, J. B., Budulac, S. E., Timens, W., van Wijngaarden, S., Schrumpf, J. A., Rabe, K. F., Postma, D. S., Sterk, P. J. & Hiemstra, P. S. Smoking status and anti-inflammatory macrophages in bronchoalveolar lavage and induced sputum in COPD. *Respir. Res.* (2011). doi:10.1186/1465-9921-12-34
83. Hodge, S., Hodge, G., Ahern, J., Jersmann, H., Holmes, M. & Reynolds, P. N. Smoking alters alveolar macrophage recognition and phagocytic ability: Implications in chronic obstructive pulmonary disease. *Am. J. Respir. Cell Mol. Biol.* **37,** 748–755 (2007).
84. Keatings, V. M., Collins, P. D., Scott, D. M. & Barnes, P. J. Differences in Interleukin-8 and Tumor Necrosis Facfor-α in Induced Sputum from Patients with Chronic Obstructive Pulmonary Disease or Asthma. *Am. J. Respir. Crit. Care Med.* (1996). doi:10.1164/ajrccm.153.2.8564092
85. Barnes, P. J., Shapiro, S. D. & Pauwels, R. A. Chronic obstructive pulmonary disease: Molecular and cellular mechanisms. *Eur. Respir. J.* (2003). doi:10.1183/09031936.03.00040703
86. Di Stefano, A., Caramori, G., Oates, T., Capelli, A., Lusuardi, M., Gnemmi, I., Ioli, F., Chung, K. F., Donner, C. F., Barnes, P. J. & Adcock, I. M. Increased expression of nuclear factor-κB in bronchial biopsies from smokers and patients with COPD. *Eur. Respir. J.* (2002). doi:10.1183/09031936.02.00272002
87. Hurd, S. S. & Pauwels, R. Global Initiative for Chronic Obstructive Lung Diseases (GOLD). *Pulm. Pharmacol. Ther.* (2002). doi:10.1006/pupt.2002.0381
88. Vlahos, R. & Bozinovski, S. Role of alveolar macrophages in chronic obstructive pulmonary disease. *Front. Immunol.* **5,** 1–7 (2014).
89. Patel, S. K. & Janjic, J. M. Macrophage targeted theranostics as personalized

nanomedicine strategies for inflammatory diseases. *Theranostics* (2015). doi:10.7150/thno.9476

90. Patel, B., Gupta, N. & Ahsan, F. Particle engineering to enhance or lessen particle uptake by alveolar macrophages and to influence the therapeutic outcome. *Eur. J. Pharm. Biopharm.* **89,** 163–174 (2015).
91. Tran, T. H. & Amiji, M. M. Targeted delivery systems for biological therapies of inflammatory diseases. *Expert Opin. Drug Deliv.* (2015). doi:10.1517/17425247.2015.972931
92. Majmudar, M. D., Yoo, J., Keliher, E. J., Truelove, J. J., Iwamoto, Y., Sena, B., Dutta, P., Borodovsky, A., Fitzgerald, K., Di Carli, M. F., Libby, P., Anderson, D. G., Swirski, F. K., Weissleder, R. & Nahrendorf, M. Polymeric nanoparticle PET/MR imaging allows macrophage detection in atherosclerotic plaques. *Circ. Res.* (2013). doi:10.1161/CIRCRESAHA.111.300576
93. Harel-Adar, T., Mordechai, T. Ben, Amsalem, Y., Feinberg, M. S., Leor, J. & Cohen, S. Modulation of cardiac macrophages by phosphatidylserine-presenting liposomes improves infarct repair. *Proc. Natl. Acad. Sci. U. S. A.* (2011). doi:10.1073/pnas.1015623108
94. Komano, Y., Yagi, N., Onoue, I., Kaneko, K., Miyasaka, N. & Nanki, T. Arthritic joint-targeting small interfering RNA-encapsulated liposome: Implication for treatment strategy for rheumatoid arthritis. *J. Pharmacol. Exp. Ther.* (2012). doi:10.1124/jpet.111.185884
95. Patel, S. K., Zhang, Y., Pollock, J. A. & Janjic, J. M. Cyclooxgenase-2 Inhibiting Perfluoropoly (Ethylene Glycol) Ether Theranostic Nanoemulsions-In Vitro Study. *PLoS One* (2013). doi:10.1371/journal.pone.0055802
96. Park, H., Kim, S., Kim, S., Song, Y., Seung, K., Hong, D., Khang, G. & Lee, D. Antioxidant and anti-inflammatory activities of hydroxybenzyl alcohol releasing biodegradable polyoxalate nanoparticles. *Biomacromolecules* (2010). doi:10.1021/bm100474w
97. Keatings, V. M., Jatakanon, A., Worsdell, Y. M. & Barnes, P. J. Effects of inhaled and oral glucocorticoids on inflammatory indices in asthma and

COPD. *Am. J. Respir. Crit. Care Med.* (1997). doi:10.1164/ajrccm.155.2.9032192

98. Culpitt, S. V., Maziak, W., Loukidis, S., Nightingale, J. A., Matthews, J. L. & Barnes, P. J. Effect of high dose inhaled steroid on cells, cytokines, and proteases in induced sputum in chronic obstructive pulmonary disease. *Am. J. Respir. Crit. Care Med.* (1999). doi:10.1164/ajrccm.160.5.9811058

99. Culpitt, S. V., Rogers, D. F., Shah, P., De Matos, C., Russell, R. E. K., Donnelly, L. E. & Barnes, P. J. Impaired inhibition by dexamethasone of cytokine release by alveolar macrophages from patients with chronic obstructive pulmonary disease. *Am. J. Respir. Crit. Care Med.* (2003). doi:10.1164/rccm.200204-298OC

100. Harvey, C. J., Thimmulappa, R. K., Sethi, S., Kong, X., Yarmus, L., Brown, R. H., David, F.-K., Wise, R. & Biswal, S. Targeting Nrf2 Signaling Improves Bacterial Clearance by Alveolar Macrophages in Patients with COPD and in a Mouse Model. *Sci. Transl. Med.* **3,** 78ra32 (2011).

101. Li, N., Alam, J., Venkatesan, M. I., Eiguren-Fernandez, A., Schmitz, D., Di Stefano, E., Slaughter, N., Killeen, E., Wang, X., Huang, A., Wang, M., Miguel, A. H., Cho, A., Sioutas, C. & Nel, A. E. Nrf2 Is a Key Transcription Factor That Regulates Antioxidant Defense in Macrophages and Epithelial Cells: Protecting against the Proinflammatory and Oxidizing Effects of Diesel Exhaust Chemicals. *J. Immunol.* **173,** 3467–3481 (2004).

102. Kensler, T. W., Wakabayashi, N. & Biswal, S. Cell Survival Responses to Environmental Stresses Via the Keap1-Nrf2-ARE Pathway. *Annu. Rev. Pharmacol. Toxicol.* (2007). doi:10.1146/annurev.pharmtox.46.120604.141046

103. Iizuka, T., Ishii, Y., Itoh, K., Kiwamoto, T., Kimura, T., Matsuno, Y., Morishima, Y., Hegab, A. E., Homma, S., Nomura, A., Sakamoto, T., Shimura, M., Yoshida, A., Yamamoto, M. & Sekizawa, K. Nrf2-deficient mice are highly susceptible to cigarette smoke-induced emphysema. *Genes to Cells* (2005). doi:10.1111/j.1365-2443.2005.00905.x

104. Suzuki, M., Betsuyaku, T., Ito, Y., Nagai, K., Nasuhara, Y., Kaga, K., Kondo, S. & Nishimura, M. Down-regulated NF-E2-related factor 2 in pulmonary macrophages of aged smokers and patients with chronic obstructive

pulmonary disease. *Am. J. Respir. Cell Mol. Biol.* (2008). doi:10.1165/rcmb.2007-0424OC

105. Bewley, M. A., Budd, R. C., Ryan, E., Cole, J., Collini, P., Marshall, J., Kolsum, U., Beech, G., Emes, R. D., Tcherniaeva, I., Berbers, G. A. M., Walmsley, S. R., Donaldson, G., Wedzicha, J. A., Kilty, I., Rumsey, W., Sanchez, Y., Brightling, C. E., Donnelly, L. E., Barnes, P. J., Singh, D., Whyte, M. K. B. & Dockrell, D. H. Opsonic phagocytosis in chronic obstructive pulmonary disease is enhanced by Nrf2 agonists. *Am. J. Respir. Crit. Care Med.* **198,** 739–750 (2018).
106. Albert, R. K., Connett, J., Bailey, W. C., Casaburi, R., Cooper, J. A. D., Criner, G. J., Curtis, J. L., Dransfield, M. T., Han, M. L. K., Lazarus, S. C., Make, B., Marchetti, N., Martinez, F. J., Madinger, N. E., McEvoy, C., Niewoehner, D. E., Porsasz, J., Price, C. S., Reilly, J., Scanlon, P. D., Sciurba, F. C., Scharf, S. M., Washko, G. R., Woodruff, P. G. & Anthonisen, N. R. Azithromycin for prevention of exacerbations of COPD. *N. Engl. J. Med.* (2011). doi:10.1056/NEJMoa1104623
107. Hodge, S., Hodge, G., Jersmann, H., Matthews, G., Ahern, J., Holmes, M. & Reynolds, P. N. Azithromycin improves macrophage phagocytic function and expression of mannose receptor in chronic obstructive pulmonary disease. *Am. J. Respir. Crit. Care Med.* **178,** 139–148 (2008).
108. Blasi, F., Bonardi, D., Aliberti, S., Tarsia, P., Confalonieri, M., Amir, O., Carone, M., Di Marco, F., Centanni, S. & Guffanti, E. Long-term azithromycin use in patients with chronic obstructive pulmonary disease and tracheostomy. *Pulm. Pharmacol. Ther.* (2010). doi:10.1016/j.pupt.2009.12.002
109. Weissleder, R. & Pittet, M. J. Imaging in the era of molecular oncology. *Nature* **452,** 580–589 (2008).
110. Bremer, C., Ntziachristos, V. & Weissleder, R. Optical-based molecular imaging: contrast agents and potential medical applications. *Eur. Radiol.* **13,** 231–243 (2003).
111. Weissleder, R. & Mahmood, U. Molecular Imaging. *Radiology* **219,** 316–333 (2001).

112. Dorward, D. A., Lucas, C. D., Rossi, A. G., Haslett, C. & Dhaliwal, K. Imaging inflammation: Molecular strategies to visualize key components of the inflammatory cascade, from initiation to resolution. *Pharmacol. Ther.* **135,** 182–199 (2012).

113. Hounsfield, G. N. Computerized transverse axial scanning (tomography): I. Description of system. *Br. J. Radiol.* (1973). doi:10.1259/0007-1285-46-552-1016

114. Davies, T. W. & Davies, M. Mass radiography in Wales experience with a mobile unit. *Br. J. Tuberc. Dis. Chest* (1945).

115. Mahajan, A. & Cook, G. in *Basic Sci. PET Imaging* (2016). doi:10.1007/978-3-319-40070-9_18

116. Nikolaou, K., Flohr, T., Knez, A., Rist, C., Wintersperger, B., Johnson, T., Reiser, M. F. & Becker, C. R. Advances in cardiac CT imaging: 64-slice scanner. *Int. J. Cardiovasc. Imaging* (2004). doi:10.1007/s10554-004-7015-1

117. Ametamey, S. M., Honer, M. & Schubiger, P. A. Molecular imaging with PET. *Chem. Rev.* **108,** 1501–1516 (2008).

118. Gallagher, B. M., Fowler, J. S., Gutterson, N. I., MacGregor, R. R., Wan, C. N. & Wolf, A. P. Metabolic trapping as a principle of radiopharmaceutical design: Some factors responsible for the biodistribution of [18F] 2-deoxy-2- fluoro-D-glucose. *J. Nucl. Med.* (1978).

119. Choy, G., Choyke, P. & Libutti, S. K. Current Advances in Molecular Imaging: Noninvasive in Vivo Bioluminescent and Fluorescent Optical Imaging in Cancer Research. *Mol. Imaging* **2,** 303–312 (2003).

120. Qin, C., Zhu, S. & Tian, J. New optical molecular imaging systems. *Curr. Pharm. Biotechnol.* **11,** 620–7 (2010).

121. Ntziachristos, V. Fluorescence Molecular Imaging. *Annu. Rev. Biomed. Eng.* **8,** 1–33 (2006).

122. Day, R. N. & Davidson, M. W. The fluorescent protein palette: Tools for cellular imaging. *Chem. Soc. Rev.* (2009). doi:10.1039/b901966a

123. Panchuk-Voloshina, N., Haugland, R. P., Bishop-Stewart, J., Bhalgat, M. K.,

Millard, P. J., Mao, F., Leung, W. Y. & Haugland, R. P. Alexa dyes, a series of new fluorescent dyes that yield exceptionally bright, photostable conjugates. *J. Histochem. Cytochem.* (1999). doi:10.1177/002215549904700910

124. Pauli, J., Licha, K., Berkemeyer, J., Grabolle, M., Spieles, M., Wegner, N., Welker, P. & Resch-Genger, U. New fluorescent labels with tunable hydrophilicity for the rational design of bright optical probes for molecular imaging. *Bioconjug. Chem.* (2013). doi:10.1021/bc4000349

125. Mittag, A. & Tarnok, A. *Recent Advances in Cytometry Applications: Preclinical, Clinical, and Cell Biology*. *Methods Cell Biol.* (2011). doi:10.1016/B978-0-12-385493-3.00001-2

126. Haller, J., Hyde, D., Deliolanis, N., De Kleine, R., Niedre, M. & Ntziachristos, V. Visualization of pulmonary inflammation using noninvasive fluorescence molecular imaging. *J. Appl. Physiol.* (2008). doi:10.1152/japplphysiol.00959.2007

127. Filner, J. J., Bonura, E. J., Lau, S. T., Abounasr, K. K., Naidich, D., Morice, R. C., Eapen, G. A., Jimenez, C. A., Casal, R. F. & Ost, D. Bronchoscopic fibered confocal fluorescence microscopy image characteristics and pathologic correlations. *J. Bronchology Interv. Pulmonol.* **18,** 23–30 (2011).

128. Thiberville, L., Moreno-Swirc, S., Vercauteren, T., Peltier, E., Cavé, C. & Bourg Heckly, G. *In Vivo* Imaging of the Bronchial Wall Microstructure Using Fibered Confocal Fluorescence Microscopy. *Am. J. Respir. Crit. Care Med.* **175,** 22–31 (2007).

129. Krstaji, N., Akram, A. R., Choudhary, T. R., Mcdonald, N., Tanner, M. G., Pedretti, E., Dalgarno, P. A., Scholefield, E., John, M., Moore, A., Bradley, M. & Dhaliwal, K. Two-color widefield fluorescence microendoscopy enables multiplexed molecular imaging of the distal human lung. **4418,** 4414–4418 (2015).

130. Krstajić, N., Mills, B., Murray, I. & Marshall, A. Low-cost high sensitivity pulsed endomicroscopy to visualize tricolor optical signatures. *J. Biomed. Opt.* **23,** 1 (2018).

131. Thiberville, L., Salau, M., Lachkar, S. & Dominique, S. Human in vivo fluorescence microimaging of the alveolar ducts and sacs during bronchoscopy. **33,** 974–985 (2009).
132. Cremer, C. & Cremer, T. Considerations on a laser-scanning-microscope with high resolution and depth of field. *Microsc. Acta* (1978).
133. Weissleder, R. & Ntziachristos, V. Shedding light onto live molecular targets. *Nat. Med.* **9,** 123–128 (2003).
134. Akram, A. R., Avlonitis, N., Lilienkampf, A., Perez-Lopez, A. M., McDonald, N., Chankeshwara, S. V, Scholefield, E., Haslett, C., Bradley, M. & Dhaliwal, K. A Labelled-Ubiquicidin Antimicrobial Peptide for Immediate In Situ Optical Detection of Live Bacteria in Human Alveolar Lung Tissue. *Chem. Sci.* 6971–6979 (2015). doi:10.1039/C5SC00960J
135. Akram, A. R., Chankeshwara, S. V., Scholefield, E., Aslam, T., McDonald, N., Megia-Fernandez, A., Marshall, A., Mills, B., Avlonitis, N., Craven, T. H., Smyth, A. M., Collie, D. S., Gray, C., Hirani, N., Hill, A. T., Govan, J. R., Walsh, T., Haslett, C., Bradley, M. & Dhaliwal, K. In situ identification of Gram-negative bacteria in human lungs using a topical fluorescent peptide targeting lipid A. *Sci. Transl. Med.* (2018). doi:10.1126/scitranslmed.aal0033
136. Craven, T. H., Avlonitis, N., McDonald, N., Walton, T., Scholefield, E., Akram, A. R., Walsh, T. S., Haslett, C., Bradley, M. & Dhaliwal, K. Super-silent FRET Sensor Enables Live Cell Imaging and Flow Cytometric Stratification of Intracellular Serine Protease Activity in Neutrophils. *Sci. Rep.* (2018). doi:10.1038/s41598-018-31391-9
137. Han, W., Zaynagetdinov, R., Yull, F. E., Polosukhin, V. V, Gleaves, L. a, Tanjore, H., Young, L. R., Peterson, T. E., Manning, H. C., Prince, L. S. & Blackwell, T. S. Molecular Imaging of Folate Receptor Beta Positive Macrophages During Acute Lung Inflammation. *Am. J. Respir. Cell Mol. Biol.* **53,** 50–59 (2014).
138. Salazar, M. D. A. & Ratnam, M. The folate receptor: What does it promise in tissue-targeted therapeutics? *Cancer Metastasis Rev.* **26,** 141–152 (2007).

139. Tedeschi, P. M., Markert, E. K., Gounder, M., Lin, H., Dvorzhinski, D., Dolfi, S. C., Chan, L. L.-Y., Qiu, J., DiPaola, R. S., Hirshfield, K. M., Boros, L. G., Bertino, J. R., Oltvai, Z. N. & Vazquez, A. Contribution of serine, folate and glycine metabolism to the ATP, NADPH and purine requirements of cancer cells. *Cell Death Dis.* **4,** e877 (2013).

140. Baker, D. W., Zhou, J., Tsai, Y. T., Patty, K. M., Weng, H., Tang, E. N., Nair, A., Hu, W. J. & Tang, L. Development of optical probes for in vivo imaging of polarized macrophages during foreign body reactions. *Acta Biomater.* **10,** 2945–2955 (2014).

141. Lin, V. S., Dickinson, B. C. & Chang, C. J. in *Methods Enzymol.* (2013). doi:10.1016/B978-0-12-405883-5.00002-8

142. Fernández, A. & Vendrell, M. Smart fluorescent probes for imaging macrophage activity. *Chem. Soc. Rev.* **45,** 1182–96 (2016).

143. Vázquez-Romero, A., Kielland, N., Arévalo, M. J., Preciado, S., Mellanby, R. J., Feng, Y., Lavilla, R. & Vendrell, M. Multicomponent reactions for de novo synthesis of bodipy probes: In vivo imaging of phagocytic macrophages. *J. Am. Chem. Soc.* **135,** 16018–16021 (2013).

144. Jiang, L., Salao, K., Li, H., Rybicka, J. M., Yates, R. M., Luo, X. W., Shi, X. X., Kuffner, T., Tsai, V. W. W., Husaini, Y., Wu, L., Brown, D. A., Grewal, T., Brown, L. J., Curmi, P. M. G. & Breit, S. N. Intracellular chloride channel protein CLIC1 regulates macrophage function through modulation of phagosomal acidification. *J. Cell Sci.* (2012). doi:10.1242/jcs.110072

145. Chagnon, F., Bourgouin, A., Lebel, R., Bonin, M. A., Marsault, E., Lepage, M. & Lesur, O. Smart imaging of acute lung injury: Exploration of myeloperoxidase activity using in vivo endoscopic confocal fluorescence microscopy. *Am. J. Physiol. - Lung Cell. Mol. Physiol.* (2015). doi:10.1152/ajplung.00289.2014

146. Haslett, C., Guthrie, L. A., Kopaniak, M. M., Johnston, R. B. & Henson, P. M. Modulation of multiple neutrophil functions by preparative methods or trace concentrations of bacterial lipopolysaccharide. *Am. J. Pathol.* (1985).

147. Parker, H. E., Stone, J. M., Marshall, A. D. L., Choudhary, T. R., Thomson, R. R., Dhaliwal, K. & Tanner, M. G. Fibre-based spectral ratio endomicroscopy for contrast enhancement of bacterial imaging and pulmonary autofluorescence. *Biomed. Opt. Express* **10,** 1856 (2019).

148. Stone, J. M., Wood, H. A. C., Harrington, K. & Birks, T. A. Low index contrast imaging fibers. *Opt. Lett.* (2017). doi:10.1364/ol.42.001484

149. Wynn, T. a., Chawla, A. & Pollard, J. W. Origins and Hallmarks of Macrophages: Development, Homeostasis, and Disease. *Nature* **496,** 445–455 (2013).

150. Gordon, S. & Martinez, F. O. Alternative activation of macrophages: Mechanism and functions. *Immunity* (2010). doi:10.1016/j.immuni.2010.05.007

151. Martinez, F. O., Helming, L. & Gordon, S. Alternative activation of macrophages: an immunologic functional perspective. *Annu. Rev. Immunol.* **27,** 451–483 (2009).

152. Parisi, L., Gini, E., Baci, D., Tremolati, M., Fanuli, M., Bassani, B., Farronato, G., Bruno, A. & Mortara, L. Macrophage Polarization in Chronic Inflammatory Diseases: Killers or Builders? *J. Immunol. Res.* (2018). doi:10.1155/2018/8917804

153. Daigneault, M., Preston, J. A., Marriott, H. M., Whyte, M. K. B. & Dockrell, D. H. The identification of markers of macrophage differentiation in PMA-stimulated THP-1 cells and monocyte-derived macrophages. *PLoS One* **5,** (2010).

154. Mendoza-Coronel, E. & Castañón-Arreola, M. Comparative evaluation of in vitro human macrophage models for mycobacterial infection study. *Pathog. Dis.* **74,** 1–7 (2016).

155. Bosshart, H. & Heinzelmann, M. THP-1 cells as a model for human monocytes. *Ann. Transl. Med.* (2016). doi:10.21037/atm.2016.08.53

156. Sundström, C. & Nilsson, K. Establishment and characterization of a human histiocytic lymphoma cell line (U-937). *Int. J. Cancer* (1976).

doi:10.1002/ijc.2910170504

157. Fuentes, A. L., Millis, L., Vapenik, J. & Sigola, L. Lipopolysaccharide-mediated enhancement of zymosan phagocytosis by RAW 264.7 macrophages is independent of opsonins, laminarin, mannan, and complement receptor 3. *J. Surg. Res.* (2014). doi:10.1016/j.jss.2014.03.024

158. Wang, B., Sullivan, J. A., Sullivan, G. W. & Mandell, G. L. Role of specific antibody in interaction of leptospires with human monocytes and monocyte-derived macrophages. *Infect. Immun.* (1984).

159. Louise, O., Amadori, M., Ritelli, M., Tagliabue, S. & Pacciarini, M. L. in *Diagnostic Bacteriol. Protoc.* (2006). doi:10.1385/1-59745-143-6:203

160. Martinez, F. O. & Gordon, S. The M1 and M2 paradigm of macrophage activation: time for reassessment. *F1000Prime Rep.* **6,** 1–13 (2014).

161. Poh, A. R. & Ernst, M. Targeting Macrophages in Cancer: From Bench to Bedside. *Front. Oncol.* (2018). doi:10.3389/fonc.2018.00049

162. Forrester, M. A., Wassall, H. J., Hall, L. S., Cao, H., Wilson, H. M., Barker, R. N. & Vickers, M. A. Similarities and differences in surface receptor expression by THP-1 monocytes and differentiated macrophages polarized using seven different conditioning regimens. *Cell. Immunol.* (2018). doi:10.1016/j.cellimm.2018.07.008

163. Gordon, S. & Plüddemann, A. Tissue macrophages: Heterogeneity and functions. *BMC Biol.* (2017). doi:10.1186/s12915-017-0392-4

164. Liu, Y., Hughes, J., Savill, J., Cousin, J. M., Haslett, C., Dransfield, I., Rossi, A. G., Van Damme, J. & Seckl, J. R. Glucocorticoids promote nonphlogistic phagocytosis of apoptotic leukocytes. *J. Immunol.* **162,** 3639–3646 (1999).

165. Kapellos, T. S., Taylor, L., Lee, H., Cowley, S. A., James, W. S., Iqbal, A. J. & Greaves, D. R. A novel real time imaging platform to quantify macrophage phagocytosis. *Biochem. Pharmacol.* **116,** 107–119 (2016).

166. Helgason, C. & Miller, C. *Basic Cell Culture Protocols*. (Humana Press, 2005).

167. Chow, C.-W., Downey, G. P. & Grinstein, S. in *Curr. Protoc. Cell Biol.* (2004). doi:10.1002/0471143030.cb1507s22

168. Jersmann, H. P. A., Ross, K. A., Vivers, S., Brown, S. B., Haslett, C. & Dransfield, I. Phagocytosis of apoptotic cells by human macrophages: Analysis by multiparameter flow cytometry. *Cytometry* **51A,** 7–15 (2003).

169. Drevets, D. a & Campbell, P. a. Macrophage phagocytosis: use of fluorescence microscopy to distinguish between extracellular and intracellular bacteria. *J. Immunol. Methods* **142,** 31–8 (1991).

170. Russo-Marie, F. Macrophages and the glucocorticoids. *J. Neuroimmunol.* (1992). doi:10.1016/0165-5728(92)90144-A

171. Giles, K. M., Ross, K., Rossi, a G., Hotchin, N. a, Haslett, C. & Dransfield, I. Glucocorticoid augmentation of macrophage capacity for phagocytosis of apoptotic cells is associated with reduced p130Cas expression, loss of paxillin/pyk2 phosphorylation, and high levels of active Rac. *J. Immunol.* **167,** 976–986 (2001).

172. Song, M. Y., Kim, E. K., Moon, W. S., Park, J. W., Kim, H. J., So, H. S., Park, R., Kwon, K. B. & Park, B. H. Sulforaphane protects against cytokine- and streptozotocin-induced β-cell damage by suppressing the NF-κB pathway. *Toxicol. Appl. Pharmacol.* (2009). doi:10.1016/j.taap.2008.11.007

173. Suganuma, H., Fahey, J. W., Bryan, K. E., Healy, Z. R. & Talalay, P. Stimulation of phagocytosis by sulforaphane. *Biochem. Biophys. Res. Commun.* **405,** 146–151 (2011).

174. Grage-Griebenow, E., Flad, H. D. & Ernst, M. Heterogeneity of human peripheral blood monocyte subsets. *J. Leukoc. Biol.* (2001).

175. Dransfield, I., Zagórska, A., Lew, E. D., Michail, K. & Lemke, G. Mer receptor tyrosine kinase mediates both tethering and phagocytosis of apoptotic cells. *Cell Death Dis.* (2015). doi:10.1038/cddis.2015.18

176. Gordon, S. & Taylor, P. R. MONOCYTE AND MACROPHAGE HETEROGENEITY. **5,** 953–964 (2005).

177. Tabata, Y. & Ikada, Y. in *New Polym. Mater.* (2006). doi:10.1007/bfb0043062

178. Schliwa, M. Action of cytochalasin D on cytoskeletal networks. *J. Cell Biol.* (1982). doi:10.1083/jcb.92.1.79

179. Miksa, M., Komura, H., Wu, R., Shah, K. G. & Wang, P. A novel method to determine the engulfment of apoptotic cells by macrophages using pHrodo succinimidyl ester. *J. Immunol. Methods* (2009). doi:10.1016/j.jim.2008.11.019

180. Tedesco, S., De Majo, F., Kim, J., Trenti, A., Trevisi, L., Fadini, G. P., Bolego, C., Zandstra, P. W., Cignarella, A. & Vitiello, L. Convenience versus biological significance: Are PMA-differentiated THP-1 cells a reliable substitute for blood-derived macrophages when studying in vitro polarization? *Front. Pharmacol.* **9,** 1–13 (2018).

181. Biswas, S. K. & Mantovani, A. Macrophage plasticity and interaction with lymphocyte subsets: Cancer as a paradigm. *Nat. Immunol.* (2010). doi:10.1038/ni.1937

182. Ambarus, C. A., Krausz, S., van Eijk, M., Hamann, J., Radstake, T. R. D. J., Reedquist, K. A., Tak, P. P. & Baeten, D. L. P. Systematic validation of specific phenotypic markers for in vitro polarized human macrophages. *J. Immunol. Methods* (2012). doi:10.1016/j.jim.2011.10.013

183. Eligini, S., Crisci, M., Bono, E., Songia, P., Tremoli, E., Colombo, G. I. & Colli, S. Human monocyte-derived macrophages spontaneously differentiated in vitro show distinct phenotypes. *J. Cell. Physiol.* (2013). doi:10.1002/jcp.24301

184. Bowdish, D. M. E., Loffredo, M. S., Mukhopadhyay, S., Mantovani, A. & Gordon, S. Macrophage receptors implicated in the 'adaptive' form of innate immunity. *Microbes Infect.* (2007). doi:10.1016/j.micinf.2007.09.002

185. Saghaeian-Jazi, M., Mohammadi, S. & Sedighi, S. Culture and Differentiation of Monocyte Derived Macrophages Using Human Serum: An Optimized Method. *Zahedan J Res Med Sci. Press* **18,** 6–10 (2016).

186. Pouniotis, D. S., Plebanski, M., Apostolopoulos, V. & McDonald, C. F. Alveolar macrophage function is altered in patients with lung cancer. *Clin. Exp. Immunol.* **143,** 363–372 (2006).

187. He, C., Hu, Y., Yin, L., Tang, C. & Yin, C. Effects of particle size and surface charge on cellular uptake and biodistribution of polymeric nanoparticles. *Biomaterials* **31,** 3657–3666 (2010).

188. Enomoto, R., Imamori, M., Seon, A., Yoshida, K., Furue, A. & Tsuruda, H. Proposal for a new evaluation of phagocytosis using different sizes of fluorescent polystyrene microspheres. **2013,** 556–563 (2013).

189. Sethi, S. & Murphy, T. F. Bacterial infection in chronic obstructive pulmonary disease in 2000: A state-of-the-art review. *Clin. Microbiol. Rev.* (2001). doi:10.1128/CMR.14.2.336-363.2001

190. Martin, K. R., Ohayon, D. & Witko-Sarsat, V. Promoting apoptosis of neutrophils and phagocytosis by macrophages: Novel strategies in the resolution of inflammation. *Swiss Med. Wkly.* **145,** 1–10 (2015).

191. Krysko, D. V., D'Herde, K. & Vandenabeele, P. Clearance of apoptotic and necrotic cells and its immunological consequences. *Apoptosis* (2006). doi:10.1007/s10495-006-9527-8

192. Lea, S., Plumb, J., Metcalfe, H., Spicer, D., Woodman, P., Fox, J. C. & Singh, D. The effect of peroxisome proliferatoractivated receptor-c ligands on in vitro and in vivo models of COPD. *Eur. Respir. J.* (2014). doi:10.1183/09031936.00187812

193. Hodge, S., Hodge, G., Jersmann, H., Matthews, G., Ahern, J., Holmes, M. & Reynolds, P. N. Azithromycin improves macrophage phagocytic function and expression of mannose receptor in chronic obstructive pulmonary disease. *Am. J. Respir. Crit. Care Med.* **178,** 139–148 (2008).

194. Martinez-Pomares, L. The mannose receptor. *J. Leukoc. Biol.* **92,** 1177–1186 (2012).

195. Allavena, P., Chieppa, M., Monti, P. & Piemonti, L. From Pattern Recognition Receptor to Regulator of Homeostasis: The Double-Faced Macrophage Mannose Receptor. *Crit. Rev. Immunol.* **24,** 179–192 (2004).

196. Pontow, S. E., Kery, V. & Stahl, P. D. Mannose Receptor. *Int. Rev. Cytol.* (1993). doi:10.1016/S0074-7696(08)62606-6

197. Martinez-Pomares, L. The mannose receptor. *J. Leukoc. Biol.* (2012). doi:10.1189/jlb.0512231

198. Gazi, U. & Martinez-Pomares, L. Influence of the mannose receptor in host

immune responses. *Immunobiology* **214,** 554–561 (2009).

199. Gazi, U., Rosas, M., Singh, S., Heinsbroek, S., Haq, I., Johnson, S., Brown, G. D., Williams, D. L., Taylor, P. R. & Martinez-Pomares, L. Fungal recognition enhances mannose receptor shedding through dectin-1 engagement. *J. Biol. Chem.* (2011). doi:10.1074/jbc.M110.185025
200. Taylor, P. R., Gordon, S. & Martinez-Pomares, L. The mannose receptor: Linking homeostasis and immunity through sugar recognition. *Trends Immunol.* **26,** 104–110 (2005).
201. Stahl, P. D. & Ezekowitz, R. a. The mannose receptor is a pattern recognition receptor involved in host defense. *Curr. Opin. Immunol.* **10,** 50–55 (1998).
202. Sallusto, F. Dendritic cells use macropinocytosis and the mannose receptor to concentrate macromolecules in the major histocompatibility complex class II compartment: downregulation by cytokines and bacterial products. *J. Exp. Med.* (1995). doi:10.1084/jem.182.2.389
203. East, L. & Isacke, C. M. The mannose receptor family. *Biochim. Biophys. Acta - Gen. Subj.* **1572,** 364–386 (2002).
204. Mantovani, A., Sozzani, S., Locati, M., Allavena, P. & Sica, A. Macrophage polarization: Tumor-associated macrophages as a paradigm for polarized M2 mononuclear phagocytes. *Trends Immunol.* **23,** 549–555 (2002).
205. Gan, J., Dou, Y., Li, Y., Wang, Z., Wang, L., Liu, S., Li, Q., Yu, H., Liu, C., Han, C., Huang, Z., Zhang, J., Wang, C. & Dong, L. Producing anti-inflammatory macrophages by nanoparticle-triggered clustering of mannose receptors. *Biomaterials* **178,** 95–108 (2018).
206. Ponzoni, M., Pastorino, F., Di Paolo, D., Perri, P. & Brignole, C. Targeting macrophages as a potential therapeutic intervention: Impact on inflammatory diseases and cancer. *Int. J. Mol. Sci.* (2018). doi:10.3390/ijms19071953
207. Movahedi, K., Laoui, D., Gysemans, C., Baeten, M., Stangé, G., Van Bossche, J. Den, Mack, M., Pipeleers, D., In't Veld, P., De Baetselier, P. & Van Ginderachter, J. A. Different tumor microenvironments contain functionally

distinct subsets of macrophages derived from Ly6C(high) monocytes. *Cancer Res.* (2010). doi:10.1158/0008-5472.CAN-09-4672

208. Karnevi, E., Andersson, R. & Rosendahl, A. H. Tumour-educated macrophages display a mixed polarisation and enhance pancreatic cancer cell invasion. *Immunol. Cell Biol.* (2014). doi:10.1038/icb.2014.22
209. Van Ginderachter, J. A., Movahedi, K., Hassanzadeh Ghassabeh, G., Meerschaut, S., Beschin, A., Raes, G. & De Baetselier, P. Classical and alternative activation of mononuclear phagocytes: Picking the best of both worlds for tumor promotion. *Immunobiology* (2006). doi:10.1016/j.imbio.2006.06.002
210. Grivennikov, S. I., Greten, F. R. & Karin, M. Immunity, Inflammation, and Cancer. *Cell* (2010). doi:10.1016/j.cell.2010.01.025
211. Movahedi, K., Laoui, D., Gysemans, C., Baeten, M., Stangé, G., Van Bossche, J. Den, Mack, M., Pipeleers, D., In't Veld, P., De Baetselier, P. & Van Ginderachter, J. A. Different tumor microenvironments contain functionally distinct subsets of macrophages derived from Ly6C(high) monocytes. *Cancer Res.* (2010). doi:10.1158/0008-5472.CAN-09-4672
212. Movahedi, K., Schoonooghe, S., Laoui, D., Houbracken, I., Waelput, W., Breckpot, K., Bouwens, L., Lahoutte, T., De Baetselier, P., Raes, G., Devoogdt, N. & Van Ginderachter, J. A. Nanobody-based targeting of the macrophage mannose receptor for effective in vivo imaging of tumor-associated macrophages. *Cancer Res.* **72,** 4165–4177 (2012).
213. Carter, P. Improving the efficacy of antibody-based cancer therapies. *Nat. Rev. Cancer* (2001).
214. Muyldermans, S., Baral, T. N., Retamozzo, V. C., De Baetselier, P., De Genst, E., Kinne, J., Leonhardt, H., Magez, S., Nguyen, V. K., Revets, H., Rothbauer, U., Stijlemans, B., Tillib, S., Wernery, U., Wyns, L., Hassanzadeh-Ghassabeh, G. & Saerens, D. Camelid immunoglobulins and nanobody technology. *Vet. Immunol. Immunopathol.* (2009). doi:10.1016/j.vetimm.2008.10.299
215. Van Bockstaele, F., Holz, J. B. & Revets, H. The development of nanobodies

for therapeutic applications. *Curr. Opin. Investig. Drugs* (2009).

216. Movahedi, K., Schoonooghe, S., Laoui, D., Houbracken, I., Waelput, W., Breckpot, K., Bouwens, L., Lahoutte, T., De Baetselier, P., Raes, G., Devoogdt, N. & Van Ginderachter, J. A. Nanobody-Based Targeting of the Macrophage Mannose Receptor for Effective In Vivo Imaging of Tumor-Associated Macrophages. *Cancer Res.* **72,** 4165–4177 (2012).
217. Vera, D. R., Wallace, a M., Hoh, C. K. & Mattrey, R. F. A synthetic macromolecule for sentinel node detection: (99m)Tc-DTPA-mannosyl-dextran. *J. Nucl. Med.* (2001).
218. Azad, A. K., Rajaram, M. V. S., Metz, W. L., Cope, F. O., Blue, M. S., Vera, D. R. & Schlesinger, L. S. γ-Tilmanocept, a New Radiopharmaceutical Tracer for Cancer Sentinel Lymph Nodes, Binds to the Mannose Receptor (CD206). *J. Immunol.* **195,** 2019–2029 (2015).
219. Kim, J. B., Park, K., Ryu, J., Lee, J. J., Lee, M. W., Cho, H. S., Nam, H. S., Park, O. K., Song, J. W., Kim, T. S., Oh, D. J., Gweon, D. G., Oh, W. Y., Yoo, H. & Kim, J. W. Intravascular optical imaging of high-risk plaques in vivo by targeting macrophage mannose receptors. *Sci. Rep.* **6,** 1–11 (2016).
220. Tahara, N., Mukherjee, J., De Haas, H. J., Petrov, A. D., Tawakol, A., Haider, N., Tahara, A., Constantinescu, C. C., Zhou, J., Boersma, H. H., Imaizumi, T., Nakano, M., Finn, A., Fayad, Z., Virmani, R., Fuster, V., Bosca, L. & Narula, J. 2-deoxy-2-[18F]fluoro-d-mannose positron emission tomography imaging in atherosclerosis. *Nat. Med.* (2014). doi:10.1038/nm.3437
221. Donnelly, L. E. & Barnes, P. J. Defective phagocytosis in airways disease. *Chest* **141,** 1055–1062 (2012).
222. Hodge, S., Hodge, G., Jersmann, H., Matthews, G., Ahern, J., Holmes, M. & Reynolds, P. N. Azithromycin improves macrophage phagocytic function and expression of mannose receptor in chronic obstructive pulmonary disease. *Am. J. Respir. Crit. Care Med.* **178,** 139–148 (2008).
223. Hodge, S., Hodge, G., Brozyna, S., Jersmann, H., Holmes, M. & Reynolds, P. N. Azithromycin increases phagocytosis of apoptotic bronchial epithelial cells

by alveolar macrophages. *Eur. Respir. J.* **28,** 486–495 (2006).

224. Hodge, S. & Reynolds, P. N. Low-dose azithromycin improves phagocytosis of bacteria by both alveolar and monocyte-derived macrophagesin chronic obstructive pulmonary disease subjects. *Respirology* **17,** 802–807 (2012).
225. Wileman, T. E., Lennartz, M. R. & Stahl, P. D. Identification of the macrophage mannose receptor as a 175-kDa membrane protein. *Proc. Natl. Acad. Sci.* (1986). doi:10.1073/pnas.83.8.2501
226. Stein, M., Keshav, S., Harris, N. & Gordon, S. Interleukin 4 potently enhances murine macrophage mannose receptor activity: a marker of alternative immunologic macrophage activation. *J. Exp. Med.* **176,** 287–292 (1992).
227. Harris, N., Super, M., Rits, M., Chang, G. & Ezekowitz, R. A. Characterization of the murine macrophage mannose receptor: demonstration that the downregulation of receptor expression mediated by interferon-gamma occurs at the level of transcription. *Blood* (1992).
228. Takei, H., Araki, A., Watanabe, H., Ichinose, A. & Sendo, F. Rapid killing of human neutrophils by the potent activator phorbol 12-myristate 13-acetate (PMA) accompanied by changes different from typical apoptosis or necrosis. *J. Leukoc. Biol.* (1996). doi:10.1002/jlb.59.2.229
229. Keller, H. U. Diacylglycerols and PMA are particularly effective stimulators of fluid pinocytosis in human neutrophils. *J. Cell. Physiol.* (1990). doi:10.1002/jcp.1041450311
230. Li, G., D'Souza-Schorey, C., Barbieri, M. A., Roberts, R. L., Klippel, A., Williams, L. T. & Stahl, P. D. Evidence for phosphatidylinositol 3-kinase as a regulator of endocytosis via activation of Rab5. *Proc. Natl. Acad. Sci.* (1995). doi:10.1073/pnas.92.22.10207
231. Macia, E., Ehrlich, M., Massol, R., Boucrot, E., Brunner, C. & Kirchhausen, T. Dynasore, a Cell-Permeable Inhibitor of Dynamin. *Dev. Cell* (2006). doi:10.1016/j.devcel.2006.04.002
232. Taylor, M. E., Conary, J. T., Lennartz, M. R., Stahl, P. D. & Drickamer, K. Primary structure of the mannose receptor contains multiple motifs

resembling carbohydrate-recognition domains. *J. Biol. Chem.* (1990).

233. Garrido, V. V., Dulgerian, L. R., Stempin, C. C. & Cerbán, F. M. The increase in mannose receptor recycling favors arginase induction and trypanosoma cruzi survival in macrophages. *Int. J. Biol. Sci.* (2011). doi:10.7150/ijbs.7.1257
234. Vigerust, D. J. & Vick, S. Stable Expression and Characterization of an Optimized Mannose Receptor. *J. Clin. Cell. Immunol.* (2015). doi:10.4172/2155-9899.1000330
235. Chakravarty, R., Goel, S. & Cai, W. Nanobody: The 'magic bullet' for molecular imaging? *Theranostics* **4,** 386–398 (2014).
236. Jenkinson, D. R., Cadby, A. J. & Jones, S. The Synthesis and Photophysical Analysis of a Series of 4-Nitrobenzochalcogenadiazoles for Super-Resolution Microscopy. *Chem. - A Eur. J.* (2017). doi:10.1002/chem.201702289
237. Akram, A. R., Chankeshwara, S. V., Scholefield, E., Aslam, T., McDonald, N., Megia-Fernandez, A., Marshall, A., Mills, B., Avlonitis, N., Craven, T. H., Smyth, A. M., Collie, D. S., Gray, C., Hirani, N., Hill, A. T., Govan, J. R., Walsh, T., Haslett, C., Bradley, M. & Dhaliwal, K. In situ identification of Gram-negative bacteria in human lungs using a topical fluorescent peptide targeting lipid A. *Sci. Transl. Med.* **10,** (2018).
238. Benson, S., Fernandez, A., Barth, N. D., de Moliner, F., Horrocks, M. H., Herrington, C. S., Abad, J. L., Delgado, A., Kelly, L., Chang, Z., Feng, Y., Nishiura, M., Hori, Y., Kikuchi, K. & Vendrell, M. SCOTfluors: Small, Conjugatable, Orthogonal, and Tunable Fluorophores for In Vivo Imaging of Cell Metabolism. *Angew. Chemie - Int. Ed.* (2019). doi:10.1002/anie.201900465
239. Mosser, D. M. & Edwards, J. P. Exploring the full spectrum of macrophage activation. *Nat. Rev. Immunol.* (2008). doi:10.1038/nri2448
240. Galván-Peña, S. & O'Neill, L. A. J. Metabolic reprograming in macrophage polarization. *Front. Immunol.* **5,** 1–6 (2014).
241. Biswas, S. K. & Mantovani, A. Orchestration of metabolism by macrophages. *Cell Metab.* (2012). doi:10.1016/j.cmet.2011.11.013
242. Eto, K., Tsubamoto, Y., Terauchi, Y., Sugiyama, T., Kishimoto, T., Takahashi,

N., Yamauchi, N., Kubota, N., Murayama, S., Aizawa, T., Akanuma, Y., Aizawa, S., Kasai, H., Yazaki, Y. & Kadowaki, T. Role of NADH shuttle system in glucose-induced activation of mitochondrial metabolism and insulin secretion. *Science (80-.).* (1999). doi:10.1126/science.283.5404.981

243. Alfonso-García, A., Smith, T. D., Datta, R., Luu, T. U., Gratton, E., Potma, E. O. & Liu, W. F. Label-free identification of macrophage phenotype by fluorescence lifetime imaging microscopy. *J. Biomed. Opt.* **21,** 46005 (2016).
244. Lakowicz, J. R., Szmacinski, H., Nowaczyk, K. & Johnson, M. L. Fluorescence lifetime imaging of free and protein-bound NADH. *Proc. Natl. Acad. Sci.* (1992). doi:10.1073/pnas.89.4.1271
245. Szulczewski, J. M., Inman, D. R., Entenberg, D., Ponik, S. M., Aguirre-Ghiso, J., Castracane, J., Condeelis, J., Eliceiri, K. W. & Keely, P. J. In Vivo Visualization of Stromal Macrophages via label-free FLIM-based metabolite imaging. *Sci. Rep.* **6,** 1–9 (2016).
246. Sunakawa, Y., Stintzing, S., Cao, S., Heinemann, V., Cremolini, C., Falcone, A., Yang, D., Zhang, W., Ning, Y., Stremitzer, S., Matsusaka, S., Yamauchi, S., Parekh, A., Okazaki, S., Berger, M. D., Graver, S., Mendez, A., Scherer, S. J., Loupakis, F. & Lenz, H. J. Variations in genes regulating tumor-associated macrophages (TAMs) to predict outcomes of bevacizumab-based treatment in patients with metastatic colorectal cancer: Results from TRIBE and FIRE3 trials. *Ann. Oncol.* (2015). doi:10.1093/annonc/mdv474
247. Zhang, B., Zhang, Y., Zhao, J., Wang, Z., Wu, T., Ou, W., Wang, J., Yang, B., Zhao, Y., Rao, Z. & Gao, J. M2-polarized macrophages contribute to the decreased sensitivity of EGFR-TKIs treatment in patients with advanced lung adenocarcinoma. *Med. Oncol.* (2014). doi:10.1007/s12032-014-0127-0
248. Bertani, F. R., Mozetic, P., Fioramonti, M., Iuliani, M., Ribelli, G., Pantano, F., Santini, D., Tonini, G., Trombetta, M., Businaro, L., Selci, S. & Rainer, A. Classification of M1/M2-polarized human macrophages by label-free hyperspectral reflectance confocal microscopy and multivariate analysis. *Sci. Rep.* **7,** 1–9 (2017).

249. Forbes, B., O'Lone, R., Allen, P. P., Cahn, A., Clarke, C., Collinge, M., Dailey, L. A., Donnelly, L. E., Dybowski, J., Hassall, D., Hildebrand, D., Jones, R., Kilgour, J., Klapwijk, J., Maier, C. C., McGovern, T., Nikula, K., Parry, J. D., Reed, M. D., Robinson, I., Tomlinson, L. & Wolfreys, A. Challenges for inhaled drug discovery and development: Induced alveolar macrophage responses. *Adv. Drug Deliv. Rev.* **71,** 15–33 (2014).

250. Li, Y. & Liu, T. M. Discovering macrophage functions using in Vivo optical imaging techniques. *Front. Immunol.* **9,** 1–20 (2018).

251. Sköld, C. M., Eklund, A., Halldén, G. & Hed, J. Autofluorescence in human alveolar macrophages from smokers: relation to cell surface markers and phagocytosis. *Exp. Lung Res.* **15,** 823–835 (1989).

252. Njoroge, J. M., Mitchell, L. B., Centola, M., Kastner, D., Raffeld, M. & Miller, J. L. Characterization of viable autofluorescent macrophages among cultured peripheral blood mononuclear cells. *Cytometry* **44,** 38–44 (2001).

253. Aubin, J. E. Autofluorescence of viable cultured mammalian cells. *J. Histochem. Cytochem.* (1979). doi:10.1177/27.1.220325

254. Billinton, N. & Knight, A. W. Seeing the wood through the trees: A review of techniques for distinguishing green fluorescent protein from endogenous autofluorescence. *Anal. Biochem.* (2001). doi:10.1006/abio.2000.5006

255. Umino, T., Sköld, C. M., Pirruccello, S. J., Spurzem, J. R. & Rennard, S. I. Two-colour flow-cytometric analysis of pulmonary alveolar macrophages from smokers. *Eur. Respir. J.* (1999). doi:10.1034/j.1399-3003.1999.13d33.x

256. Song, W., Wang, W., Dou, L.-Y., Wang, Y., Xu, Y., Chen, L.-F. & Yan, X.-W. The implication of cigarette smoking and cessation on macrophage cholesterol efflux in coronary artery disease patients. *J. Lipid Res.* (2015). doi:10.1194/jlr.p055491

257. Morrell, E. D., Wiedeman, A., Long, S. A., Gharib, S. A., West, T. E., Skerrett, S. J., Wurfel, M. M. & Mikacenic, C. Cytometry TOF identifies alveolar macrophage subtypes in acute respiratory distress syndrome. *JCI Insight* (2018). doi:10.1172/jci.insight.99281

258. Hodge, S. J., Hodge, G. L., Holmes, M. & Reynolds, P. N. Flow cytometric characterization of cell populations in bronchoalveolar lavage and bronchial brushings from patients with chronic obstructive pulmonary disease. *Cytom. Part B - Clin. Cytom.* (2004). doi:10.1002/cyto.b.20020

259. Pauly, J. L., Allison, E. M., Hurley, E. L., Nwogu, C. E., Wallace, P. K. & Paszkiewicz, G. M. Fluorescent human lung macrophages analyzed by spectral confocal laser scanning microscopy and multispectral cytometry. *Microsc. Res. Tech.* **67,** 79–89 (2005).

260. Pedretti, E., Tanner, M. G., Choudhary, T. R., Krstajić, N., Megia-Fernandez, A., Henderson, R. K., Bradley, M., Thomson, R. R., Girkin, J. M., Dhaliwal, K. & Dalgarno, P. A. High-speed dual color fluorescence lifetime endomicroscopy for highly-multiplexed pulmonary diagnostic applications and detection of labeled bacteria. *Biomed. Opt. Express* **10,** 181 (2019).

261. Alfonso-Garcia, A., Haudenschild, A. K. & Marcu, L. Label-free assessment of carotid artery biochemical composition using fiber-based fluorescence lifetime imaging. *Biomed. Opt. Express* (2018). doi:10.1364/boe.9.004064

262. Wallrabe, H. & Periasamy, A. Imaging protein molecules using FRET and FLIM microscopy. *Curr. Opin. Biotechnol.* (2005). doi:10.1016/j.copbio.2004.12.002

263. Lin, H.-J., Herman, P. & Lakowicz, J. R. Fluorescence lifetime-resolved pH imaging of living cells. *Cytometry* (2003). doi:10.1002/cyto.a.10028

264. Seth, S., Akram, A. R., Dhaliwal, K. & Williams, C. K. I. Estimating bacterial and cellular load in FCFM imaging †. *J. Imaging* (2018). doi:10.3390/jimaging4010011